Università degli Studi della Basilicata

Dottorato di Ricerca in
Ingegneria per l'Innovazione e lo Sviluppo Sostenibile

HYDROGEOLOGY AND NUMERICAL MODELING OF COASTAL GROUNDWATER
RESOURCES FOCUSING ON SALINIZATION RISK IN THE METAPONTO PLAIN
(BASILICATA, SOUTHERN ITALY)

Settore Scientifico-Disciplinare GEO/05

Coordinatrice del Dottorato
Prof.ssa Aurelia Sole

Dottoranda
Dott.ssa Rosalba Muzzillo

Relatore
Prof. Francesco Sdao

Co-tutor
Ing. Maurizio Polemio
Prof.ssa Filomena Canora

Ciclo XXXV

University of Basilicata

Doctoral research programme in
Engineering for Innovation and Sustainable Development

HYDROGEOLOGY AND NUMERICAL MODELING OF COASTAL GROUNDWATER
RESOURCES FOCUSING ON SALINIZATION RISK IN THE METAPONTO PLAIN
(BASILICATA, SOUTHERN ITALY)

Discipline GEO/05 - Engineering Geology

Coordinator of the Ph.D. programme   **Ph.D. student**
Prof. Aurelia Sole   Dr. Rosalba Muzzillo

Supervisor
Prof. Francesco Sdao

Co-supervisor
Dr. Eng. Maurizio Polemio
Prof. Filomena Canora

XXXV Cycle

Acknowledgements

Table of contents

1. List of figures and tables

2. Summary

Coastal aquifers, defined as the domains where continental fresh groundwater and seawater meet (Post, 2005), represent a valuable source of water supply, but they are particularly sensitive to natural and anthropogenic changes.

The phenomenon of seawater intrusion (hereinafter SWI), defined as the movement of salt water invading freshwater aquifers, represents the most typical hydrogeological problem for coastal aquifers. SWI is one of the main causes of groundwater being unsuitable both for drinking and irrigation use. It also affects coastal environments by changing the soil chemistry, reducing fertility, and impacting local ecosystems.

The most common causes of SWI are aquifer overutilization and, locally, overpumping, but this phenomenon can be further worsened by the effects of climate change. With sea levels rising, the saline front (the interface between fresh water and salt water) can advance landward and further upstream into coastal estuaries. This process can be aggravated by drought and reduced rainfall. The resulting increase in water salinity can threaten coastal areas' flora and fauna and damage delicate habitats such as marshes and wetlands. Around 680 million people live in low-lying coastal zones - that is expected to increase to a billion by 2050 (2022 UN Ocean Conference[1]). Furthermore, coastal areas, especially coastal plains, are generally very important from an economic, social, and environmental point of view due to the presence of agricultural and productive activities, residential and tourism settlements, wooded areas, and wetlands of high ecological value (Vespasiano, et al., 2019; Erostate, et al., 2020).

In terms of the involved global population, SWI is one of the primary genetic sources of groundwater salinization, which affects 16% of the world land area (Polemio & Zuffianò, 2020).

The phenomenon of SWI as a result of groundwater over-exploitation is a significant concern in many European aquifers (Scheidleger et al., 2004; EEA, 2012). In the Mediterranean regions coastal aquifers are important reservoirs of water resources intended for drinking, but at the same time they are hydrogeological systems extremely vulnerable to pollution phenomena due to anthropogenic pressure and to the effects of climate change. Italy is one of the countries most affected by SWI due to overexploitation and climate change (Romanazzi & Polemio, 2013).

The risk of groundwater's qualitative degradation highlights the importance of developing and applying efficient methods for the prevention and mitigation of salinization processes. The detailed knowledge of coastal aquifer systems and the assessment of vulnerability and risk to the phenomenon of SWI can contribute to more effective management and protection of groundwater resources.

This thesis represents the conclusion of a three-year research activity conducted as part of the Ph.D. program under the Joint Research Agreement signed between the University of Basilicata, ENI, and CNR (Italian National Research Council). The scholarship, funded by ENI, belongs to the curriculum *Methods and Technologies for Environmental Monitoring and Protection* about the pre-assigned topic "Optimal management of coastal groundwater resources focusing on salinization and subsidence risks". The main objectives were the evaluation and modeling of the SWI process in the Metaponto coastal aquifer (Basilicata, southern Italy) by analysing the intrinsic geological and hydrogeological characteristics of the coastal plain and external factors such as excessive withdrawals and climate change causing recharge modification.

---

[1] https://www.un.org/en/conferences/ocean2022/facts-figures

Among the various Italian coastal aquifers subject to SWI, this area was chosen because, in addition to the effects of climate change, other anthropogenic aspects also play a significant role in facilitating the SWI process. The Metaponto coastal plain is intensively cultivated, and groundwater resources are important for economic growth in terms of tourism and agriculture (Polemio et al., 2005). The plain represents an important area for the entire Basilicata region, both for its marked agricultural vocation and for the presence of residential settlements, tourist facilities, wooded areas and wetlands. Five protected sites located near the river mouths are included in the Natura 2000 network thanks to the high ecological value of their flora and fauna.

During the 20th century, the anthropogenic impact, mainly linked to the development of modern irrigation systems, land reclamation works, the overexploitation of wells, and agricultural and industrial activities, has significantly modified the plain. The land reclamation works of the marshy areas started in the 1930s have helped to lower the water table and, at the same time, the excavation of the drainage channels has facilitated the circulation of salt water also far from the coast. The coastline modifications through the construction of ports, and the phenomenon of coastal regression due to climatic variations and the progressive human changes to the beach, must also be considered. These land use changes negatively impacted the hydrogeological system threatening groundwater availability and quality along the plain and intensifying the risk of aquifer pollution. These modifications also magnified soil salinization and SWI risks.

Groundwater resources are particularly exposed to quantitative degradation due to the historically unfavourable climatic conditions worsened by climate change and the growing water demand, and to qualitative degradation caused by the SWI. Low rainfall (mean annual value of 538 mm) and moderate temperature (mean annual value equal to 16.3 °C), typical of a Mediterranean climate, cause low aquifer recharge (Muzzillo et al., 2021a; Muzzillo et al., 2022).

The surface and sub-surface structure of the study area, characterized by the presence of marine terraces, coastal plains, and paleo-riverbeds, is the result of evolutionary processes of sedimentation, erosion, and sea level variations due to the action of marine and fluvial morphological agents.

From a geological point of view, the area belongs to the sedimentary succession of the Fossa Bradanica, made up, from bottom to top, of the Sub-Apennine Clays Formation (Upper Pliocene?-Middle Pleistocene) (Vezzani, 1967; Parea, 1986), passing upwards to the Terraced Marine Deposits (Middle-Upper Pleistocene) and the alluvial and coastal deposits (Upper Pleistocene?-Holocene), in discordance on the Sub-Apennine Clays (Tropeano et al., 2002; Pescatore et al., 2009; Cilumbriello et al., 2010; Sabato et al., 2018). The hydrogeology of the plain is characterized by the presence of a complex coastal aquifer system.

The application of the inverse hydrogeological water balance (Celico, 1988; Cotecchia et al., 1990; Civita, 2005; Canora et al., 2018; Canora & Sdao, 2020) and the characterization of the hydrogeological complexes allowed us to calculate the effective infiltration, equal to about 34 Mm^3/year.

The investigations conducted and the data collected allowed the reconstruction of the geolithological and hydrogeological structure of the various aquifers present in the study area and the definition of the chemical-physical characteristics of the groundwater (Cilumbriello et al., 2010; Muzzillo et al., 2021a; Muzzillo et al., 2021b). In particular, the hydrochemical characteristics and the spatial distribution of the groundwater electrical conductivity showed that the coastal aquifer is partially affected by the phenomenon of SWI (Polemio et al., 2002; Muzzillo et al., 2021a; Muzzillo et al., 2021b). Firstly, in this Ph.D. research project, the proneness to SWI was explored with a

multidisciplinary approach based on geophysical and hydrochemical investigations. Defining the main hydrostratigraphic features can help prevent the worsening of SWI: detailed knowledge of the aquifer bottom is important to support groundwater management. For this purpose, a significant portion of the coastal plain was selected between the Agri and Cavone Rivers. Geoelectrical measurements recorded along three Electrical Resistivity Tomography (ERT) profiles showed where the aquifer bottom pattern is deeply incised by paleovalleys. The hydrochemical study focused on 49 groundwater samples for which on-site chemical-physical parameters (electrical conductivity at 25 °C, temperature, and pH) and main ions (Na^+, K^+, Ca^{2+}, Mg^{2+}, Cl^-, NO_3^-, SO_4^{2-}, and HCO_3^-) were determined. The hydrochemical data highlighted the areas with higher SWI proneness, especially where the aquifer bottom is very deep below sea level, even far from the coast.

Subsequently, the chemical-physical parameters of 53 groundwater samples collected between Cavone and Bradano Rivers were detected on-site using a multiparametric probe (electrical conductivity at 25 °C, temperature, and pH), and the main ions (Na^+, K^+, Ca^{2+}, Mg^{2+}, Cl^-, NO_3^-, SO_4^{2-} and HCO_3^-) were determined using ion chromatography methods. The concentrations of the main constituents were reported in a Piper diagram, which made it possible to represent the geochemical facies and the types of analysed groundwater. Despite a significant dispersion of the representative points of groundwater chemistry, it was possible to recognize two main types: the bicarbonate-alkaline-earthy facies (typical of the groundwater of marine terraces and alluvial deposits) and the sulphate-chlorinated alkaline facies (referable to samples of wells located in coastal deposits). The distribution of the main dissolved ions in groundwater showed, in most cases, the enrichment of Ca^{2+} together with the depletion of Na^+ and K^+, indicating a progressive mixing with seawater.

After the description of the geological and hydrogeological setting (with the inverse hydrogeological water balance) and the hydrochemical characterization, the groundwater vulnerability assessment of the Metaponto coastal plain was conducted.

Firstly, the assessment of the intrinsic vulnerability of the coastal aquifer was carried out by the GIS-based application of the SINTACS method (Civita & De Maio, 1997). It considers seven aquifer parameters: water table depth, effective infiltration, unsaturated conditions, soil media, aquifer media, hydraulic conductivity, and topography. Furthermore, to consider the anthropogenic influence in the study area, the SINTACS method was modified by adding the parameter of land use (LU). The SINTACS and SINTACS-LU vulnerability indexes were provided by summing the product of ratings and weights assigned to each parameter. The intrinsic vulnerability maps showed three classes ranging from low to high vulnerability. In both cases, the south-eastern part of the coastal plain, closest to the sea, is characterized by the high vulnerability class, indicating that it is the most vulnerable to contamination due to the intrinsic hydrogeological factors. The wide central part of the study area shows the moderate vulnerability class, whereas the low one is scattered in small portions in the northern part of the plain, which represent the areas less contaminable in space and time in the case of potential pollution. In the SINTACS-LU map, some areas classified as highly vulnerable in the SINTACS method show a minor vulnerability class. These areas are localized in natural and wooded sectors of the Metaponto plain, which are less populated and where the human impact on the groundwater is minimal.

Then, the groundwater vulnerability to SWI was evaluated through the GALDIT method application, also conducted using the QGIS open-source geographic information system. GALDIT is an overlay-index method with scores and weights specific for the vulnerability to SWI assessment in coastal aquifers (Chachadi & Lobo Ferreira, 2001; Chachadi & Lobo Ferreira, 2005; Lobo Ferreira et al., 2005). It allows the determination and zoning of the vulnerability index by taking into consideration

the intrinsic parameters of the aquifer, such as type of aquifer (G), hydraulic conductivity (A), groundwater level (L), distance from the coastline (D), the impact of the existing status of SWI in the area (I) and aquifer thickness (T). The vulnerability map produced has three classes: low, moderate, and high, covering 70.40%, 22.65%, and 6.95% of the study area, respectively. The high vulnerability to SWI is detected along the coastal strip, within 500 m from the coast, covering an extension of about 20 km^2. The high class is located close to the coast due to the proximity to the sea, the greater thickness of the aquifer, and the shallow freshwater-seawater interface. Areas characterized by moderate vulnerability extend, on average, up to 4 km in correspondence with the Agri and Cavone Rivers, with a width of about 7 km between the Basento and Bradano Rivers. In these zones, the aquifer thickness is greater than 10 m, and the highest values of groundwater electrical conductivity are found. The low vulnerability covers most of the study area and is detected where the piezometric altitude is highest, and the electrical conductivity of the groundwater has the lowest values. The vulnerability zoning reveals that the propensity to SWI is accentuated from SW to NE, widening from the coast towards inland.

The sensitivity analysis was conducted to evaluate the influence of the parameters and weights on the final vulnerability indexes obtained with the SINTACS, SINTACS-LU, and GALDIT methods.

In the last part of the thesis, the research performed to conceptualize and numerically model the Metaponto coastal aquifer is described. Numerical simulations were performed for the portion of the coastal plain characterized by a greater propensity to the SWI phenomenon based on the results of hydrochemical analyses and the evaluation of intrinsic vulnerability with the GALDIT method. Once the study area was selected, the geological, hydrogeological, hydrological, climatic, and hydrochemical data acquired and processed became the inputs for the numerical modeling of groundwater flow and variable-density transport. The hydrogeological and hydrochemical characterization of the aquifer was necessary to define an accurate conceptual model, the subsequent numerical simulations of the groundwater flow, and a proper modeling of the SWI phenomenon.

The MODFLOW and SEAWAT codes were used within the Visual MODFLOW Flex 7.0 software (© 2021 by Waterloo Hydrogeologic). Groundwater flow was reconstructed in the steady-state simulation under natural conditions. Subsequently, transient simulations were carried out for the years 1997-1999. Then three scenarios were simulated by considering changes in pumping rate and the impact of climate change in terms of different recharge values. With pumping rates above 100 l/s, SWI will not be negligible in the future, causing significant effects on coastal groundwater. The overall results highlight that the aquifer requires the definition of effective management criteria to avoid the progress of the SWI phenomenon.

The outcomes, in addition to improving the knowledge of the investigated area, can provide effective support for optimal groundwater management and protection, and planning of the aquifer groundwater exploitation. The groundwater flow modeling and the understanding of the mechanisms that determine salinity variations can support the implementation of management criteria facing SWI, climate change, and water demand in future scenarios linked to qualitative and quantitative changes in groundwater.

Research on this aquifer system could be continued and expanded to further improve knowledge of the salinization process. In particular, *in situ* hydrogeological and geognostic surveys could be essential for the consolidation and validation of the numerical model.

3. State of the art

Over the years, the Metaponto plain has been the subject of numerous studies and investigations with varying degrees of detail.

In 1999, the interregional project PRISMAS aimed to define and implement standard procedures for designing and exploiting a groundwater monitoring network (Martinelli & Marchetti, 2000). In the Basilicata Region, in particular, the objective was to assess the possible contamination of coastal groundwater due to SWI processes along the Ionian coast by analysing the hydrogeological characteristics of groundwater resources and their qualitative-quantitative status.

In 2001, the CRYSTECHSALIN research activity began (IV Meeting CRYStallisation TECHnologies for prevention of SALt water INtrusion. Scanzano Jonico, Italy, 26-29 September 2002). The three-year project, funded by the European Union, was aimed at testing new techniques for creating physical barriers to marine intrusion by reducing the permeability of soils through crystallization. The experimentation involved, among others, the Bradano and Metaponto Reclamation Consortium and the Bari section of the CNR's Research Institute for Geo-Hydrological Protection (Istituto di Ricerca per la Protezione Idrogeologica - IRPI). During the research activity, the hydrogeological characterization of the Metaponto plain was aimed at selecting a suitable area to host the experimentation, which was identified in the municipal territory of Scanzano Jonico.

The Bari section of the CNR IRPI (Polemio et al., 2002; Polemio et al., 2003; Polemio et al., 2005) pointed out how the coastal aquifer is subject to the risk of qualitative degradation due to anthropogenic activities in the area (groundwater extraction, agricultural and livestock practices, wastewater, and waste disposal). The research focused on hydrogeological and hydrochemical characterization. In particular, the spatial distribution of salinity, electrical conductivity, and chlorides was analysed.

Numerous studies have been conducted by various authors on the geological, hydrogeological, and stratigraphic characterization of the Metaponto plain (Tropeano et al., 2002; Pescatore et al., 2009; Cilumbriello et al., 2010). These works resulted in the creation of Sheet 508 "Policoro" of the Geological Map of Italy at a scale of 1:50.000 (Sabato et al., 2018).

The CNR Institute of methodologies for environmental analysis (IMAA) carried out geophysical and geoelectrical surveys to investigate the Metaponto plain.

Satriani et al. (2011) used ERT to evaluate resistivity contrasts and delineate the lithostratigraphic boundaries geometry. This technique is a valuable tool for reconstructing the geometry of the salt intrusion front and for identifying areas characterized by a high level of salinization. Indeed, the presence of seawater strongly reduces resistivity values.

Satriani et al. (2012) applied the 2D ERT in an area of the Metaponto coastal forest Reserve. This technique, supported by laboratory analysis of soil and water samples, revealed the presence of a saline intrusion process that caused the decline of the existing pine forest with consequent problems of erosion and desertification. The geoelectrical investigations revealed significant variations in subsurface resistivity related to the lithological characteristics of the subsurface strata. In this way, the spatial distribution of brackish and saline water in the pine forest was assessed.

Imbrenda et al. (2018) implemented a multidisciplinary study based on geophysical and remote sensing techniques, landscape ecology tools, and geospatial data analysis to monitor the Metaponto Plain. The analysis of landscape evolution performed in five protected areas of the Natura 2000 network for about 30 years (1985-2013) revealed marine intrusion processes, which promote forest degradation and limit its recovery after fires.

Summa et al. (2019) tried to identify the main mechanisms causing the soil salinization process by analysing the grain size, and mineralogical and geochemical characteristics of a pilot site in the coastal area. A critical depth of about 20 cm was identified, which influences the downward diffusion mechanism of the surface salt content.

Moreover, the geomorphology of the Metaponto coastal area was studied from borehole analysis and Horizontal-to-Vertical Spectral Ratio (HVSR) method, delineating the morphology of the top of the bedrock between the Cavone and Bradano Rivers (Tropeano, et al., 2011). Tropeano et al. (2013) suggested a high depth of this substratum, which also defined the clay bedrock incision where paleovalleys have settled and refilled.

Pastore et al. (2020) analysed the dynamics involved in groundwater level variations due to episodic rainfall supply with a kinematic dispersion wave model. The developed model was validated using a high-resolution time series of rainfall data and groundwater levels obtained from the monitoring station of Terra Montonata.

The cognitive framework outlined by the literature search and the collection of geological, lithostratigraphic and hydrogeological data available from previous researches provided a good starting point for the study of the investigated area. However, a more in-depth knowledge of the aquifer characteristics was needed to pursue its conceptual and numerical modeling.

Different approaches can be adopted to properly manage water resources in coastal areas. Hydrochemical methods can be used to highlight the saline contamination by measuring parameters such as electrical conductivity, chloride concentration, and total dissolved solids concentration. Nowadays, attention is focused on geophysical techniques as an alternative to these traditional methods to directly or indirectly detect the hydrogeological structure of the aquifer to monitor salt water in coastal aquifers (Polemio & Zuffianò, 2020). Geophysical methods are widely used to obtain geological and hydrogeological information in coastal environments. They are particularly valuable when traditional investigation techniques are too expensive, invasive or their application is not feasible. Both land- and marine-based near-surface geophysical methods can be effective in numerous applications, including water resource management, watershed-scale and coastal hydrology, and characterization of the geological and hydrogeological properties of the subsoil for natural-hazards risk assessment or the design of coastal engineering structures.

Shallow geophysical methods, such as ground-penetrating radar and seismic approaches, are widely used in sedimentology for the management of onshore environments. Seismic methods can assist hydrogeological conceptualization by providing deep geological information, such as stratigraphy features. In coastal environments, seismic methods are particularly useful to delineate the distribution of geologic units that could also be affected by the movement of salt water (Stewart, 1999).

Even if several geophysical methods can characterize coastal areas, the electrical resistivity is more closely connected and strongly related to pore water salinity. Numerous case studies of geoelectrical applications may be found in the literature (Goldman et al., 2006; Nguyen et al., 2009; Kazakis et al., 2016; Bouzaglou et al., 2018). The electrical geophysical prospecting method determines the subsoil's electrical resistivity distribution. The electrical resistivity of a geological formation is a physical characteristic that defines the resistance to the flow of electric current. The resistivity varies with the texture of the rock, nature of mineralization, and conductivity of electrolyte contained within the porous rock. Resistivity increases with grain size and drastically decreases with the increase in clay content, which is commonly dispersed throughout as coatings on grains, disseminated masses, or thin layers or lenses. In saturated rocks, low resistivity can be due to increased clay content or salinity.

Hence, resistivity surveys are the most suitable for the delineation of clayey or saline zones (Kirsch, 2009). These concepts are well defined by the Archie law in saturated medium:

$$\rho = \rho_w \varphi^{-n}$$

where ρ is the electrical resistivity of a rock, ρ_w is the resistivity of the water, φ is the fraction of porosity filled with water, and n is the cementation exponent of the rock. Therefore, electrical and electromagnetic methods could contribute to SWI studies. Several papers highlight the use of Vertical Electrical Sounding (VES) and Electrical Resistivity Tomography (ERT) for the characterization of coastal areas and the investigations of SWI phenomena (Aladejana et al., 2020; Hasan et al., 2020). The VES method defines the vertical variation of the electrical resistivity, but when the bedrock has an irregular geometry and strong lateral variations are distributed, only a spatial investigation method as the ERT has an important role in the coastal area characterization (De Franco et al., 2009; Costall et al., 2018).

In the present research, ERT method was applied in a selected portion of the Metaponto coastal plain, between the Agri and Cavone Rivers, to obtain information about the spatial distribution of the electrical resistivity in the subsoil and define the main geological and hydrogeological features. Three ERT profiles with an investigation depth of about 120 m were performed, overcoming the insufficient maximum depth investigated in the previous works (Satriani et al., 2011) and increasing the resolution of the bedrock substratum compared with the past HVSR survey. The use of continuous coring drilling data improved the reliability of geophysical result interpretation.

Considering the importance of groundwater as an essential resource nowadays and yet, the risk of pollution to which it is exposed, especially in areas of intensive agriculture with fertilizer and pesticide use, many studies in recent decades have focused on its protection and management based on vulnerability assessment. Groundwater vulnerability assessment has been widely recognized for its ability to spatially predict groundwater pollution (Adams & Foster, 1992; Civita & De Maio, 1997; Kumar & Krishna, 2018; Barbulescu, 2020; Kirlas et al., 2022). It represents a relevant tool for the groundwater resources protection and can be useful for their planning and management. The intrinsic vulnerability map provides valuable information to stakeholders interested in preventing groundwater degradation, especially under the current climate and environmental changes (Mendoza & Barmen, 2006).

Different definitions of groundwater vulnerability were proposed (Albinet & Margat, 1970; National Research Council, 1993; Vrba & Zaporec, 1994). The intrinsic vulnerability of groundwater to contamination can be described as the sensitivity of the aquifer systems, in their different geometric and hydrodynamic settings, to ingest and spread a pollutant, even mitigating its effects, and with the ability to impact the groundwater quality (Civita, 1987). Based on this definition, the aquifer vulnerability is assessed independently of the nature of pollutants resulting from human activities but refers to the geological and hydrogeological aquifer characteristics (Zwahlen, 2004).

Currently, several approaches have been proposed for assessing the vulnerability of groundwater. Different authors (Machiwal et al., 2018a; Machiwal et al., 2018b; Barbulescu, 2020; Taghavi et al., 2022) and references therein proposed comprehensive reviews about advanced approaches for the groundwater vulnerability assessment, highlighting the status and challenges of groundwater protection. In recent years, the advent and the improvement of Geographic Information Systems (GIS) greatly enhanced the different approaches. The storage, elaboration, interpretation, and representation of the numerous georeferenced data necessary to assess groundwater vulnerability at large spatial scales has become simpler than in the past (Jha et al., 2007).

The most relevant approaches elaborated in the literature to evaluate aquifer vulnerability are the following: process-based models such as SUTRA (Voss, 1984), PRZM (Carsel et al., 1985),

LEACHP (Wagenet & Hutson, 1986), GLEAMS (Leonard et al., 1987), MT3DMS (Zheng & Wang, 1999) and Hydrus (Šimunek et al., 2005); overlay and index methods such as DRASTIC (Aller et al., 1987), SINTACS (Civita & De Maio, 2000; Civita & De Maio, 2004; Civita, 2005), EPIK (Doerfliger et al., 1997) and COP (Vías et al., 2006); statistical techniques (Nolan et al., 2002; Twarakavi & Kaluarachchi, 2005); and hybrid procedures (Rupert, 2001).

All these method and technique typologies show different benefits and drawbacks. Although process-based models can create a transient representation of groundwater quality (Ostad-Ali-Askari et al., 2017; Javadinejad et al., 2019; Gupta et al., 2020; Ostad-Ali-Askari et al., 2021), they are typically utilized on small-scale domains due to the need for high quality and frequency data, as well as the high computing time and demand. Advanced statistical techniques, successfully integrated with GIS, have been applied by several researchers (Tesoriero & Voss, 1997; Stevenazzi et al., 2017). The disadvantages of these methods can be found in the requirement for large and high-quality datasets. Overlay and index methods can be easily implemented, modified, and updated, can be applied to wide domains, and usually do not need large amounts of data (Sahoo et al., 2016; Barbulescu, 2020). However, they could be affected by subjectivity in rating assignments. Hybrid procedures, which primarily combine overlay and index methods with statistical analysis, aim to overcome their limitations (Panagopoulos et al., 2006; Kazakis & Voudouris, 2015).

Many overlay and index procedures and methods have been set based on parameters derived from hydrogeological data represented by ratings and weights (Brindha & Elango, 2015; Jahromi et al., 2021).

Groundwater vulnerability assessment to SWI represents an utmost importance tool to develop and propose the most appropriate and cost-effective groundwater management and protection strategies for groundwater salinization prevention to make more resilient coastal aquifers and ecosystems.

Lobo Ferreira & Cabral (1991) defined groundwater vulnerability to SWI as "the sensitivity of groundwater quality to an imposed groundwater pumping or sea-level rise or both in the coastal belt, which is determined by the intrinsic characteristics of the aquifer". SWI into coastal groundwater highlights the importance of developing innovative and effective methods to prevent and mitigate the salinization process.

Different researchers applied several approaches, models, and methods for assessing the vulnerability to SWI in coastal aquifers (Praveena & Aris, 2009; Younes & Fahs, 2014; Kazakis et al., 2018; Mavriou et al., 2019; Moazamnia et al., 2020).

The worldwide-applied overlay-index method for assessing groundwater vulnerability to SWI is GALDIT (Kura et al., 2015; Trabelsi et al., 2016; Luoma et al., 2017; Kim et al., 2021).

Chachadi & Lobo Ferreira (2001) developed the GALDIT method for vulnerability assessment of coastal aquifers to SWI. GALDIT is the acronym for selected vulnerability indicators such as Groundwater occurrence, Aquifer hydraulic conductivity, water Level above sea level, Distance from the coastline, Impact status of existing SWI, and aquifer Thickness (meaning saturated thickness). It is a numerical ranking system based on six hydrogeological, topographic and morphological parameters with appropriately assigned ratings and weights (Chachadi & Lobo Ferreira, 2001; Chachadi & Lobo Ferreira, 2005; Lobo Ferreira et al., 2005).

The salinization risk of coastal groundwater highlights the importance of developing innovative and efficient methods to prevent and mitigate this process. A significant contribution to a proper policy of groundwater utilization, including monitoring design and planning, can be offered by scenario numerical modeling to characterize SWI modifications and develop optimal management tools for the sustainable use of these resources (Polemio & Zuffianò, 2020). Computational tools are useful in the management, control and planning of groundwater resources, allowing, among other things,

verification of the achievement of resource protection objectives. One can, for example, interpret the results of the aquifer water balance to understand the evolution of the freshwater-seawater balance following a given pumping rate. Mathematical models for analysing salt transport can be used to interpret the results of monitoring salinity and electrical conductivity of groundwater and the transition zone. This makes it possible to describe the phenomena underlying any deterioration in qualitative and quantitative status of groundwater and, thus, to control and predict its evolution. The effectiveness of interventions to restore the quantitative status of the aquifer can be evaluated, identifying new scenarios for exploiting the water resource.

In the last years, various simulation and optimization computer-based models have been applied to find proper solutions for SWI management problems (Singh, 2015). The approaches used for the simulation of SWI can be divided into two main categories: interface models and variable density models (Bakker et al., 2013). In the former, freshwater and seawater are considered two immiscible fluids of constant density separated by a sharp interface. In the latter (e.g., SEAWAT - Guo & Langevin, 2002), the transition zone between salt water and fresh water has a finite thickness, and the fluid density can vary continuously. So, they are more suitable for simulating the density-dependent groundwater flow system.

Analysis of the balance between freshwater and intruded seawater is essential for proper groundwater management. Modeling proves to be a valuable tool for solving problems both at regional scales, such as changes in the shape and position of the transition zone due to withdrawal and at local scales, such as salt-water upconing. Numerical modeling can be accomplished by finite difference or finite-element calculation methods, including three-dimensional analysis. However, any assessment must be based on knowledge of the aquifer's actual hydrogeological parameters, as well as recharge and groundwater use conditions.

Modeling the process of marine intrusion into a coastal aquifer, in which the aquifer feeding or boundary conditions may vary, must necessarily be three-dimensional, density-dependent, consider transient and dispersion phenomena.

In recent decades, the use of computational codes has become considerably widespread. The main ones are given below.

FEFLOW is a 2-3D finite element computational code particularly suitable for simulating groundwater flow phenomena of varying density in porous and cracked media under saturated and unsaturated conditions. The code makes it possible to model groundwater flow in case it is affected by density changes in the fluid due to temperature differences or the presence of contaminants. One of the main advantages of the model is the flexibility of meshing. Among its many applications are modeling salt intrusion, fresh water/salt water interface, upconing of seawater in coastal aquifers and below boreholes, and salt transport due to agricultural practices.

MODFLOW is the most widely used hydrologic model developed by the U.S. Geological Survey (USGS) in the literature, considered an international standard for the simulation and prediction of groundwater conditions and interactions with surface waters. Its modular structure provided a robust framework for integrating additional simulation capabilities to simulate coupled groundwater/surface water systems, solute transport, subsidence, parameter estimation, and groundwater management. The 3-D numerical modeling software solves flow equations using the finite difference method, modeling groundwater trends through portions of saturated soil. MODFLOW is generally limited to density-independent problems. Using MODFLOW, it is possible to calculate piezometric loading but not to model flows that depend on differences in density, as in the case of saline intrusion in a coastal aquifer. To overcome this issue, it is possible to use the software package SEAWAT, which allows groundwater modeling by coupling flow and mass transport with concentrations starting at different densities, using for flow and transport two widely accepted codes, namely, MODFLOW and MT3D.

SUTRA (Saturated-Unsaturated TRAnsport), developed by the U. S. Geological Survey (USGS), is a public domain computational code widely used for solving general hydrogeology problems because of its extreme flexibility. It is a finite element simulation model for saturated-unsaturated groundwater flow, dependent on fluid density, with energy transport or solute transport of single chemically reactive species. SUTRA can be used for the areal and cross-sectional modeling of groundwater flow systems in the saturated zone and cross-sectional modeling of flow in the unsaturated zone. Solute transport simulation using SUTRA can be employed to model the transport of natural or human-induced chemical species, including solute uptake, production, and decay processes, and can be applied to analyse contaminant transport problems in groundwater and groundwater restoration projects. In addition, solute transport simulation with SUTRA can be used for cross-sectional modeling of salt water intrusion into aquifers at local (well) or regional scales. The model employs a two-dimensional hybrid finite-element and integrated finite-difference method to approximate the governing equations that describe the two interdependent processes that are simulated: (1) fluid density-dependent saturated or unsaturated groundwater flow, (2a) transport of a solute in groundwater, which may be subject to adsorption onto the porous matrix and production or decay, or (2b) transport of thermal energy in groundwater and solid aquifer matrix[2].

The choice of the numerical code to use depends on a series of factors associated with the definition of the investigated hydrogeological problem and/or the ability of the code to successfully simulate it (Kallioras et al., 2010; Polemio et al., 2011). The choice of the most suitable model to use must result from careful consideration of the actual hydrogeological conditions of the aquifer, the possibility of finding the necessary input data, and the accuracy with which these parameters can be derived.

The first choice to be made concerns the use of a finite difference or finite element model.

Computational codes based on finite differences are usually more intuitive and easier to program. Therefore, they are widespread and widely used even for rather complex problems, but they are difficult to apply in presence of irregular geometries and special boundary conditions.

Finite element methods are very versatile and are used especially in cases of irregular domains: the computational domain, in fact, is constructed from the union of a considerable number of subdomains of elementary form.

Second, the choice of initial and boundary conditions is an extremely important step in the implementation of the chosen model, as they strongly influence the results obtained during the simulation. In particular, attention should be paid to the definition of the water balance and deciding whether to model the flow in the saturated and/or unsaturated zone.

Finally, regarding the required input parameters, the main ones are as follows:

- detailed stratigraphy (depositional environments, facies associations, thickness, lithology);
- land use;
- temperature, pH, redox potential, salinity;
- climatic data;
- evaporation rates;
- hydraulic and transport parameters (conductivity, conductance, transmissivity, dispersion, diffusion, effective porosity, composition of recharge water-salinity);
- sea level;
- outflows;
- permeability;
- piezometric surface.

---

[2] https://apps.dtic.mil/sti/citations/ADA156779

4. Study area

The Metaponto coastal plain, covering an area of about 280 km^2, is located in the southern part of the Basilicata region (Italy). It extends for about 40 km along the Ionian coast in the SW-NE direction from the Sinni River to the Bradano River, and in the SE-NW direction from the coast up to about 9 km inland. (**Fig. 1**).
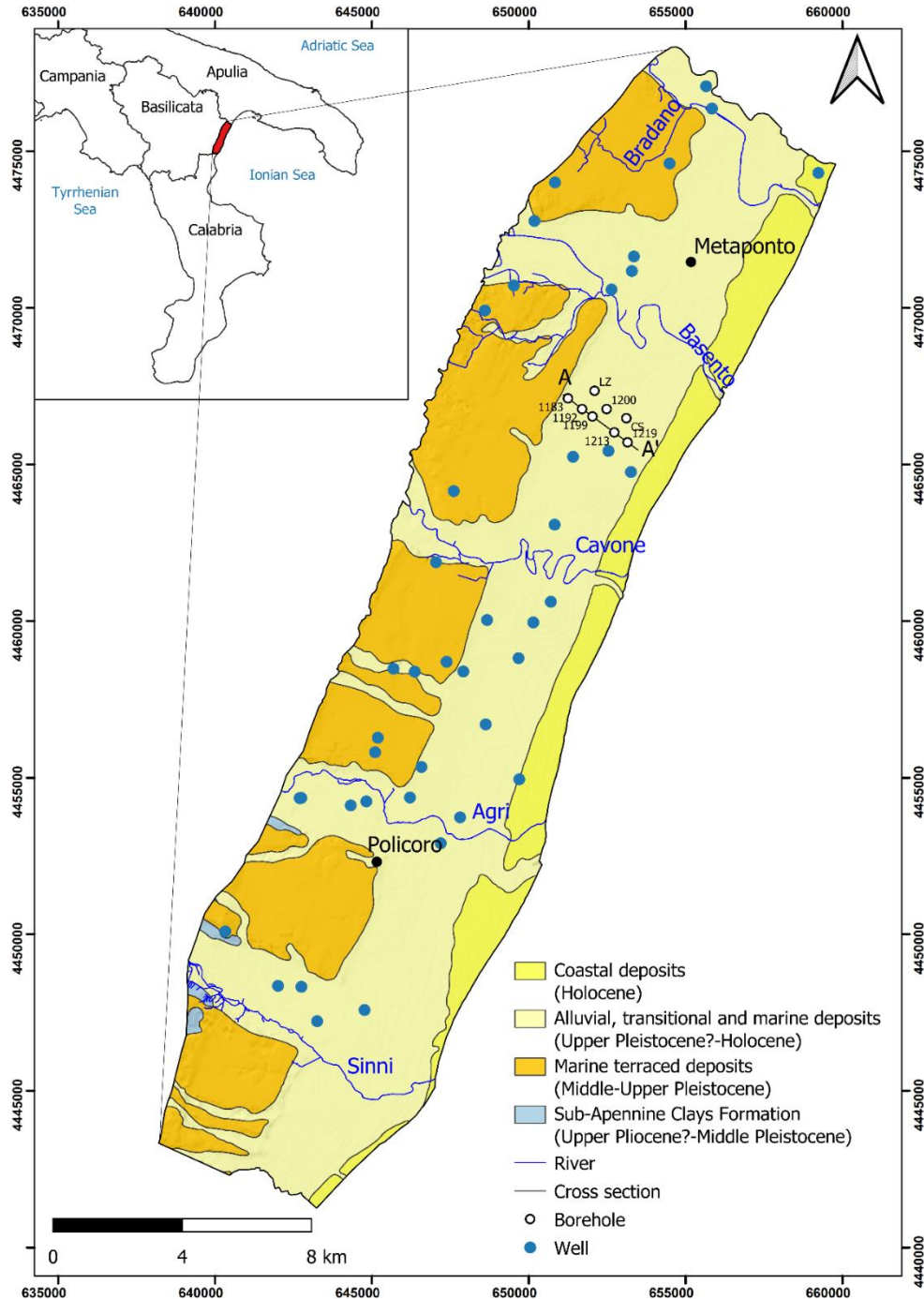
Fig. 1 *Schematic geological map of the Metaponto coastal plain, adapted from the Geological Maps of Italy at 1:100.000 and 1:50.000 scale (from Canora et al., 2022).*

The study area morphology is characterized by smooth marine terraces engraved by river valleys, which constitute the surface drainage network, and by plains close to the sea. The mean elevation and slope of the coastal area are about 20 m a.s.l. and 5%, respectively.

The main climatic characteristics of the study area are typical of the Mediterranean climate, with dry summers and mild, wet winters. Precipitation is scarce and concentrated mostly in winter. The highest rainfall rates are detected during November and December, whereas the lowest occur during July and August. The highest monthly mean temperatures are recorded during the summer period in July and August, with a value of 26.9 °C, whereas the lowest temperatures are observed in winter, with a minimum temperature in January of 9.3 °C. The hydrological balance, elaborated for the reference period from 2000 to 2015, gives 538 mm as rainfall, 465 mm as actual evapotranspiration determined following Turc's formula (Turc, 1954), and the rate of 52 mm/year as effective infiltration, which is equivalent to about 1080 l/s, as mean annual values in the study area. The annual mean value of direct runoff is 21 mm/year (Muzzillo et al., 2021a).

The demand for water resources is higher in the summer months when agricultural requests and the presence of the tourist population increase.

The morphology of the study area highlights, from the coastline moving inland, different zones. According to a general coastal model (Longhitano, 2015), the coastal subaerial sector can be divided into foreshore primarily constituted by a limited sandy deposit stretch, and backshore affected by dunes, striking mainly parallel to the shoreline, and flat variable-width zones, ranging from 2 to 5 km, constituted by fluvial deposits. The inland areas present a staircase of marine terraces succession, almost parallel to the coastline, crosscut by different rivers (Bradano, Basento, Cavone, Agri, and Sinni) with an orthogonal trend to the Ionian coast, from NE to SW. Due to the particular morphology of the territory, the rivers caused flooding and marsh areas in the peri-coastal environment. Starting from 1950, the hydraulic arrangement and land reclamation of the Metaponto coastal area, carried out by the Irrigation and Land Development Authority, have contributed to the development of the entire plain. The coastal area is characterized by the presence of numerous inhabited and tourist villages, and the primary economic activity is agriculture. Nowadays, the plain is very important for the economic growth of the region, especially regarding intensive agriculture production and tourism. During the 20th century, reclamation works and the development of modern irrigation systems favored agricultural and industrial activities, which, together with groundwater exploitation and climate change impact, have strongly modified the hydrogeological conditions of the plain (**Fig. 2**).

Fig. 2 Intensive agricultural landscape of the Metaponto coastal plain and strawberry field.

5. Geological and hydrogeological setting

The Metaponto coastal plain is located along the Ionian coastal area of the Basilicata region. From a geological point of view, it corresponds to the southernmost and more recent outcropping sector of the Bradanic Foredeep that lies between the eastern front of the Apennine chain and the western sector of the Apulia foreland (Migliorini, 1937; Pescatore, et al., 2009) (**Fig. 1**). It has undergone a progressive stage of emersion since the Middle Pleistocene (Ciaranfi et al., 1983; Doglioni et al., 1996; Corrado et al., 2017) due to the interaction between a moderate tectonic uplift (Westaway & Bridgland, 2007) and Quaternary eustatic sea-level changes (Pescatore, et al., 2009).

The geomorphological evolution of the study area is identifiable by the presence, from 380 m a.s.l. to 10-15 m a.s.l., of a staircase of marine terraces (Brückner, 1980; Caputo et al., 2010; Cilumbriello et al., 2010; Sauer et al., 2010; Gioia et al., 2020).

The marine-terrace deposits (Middle-Upper Pleistocene), constituted by thin gravel and medium-fine sands, unconformably overlie the marine silty clays of the Sub-Apennine Clays Formation (Upper Pliocene?-Middle Pleistocene) (Tropeano et al., 2002), outcropping in limited portions of the study area, mainly along the deeper incision of the fluvial network (Pescatore, et al., 2009; Tropeano, et al., 2013) (**Fig. 3**). The flat surfaces of the marine terraces, having a similar trend to the current coastline and representing the ancient coastlines of the different sea level standing phases, are crosscut by the fluvial incisions of the Sinni, Agri, Cavone, Basento, and Bradano Rivers (from SW to NE) (Parea, 1986) (**Fig. 1**).

Fig. 3 First and second order of the marine terraces of the study area.

The alluvial, transitional and marine deposits (Upper Pleistocene?-Holocene), extensively present in the coastal plain, overlay the marine grey-blue silty clays (Pescatore, et al., 2009). Silty-clayey and sandy silts layers, with interspersed sandy layers, characterize the alluvial deposits, present mainly along the river valleys and on flood plains. The transitional and marine deposits are characterized by gravel, sand, and silt layers of the deltaic and beach depositional environment, unevenly distributed mostly in the coastal plains and prograded up to the present coastal deposits (Pescatore et al., 2009; Cilumbriello et al., 2010; Tropeano et al., 2013; Sabato et al., 2018) (**Fig. 1** and **Fig. 4**).

The coastal deposits define the sandy beaches, which become sandy or gravely sandy, with pebbly lenses towards the Sinni River (Cocco, et al., 1975). Coastal dunes and wetlands made up of compact and weakly cemented sands delimit the beaches inland. (**Fig. 1** and **Fig. 5**).

Fig. 4 *Alluvial, transitional and marine deposits in proximity of the Cavone River.*

Fig. 5 *Coastal dunes and sandy beaches in the Metaponto area.*

The lithostratigraphic setting of the Metaponto coastal plain, derived from the cross-section AA' (**Fig. 7**) of the Geological Map of Italy at a scale of 1:50.000, and realized on the basis of several datasets referring to the boreholes present in the study area, highlights different stratigraphic units (**Fig. 1** and **Fig. 7**). From the bottom to the top, it consists of the irregular depth of shelf-transition clayey, clayey-silty, and clayey-sandy deposits, locally with intercalations of discontinuous gravel levels, belonging to Sub-Apennine Clays Formation (Middle-Pleistocene), reaching about 120 m below sea level. in

correspondence with the paleo river valleys (Tropeano, et al., 2013), mainly filled by estuarine deposits (Pescatore, et al., 2009; Cilumbriello, et al., 2010) (**Fig. 6**). Fluvial and/or deltaic sandy-gravelly deposits with locally clayey and clayey-silty deposits belonging to marine-terrace deposits (Upper Pleistocene) characterize the second unit.

Fig. 6 *"Biancane" erosional landforms constituted by the Sub-Apennine Clays Formation outcropping at a higher elevation than the Metaponto coastal plain (Montalbano Jonico, MT).*

The last two lithostratigraphic units constitute the buried and outcropping coastal prisms of Metaponto, both belonging to the alluvial, transitional, and marine deposits (**Fig. 7**).

Sandy, gravelly and silty deposits constitute the buried prism (Upper Pleistocene). They have filled the paleo river valleys during low-stand of sea level, the depth of which ranges between 30 and 40 m below the current sea level. These deposits, laterally discontinuous, lie by an erosional surface on the substrate and the sandy-gravelly deposits. The outcropping deposits of the coastal prisms (Upper Pleistocene-Holocene) constitute the upper unit. These medium-to-fine sandy, gravelly and silty deposits of a continental-to-transitional environment during a low-stand of relative sea level, filled the incised paleovalleys, and subsequently, the aggradation took place to form the current Metaponto coastal area.
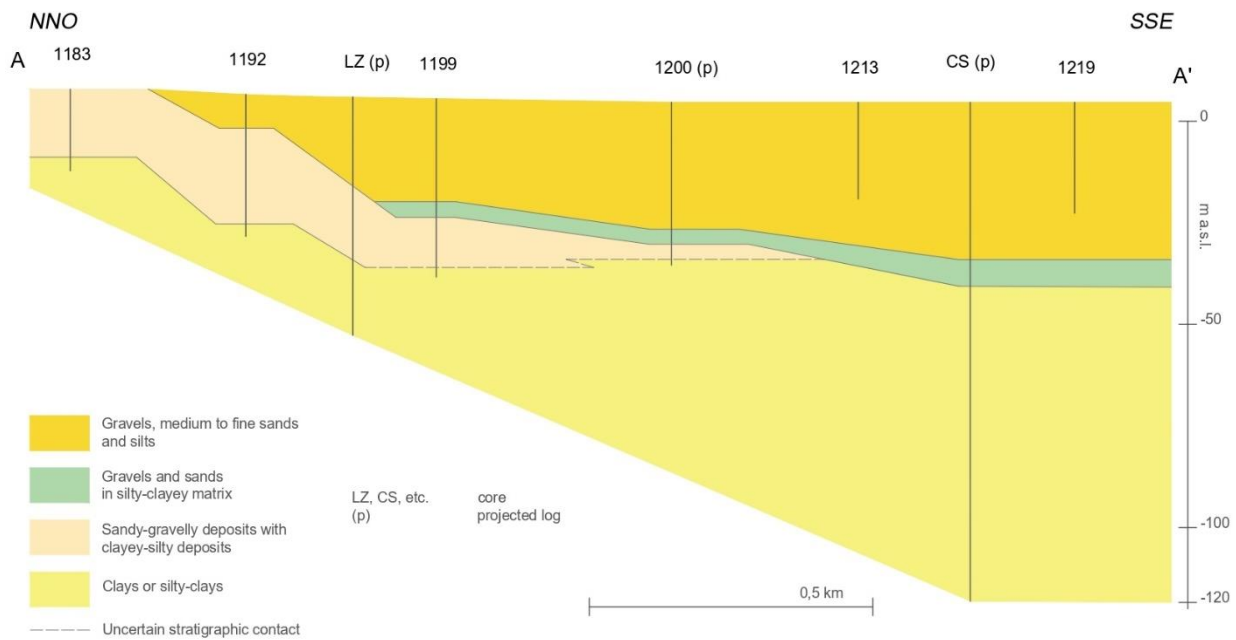
Fig. 7 *Schematic cross section AA' (see **Fig. 1** for location) of the Metaponto coastal plain stratigraphic units, adapted from the Geological Map of Italy at 1:50,000 scale (ISPRA, 2016; Sabato et al., 2018).*

The peculiar hydrogeological structure of the Metaponto coastal plain reflects the complex and articulated geological and stratigraphic context. The distinctive boundary conditions of the groundwater flow have been determined by the spatial distribution of the different formations and the geomorphological evolution of the entire area. The grey-blue clays, characterized by very low hydraulic conductivity, constitute the bottom of the entire aquifer system (Radina, 1969; Polemio et al., 2003). Different mostly unconfined aquifers can be distinguished (Polemio et al., 2005; Muzzillo et al., 2021b). They are located in the marine terraced deposits, in the alluvial deposits of river valleys, and in the coastal plain. The continuity of the aquifer that lies in the marine terraced deposits, showing medium to high hydraulic conductivity, is cut by the river valleys (Polemio et al., 2003). The aquifers of the alluvial paleo river valleys are very deep with limited lateral extension and show medium hydraulic conductivity. The coastal plain aquifer, limited in-depth, has medium-low relative hydraulic conductivity compared to the previous ones; its importance is due to the continuity across the plain. The mean and median values of the hydraulic conductivity of the plain deposits are $2.28 \cdot 10^{-4}$ and $6.53 \cdot 10^{-5}$ m/s, respectively, determined from pumping tests on a large scale referred to the entire plain (Polemio et al., 2003; Muzzillo et al., 2021b). From inland to the shore, the hydraulic conductivity decreases, but its reduction in the proximity of the coast may not be sufficient to mitigate SWI risk.

The shallow coastal aquifer corresponds to the intermediate most permeable sandy thickness, characterized by a variable particle-size distribution confined within silty clayey impermeable levels of varying extents and thicknesses (Polemio et al., 2003). The thickness of the aquifer permeable layers is greater than 10 m and generally tends to increase from the inland toward the coast. The silty clay formation constitutes the bottom of the coastal aquifer; it deepens towards the shore with an irregular surface characterized by local depressions.

The aquifer bottom gradually decreases from the Sinni to the Bradano Rivers in the SW-NE direction and, in the proximity of the coastline, it drops below sea level, potentially allowing SWI along the coast in the north-eastern direction, depending on the local hydrodynamic conditions (Polemio et al., 2002).

The effective infiltration amount of about 52 mm/y, considered as recharge of the coastal aquifer system, is modest due to the climate conditions (Muzzillo et al., 2021a). The aquifer recharge is mostly guaranteed by the discharge from the upward marine terraces' aquifer, in which the recharge areas are localized, and by river leakage. The spatial trend of the piezometric surface confirms the upstream groundwater recharge of the coastal aquifer (**Fig. 8**). The water table contour lines, nearly parallel to the coastline, allow identifying the preferential flow directions of the groundwater, oriented orthogonally to these lines, moving from the terraces to the Ionian coast.
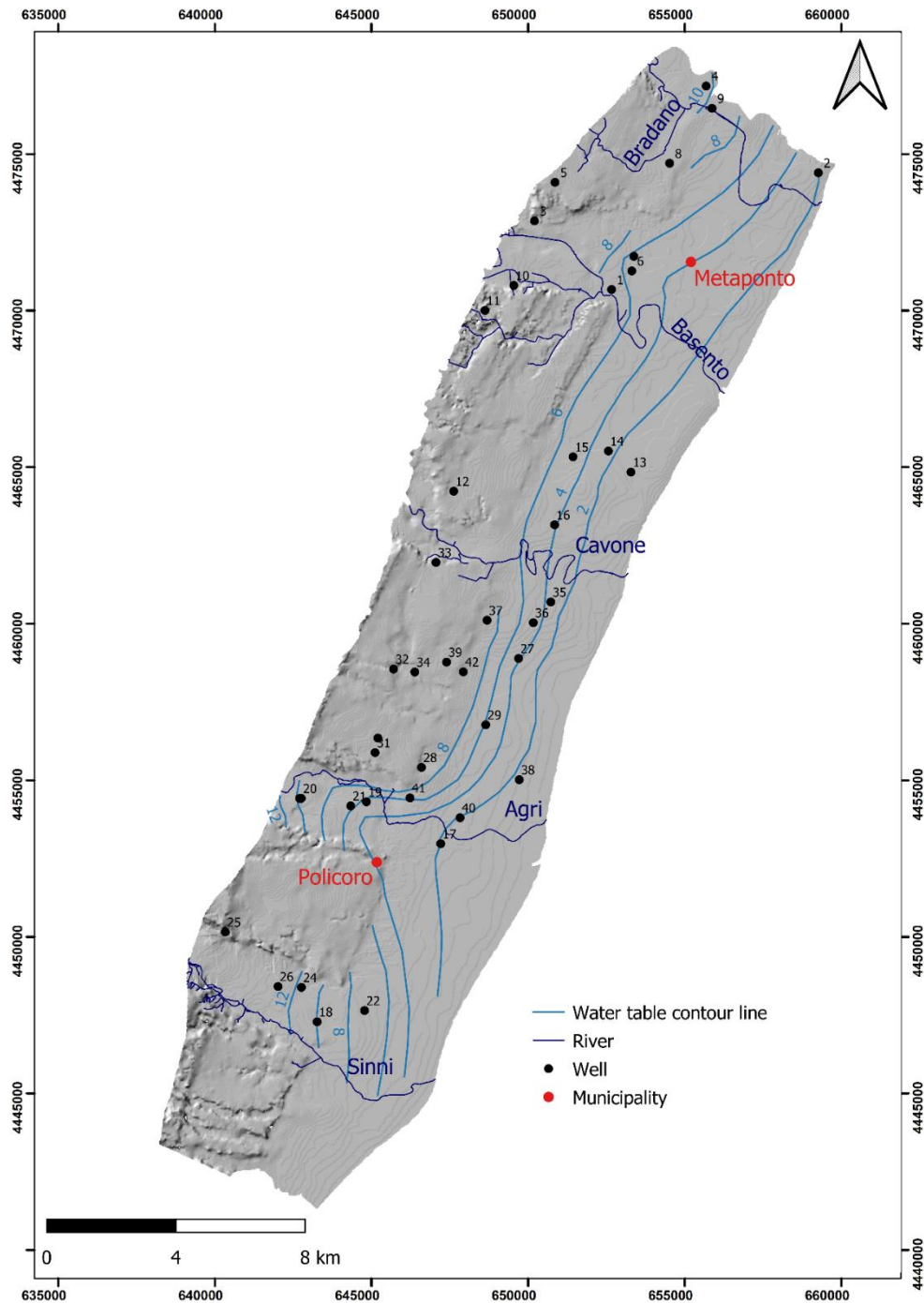
Fig. 8 *Simplified water table map of the Metaponto coastal plain (from Muzzillo et al., 2022).*

6. Materials and methodologies

6.1 Data collection

The selection of potential areas most subjected to SWI was carried out by the data analysis, considering various parameters such as depth to water, saturated aquifer thickness, depth of the shallow aquifer bottom, hydraulic conductivity, and aquifer grain size.

The collection of the historical data series and their analysis focused on geological, hydrogeological, hydrological, and hydrochemical data. The early stage of the study concerned the geological and hydrogeological description of the study area as well as the hydrochemical characterization of groundwater. The investigation was conducted on: the existing bibliography, including ISPRA geological maps, reports, and publications; hydrogeological data sets, and chemical and physical descriptions of groundwater; and maps at scales from 1:100.000 to 1:10.000.

Regarding the wells surveyed in the entire Metaponto coastal plain, stratigraphic, piezometric, and hydrochemical data are available only for some of them, since the time series come from different sources (Polemio et al., 2003).

The examined geological and hydrogeological parameters comprise: the depth to the bottom aquifer, inferred from stratigraphic surveys, the piezometric head above sea level, and the well tests. These data were used to assess additional parameters, such as the depth to water or the unsaturated zone thickness, the hydraulic conductivity, and the type of groundwater flow (phreatic or confined). The wealth of information assembled to characterize the geological and hydrological conceptualization of the Metaponto coastal plain was extracted from a vast array of sources and dates to various periods. Hence, huge efforts have been put to make data comparable and overlapping and validate the findings in keeping with the objectives of this research activity. To manage space-related information, a Geographic Information System (GIS) was used, allowing the management and organization of databases containing information relating to all the surveyed wells. All collected data were georeferenced and implemented in a geodatabase on the QGIS software.

The research activity pursued the definition of a reliable conceptual model representative of the aquifer system. A solid conceptual model can arise from a multidisciplinary approach, which schematizes reality considering the numerous factors that contribute to determine the system's behaviour and its response to external variations. This phase of the work was necessary to define the hydrostructural and hydrodynamic characteristics of the aquifer system and understand the mechanisms governing the quantity and quality aspects of water resources. Based on such a conceptual model, it was possible to perform groundwater modeling, a useful tool also in terms of groundwater management and planning.

6.2 Geophysical survey

In the first steps of the research activities, a multimethodological approach was defined to improve the aquifer knowledge, merging basic and affordable investigation techniques and integrating boreholes data, electrical resistivity profiles, and groundwater hydrochemical analyses. This approach was tested in a selected area characterizing the coastal aquifer bottom and the hydrochemical characteristics of groundwater, supporting the discussion of the variability of the bottom depressions and providing fresh-saline water mixing evidence. The geophysical approach (ERT) was used to detect the paleovalley patterns and the erosional morphology in the investigated area between the substratum (Sub-Apennine Clays Formation) and the shallow filled units, which define an important rule for SWI phenomena.

Three ERT profiles were performed between the Agri and Cavone Rivers (**Fig. 9**). They were acquired using a Syscal Pro Instruments georesistivimeter (Iris company, Orléans, France) with an electrode distance of about 20 m with 48 electrodes. Each profile was 940 m long to reach an investigation depth of about 140 m. ERT is realized by applying electrical current to the ground using well-defined electrode configurations and measuring the potential differences at the surface. It is used to assess the electrical resistivity distribution of the subsoil. Rock resistivity is of special interest for hydrogeological purposes as it allows, e.g., to discriminate between fresh water and salt water, soft-rock sandy aquifers and clayey material, and between hard rock porous/fractured aquifers and low-permeable claystones and marlstones (Kirsch, 2009). The electrode configuration affects the depth of investigation, the sensitivity to vertical and horizontal changes in the subsurface resistivity, the horizontal data coverage, and the signal strength. The raw data acquired during the survey must be processed to obtain the best possible interpretation.
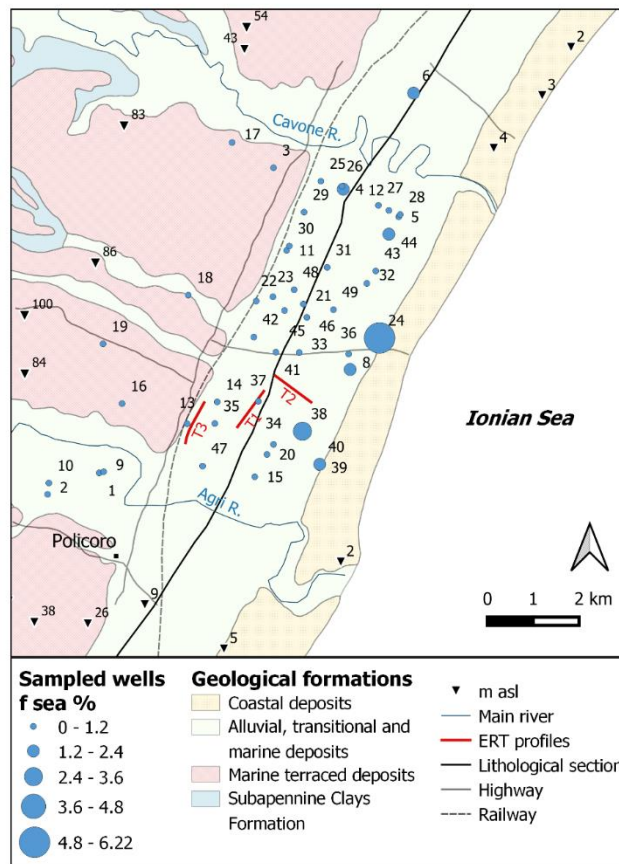
Fig. 9 *Map of the sampled wells and the locations of the Electrical Resistivity Tomography (ERT) profiles (from Muzzillo et al., 2021b).*

For this work, apparent resistivity data were analysed and converted to real resistivity values using ZondRes2D (Zond software LTD, Larnaca, Cyprus), which is a software for 2.5D interpretation of ERT. The first step was preparing the data for the inversion, which involved detection of poor data. The next step was selecting the inversion type and parameters. To transform the apparent resistivity pseudo section into a model representing the distribution of the calculated electrical resistivity in the subsurface, the Marquardt method was used. It is a classic inversion algorithm using the least-square method with regularization by damping parameters (Marquardt, 1963). Then we performed the Occam inversion, an algorithm that produces a contrast subsurface model, which is an inversion by the least-square method, using a smoothing operator and an additional contrast minimization (Constable et al., 1987).

6.3 Inverse hydrogeological water balance

The assessment of the aquifer recharge is necessary to define the priority protection measures and the sustainable management of groundwater.

In the literature, there are several direct and indirect methods for the groundwater recharge estimation, each with a different degree of approximation depending on the availability of data and space-time scales considered (Simmers, 1988).

Direct methods describe the mechanism of water percolation from the soil to the aquifer by simulating flow and storage at temporal and spatial resolutions based on meteorological, topographical, land cover, and hydrogeological input parameters.

Since in most cases not all these data are available, it is necessary to use indirect methods using variables that represent the flow of water through the soil and allow the definition of the relationship between flow and recharge (Scanlon et al., 2002).

The inverse hydrogeological water balance approach was applied to evaluate the annual groundwater recharge of the Metaponto coastal plain (Celico, 1988; Cotecchia et al., 1990; Civita, 2005; Canora et al., 2018; Canora & Sdao, 2020). This indirect methodology consists of calculating the effective infiltration considering climate data, such as rainfall and temperature, and topographic and hydrogeological parameters, such as the altitude and the characteristics of the hydrogeological complexes in the basin under consideration (Civita & De Maio, 2001; Civita, 2005). This method implemented in the GIS environment allows to derive the spatial distribution of the infiltration rate (potential recharge of the aquifer) in the hydrogeological basin based on geostructural and hydrogeological data (Canora et al., 2018).

The 5 m-resolution Digital Terrain Model (DTM) of the Metaponto coastal plain was loaded In QGIS software, and the position of the thermic and rainfall gauges, located inside or bounding the study area, was georeferenced (**Tab. 1** and **Tab. 2**).

Despite the apparent homogeneous distribution of the thermopluviometric stations within the study area, to obtain a better correlation between the precipitation data and the altitude, some stations located in the vicinity of the study area were considered due to the lack of climate monitoring points at the highest altitudes (**Tab. 1**, **Tab. 2** and **Fig. 10**).

Daily rainfall and air temperature series were collected for two different periods: 1925-1979 from the National Hydrographic Service and 2000-2015 from ALSIA (Lucanian Agency for Development and Innovation in Agriculture).

Station	Lat. N	Long. E	m (a.s.l.)
Bernalda	40°25'00.25''	16°40'49.08''	127
Metaponto	40°22'	16°49'	3
Montalbano Jonico	40°17'24''	16°34'12''	292
Nova Siri	40°09'03.32''	16°31'48.35''	300
Nova Siri Scalo	40°07'48''	16°37'48''	2
Pisticci	40°17'44.47''	16°44'00.97''	364
Policoro	40°13'12''	16°40'48''	31
Recoleta	40°15'01.63''	16°38'48.24''	83
San Basilio	40°19'02.90''	16°41'46.14''	67
San Salvatore	40°26'05.52''	16°47'46.57''	46

Tab. 1 Location and altitude (m. a.s.l.) of the National Hydrographic Service thermopluviometric gauges considered for the period 1925-1979.

Station	Lat. N	Long. E	m (a.s.l.)
Bernalda, C.da Pezzagrande	40°26'23"	16°45'45"	49
Metaponto, AASD Pantanello	40°26'24"	16°54'46"	9
Montalbano Jonico, C.da Cozzo del Fico	40°16'53"	16°36'52"	151
Montescaglioso, Fiumicello	40°28'49"	16°43'12"	45
Nova Siri, Agriturismo La Collinetta	40°8'51"	16°35'21"	136
Pisticci, C.da Castelluccio	40°21'53"	16°37'13"	189
Pisticci, Pisticci Scalo	40°24'48"	16°34'40"	49
Policoro, C.da Troyli	40°13'33"	16°37'32"	115
Policoro, Pantano Sottano	40°10'60"	16°41'17"	4
San Giorgio Lucano, Piano delle Rose	40°8'17"	16°21'49"	455
Stigliano, C.da Torre	40°23'35"	16°20'9"	285

Tab. 2 Location and altitude (m. a.s.l.) of the ALSIA thermopluviometric gauges considered for the period 2000-2015 (from Muzzillo et al., 2021a).
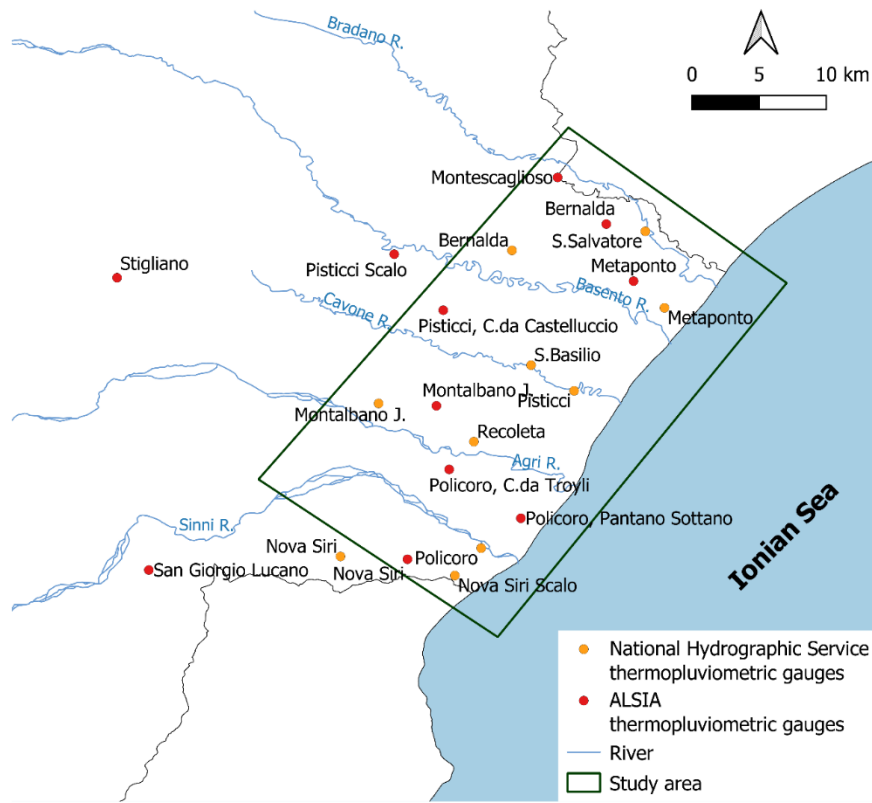
Fig. 10 Thermopluviometric gauges locations (modified from Muzzillo et al., 2021a).

The inverse hydrogeological water balance uses rainfall as the main input variable in the system. The water balance equation provides the average annual assessment of the hydrological variables:

$$P = ET_r + I + R \qquad (1)$$

where P indicates the rainfall (mm), ET_r is the amount of actual evapotranspiration (mm), I is the effective infiltration (mm) that can be considered as the active recharge, and R is the direct runoff (mm). From daily rainfall and temperature data for the reference periods, monthly and annual average values were calculated for each gauge. The monthly average temperatures were used to calculate for each gauge the corrected annual mean temperature (T_c), also depending on rainfall, by using:

$$T_c = \frac{\sum P_i T_i}{\sum P_i} \qquad (2)$$

where: P_i is the monthly average rainfall (mm) and T_i indicates the temperature (°C) of the i-th month, with i from 1 to 12, counting from January. The spatial distribution of corrected temperature and rainfall across the study area was estimated using the straight-line correlation between the thermic and pluviometric data with the altitude q by the definition of linear regression functions $T_c = f(q)$ and $P = f(q)$. These functions were used to compute the water balance within the whole study area by using a GIS-based procedure. The altitude in each cell was derived from the DTM.

The corrected temperature T_c is necessary to estimate the actual evapotranspiration. Due to the limited availability of temporal and spatial meteorological datasets, it was calculated by applying the empirical Turc's formula (Turc, 1954), based on annual rainfall and air temperature data:

$$ET_r = \frac{P}{\sqrt{0.9 + \left(\dfrac{P}{300 + 25T_c + 0.05T_c^3}\right)^2}} \tag{3}$$

where ET_r is the average real annual evapotranspiration (mm), P is the average annual rainfall (mm), and T_c is the corrected average annual temperature (°C). The reliability of Turc's empirical model was confirmed by several studies carried out in the Mediterranean basin and European areas (Turc, 1954; Santoro, 1970; Parajka & Szolgay, 1998; Allocca et al., 2014).

The effective rainfall P_e, evaluated for each cell as the difference between mean annual rainfall P (mm) and mean annual real evapotranspiration ET_r (mm), represents the sum of effective infiltration I (mm) and direct runoff R (mm):

$$P_e = P - ET_r = I + R \tag{4}$$

The effective infiltration (the water rate that percolates underground) is related to the infiltration capacity of the geological formations depending on many factors such as outcropping lithologies, soil textures, and land use, expressed by the identification of the appropriate set of potential infiltration coefficients χ (**Tab. 3**) (Civita, 2005; Canora et al., 2018). The potential infiltration coefficient was assigned to each geological formation in the area, considering the characteristics of the aquifer system and referring the permeability of the complexes to literature values (Civita, 2005).

Geological formation	χ
Alluvial, transitional and marine deposits	0,75
Coastal deposits	0,80
Marine terraced deposits	0,85
Subapennine Clays formation	0,15

Tab. 3 *Values of the potential infiltration coefficient χ.*

The effective infiltration was calculated in each cell by using effective rainfall values and potential infiltration coefficients:

$$I = P_e \cdot \chi \tag{5}$$

where I is the mean annual effective infiltration (mm), P_e is the mean annual effective rainfall (mm), and χ is the potential infiltration coefficient (dimensionless).
The direct runoff rate (the flow rate on the topographic surface) was calculated as the difference between the effective rainfall P_e and infiltration I:

$$R = P_e - I \tag{6}$$

6.4 Hydrochemical study

The hydrochemical study was conducted to define the groundwater chemical characteristics, supporting the hydrogeological conceptualization, and the existence of other relevant processes apart from fresh-salt water mixing, especially at the salt/fresh water interface, as the cation exchange processes. It focused on two sets of groundwater samples for which on-site chemical-physical parameters (electrical conductivity EC at 25 °C, temperature T and pH) and main ions (Na^+, K^+, Ca^{2+}, Mg^{2+}, Cl^-, NO_3^-, SO_4^{2-}, and HCO_3^-) were determined. The locations of the sampling points are shown in **Fig. 9** and **Fig. 11**.
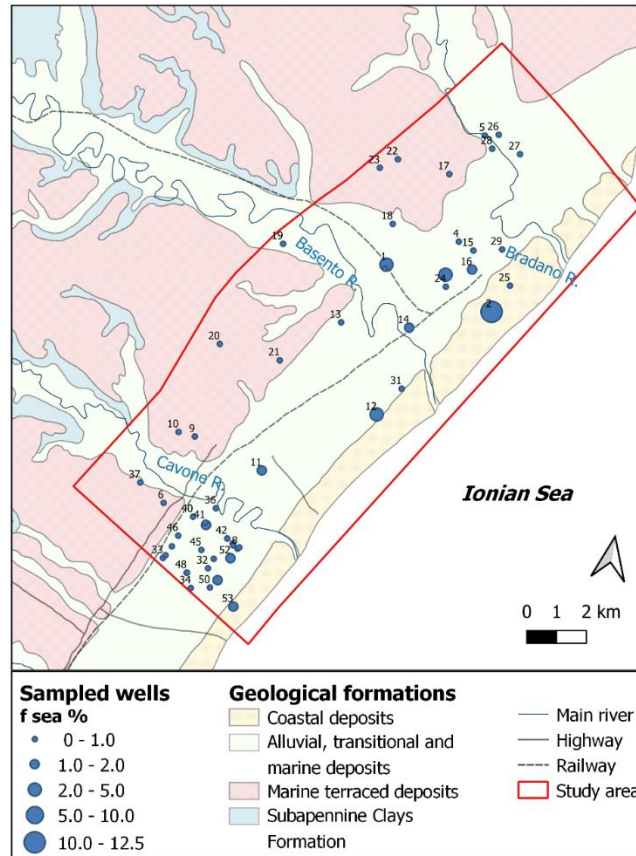
Fig. 11 *Map of the sampled wells (from Muzzillo et al., 2021a).*

Each sampled well was purged using a flow cell and a multi-parametric probe with EC, T, and pH sensors, withdrawing 3 water-well volumes in low flow conditions. After that, when steady parameter values were observed, the sampling was performed.

The water samples were filtered using a 0.45 μm membrane filter and then collected in double-capped 500 mL polyethylene bottles. The samples for cation analysis were acidified by the addition of HNO_3 to pH < 2, whereas the samples for anion analysis were unacidified.

The main constituents of waters were determined by ion chromatography (IC) methods and, for separation of both cations and anions, with conductometric detection. Total alkalinity values of the samples were determined by titration with 0.1 N HCl, to a pH end-point of 4.5.

The charge balance error was used to check the quality of the analysis results, using 5% as the threshold value. The chemical groundwater classification was supported by diagrams; in the case of seawater mixing, the Langelier-Ludwig diagram is often effective (Custodio & Llamas, 1996).

The fraction of seawater (f_{sea}) in the samples was calculated from the concentration of the chloride ion (mmol/L), which is considered conservative in the mixing process (Appelo & Postma, 2005), using the relationship:

$$f_{sea} = \frac{m_{Cl^-_{sample}} - m_{Cl^-_{fresh}}}{m_{Cl^-_{sea}} - m_{Cl^-_{fresh}}} \tag{7}$$

The expected concentration of the different ions ($m_{i,mix}$), resulting from mixing between fresh water and salt water, was calculated by:

$$m_{i,mix} = f_{sea} \cdot m_{i,sea} + (1 - f_{sea}) \cdot m_{i,fresh} \tag{8}$$

where $m_{i,sea}$ and $m_{i,fresh}$ are the concentration in seawater and freshwater of the species i, respectively. The enrichment or depletion ($m_{i,react}$) of the species i was then obtained by:

$$m_{i,react} = m_{i,sample} - m_{i,mix} \tag{9}$$

where $m_{i,react}$ may take both positive and negative value, or be equal to zero (only mixing). Positive or negative values of $m_{i,react}$ indicate the presence of geochemical processes that modify the water hydrochemistry in addition to simple mixing.

As endpoints were used the seawater samples and pure fresh groundwater samples, corresponding to wells, which showed the lowest chloride concentration.

6.5 Groundwater vulnerability

6.5.1 SINTACS and SINTACS-LU methods

Firstly, the SINTACS method, belonging to the GIS-based overlay and index approaches (Civita & De Maio, 1997), was selected and applied in the Metaponto coastal plain to assess the intrinsic vulnerability to pollution. The SINTACS method, widely utilized for determining groundwater vulnerability, represents the evolution of the DRASTIC method (Aller et al., 1987) suitable to the hydrogeological Mediterranean environments (Hamza et al., 2007; Noori et al., 2019). In this method, the hydrogeological scenarios corresponding to the weights attributable to each parameter are more numerous and flexible than in DRASTIC, which provides strings of weights for only two hydrogeological contexts. The index-based SINTACS method is easy to apply, low-cost, requires limited datasets and low computational time, and provides adequate reliability and accuracy of the results (Jahromi et al., 2021).

The acronym "SINTACS" derives from the initials of the Italian words that express the input conditioning factors used by the method to assess intrinsic vulnerability. These parameters are: (i) S (Soggiacenza) water table depth; (ii) I (Infiltrazione efficace) effective infiltration; (iii) N (Non-saturo) unsaturated zone; (iv) T (Tipologia della copertura) soil media; (v) A (Acquifero) aquifer characteristics; (vi) C (Conducibilità idraulica) hydraulic conductivity; (vii) S (Superficie topografica) topographic slope. Based on the structure of the SINTACS method (Civita & De Maio, 1997; Civita & De Maio, 2004; Civita, 2010), each hydrogeological parameter is divided into different classes, to which it is assigned ratings and relative weights.

The SINTACS index is provided using the following Equation (10):

$$SINTACS\ index = S_r S_w + I_r I_w + N_r N_w + T_r T_w + A_r A_w + C_r C_w + S_r S_w \tag{10}$$

In addition to those mentioned above, one more parameter was added to improve the accuracy in representing groundwater vulnerability: land use (LU) was included to consider the anthropogenic influence in the study area. Land cover plays a key role in relation to the pressure exerted on groundwater quality by industrial, urban, and vegetation land uses, posing a serious threat to groundwater resources (Wagenet & Hutson, 1986; Leonard et al., 1987). This parameter was ranked

depending on land use and weighted with a 5 value (**Tab. 4**). The modified SINTACS index was computed using the following Equation (11):

$$SINTACS - LU\ index = S_r S_w + I_r I_w + N_r N_w + T_r T_w + A_r A_w + C_r C_w + S_r S_w + LU_r LU_w \qquad (11)$$

where for both equations, S, I, N, T, A, C, S and LU are the above-reported parameters; r is the rating value; w is the weight assigned to each parameter.

SINTACS parameters	Range	Rating	Weight
S – water table depth (m)	5.0–10	6	5
	3.0–5.0	7	
	1.5–2.0	9	
	1.5	10	
I – effective infiltration (mm/year)	0–50	1	5
	50–65	2	
	>65	3	
N – unsaturated zone	Clay deposits	2	4
	Fine alluvial deposits	4	
	Medium-fine alluvial deposits	5	
	Coarse alluvial deposits	6	
	Sandy coastal deposits	7	
T – soil media	Clay loam	3	5
	Silty-clay loam	4	
	Loam	5	
	Sandy loam	6	
	Sandy	8	
	Coarse sand	9	
A – aquifer media	Clay	3	2
	Medium-fine alluvial complex	6	
	Coarse alluvial complex	7	
	Sandy complex	8	
C – hydraulic conductivity (m/s)	$6.53 \cdot 10^{-5}$	5	2
	$2.28 \cdot 10^{-4}$	7	
	$5.69 \cdot 10^{-3}$	9	
S – topographic slope (%)	>25	1	3
	20–25	2	
	17–20	3	
	14–17	4	
	11–14	5	
	8–11	6	
	6–8	7	
	4–6	8	
	2–4	9	
	<2	10	
LU – land use	Pastures, Forests	3	5
	Beaches, dunes, sands	4	
	Olive groves, Vineyards	5	
	Mining areas	6	
	Annual crops, Fruit trees, Urban areas	7	
	Industrial areas, Wetlands	8	
	Intensive agriculture	9	

Tab. 4 Ranges, ratings and weights of SINTACS and SINTACS-LU parameters (from Canora et al., 2022).

The data implementation and processing were performed in a GIS environment. The advantages of GIS are identifiable in the ability to store, organize and analyse uniquely georeferenced spatial geographic data and the efficiency in combining different layers of information. Eight layers (one for each parameter) were prepared and processed to produce the groundwater vulnerability maps and reclassify the indexes (**Fig. 12**).
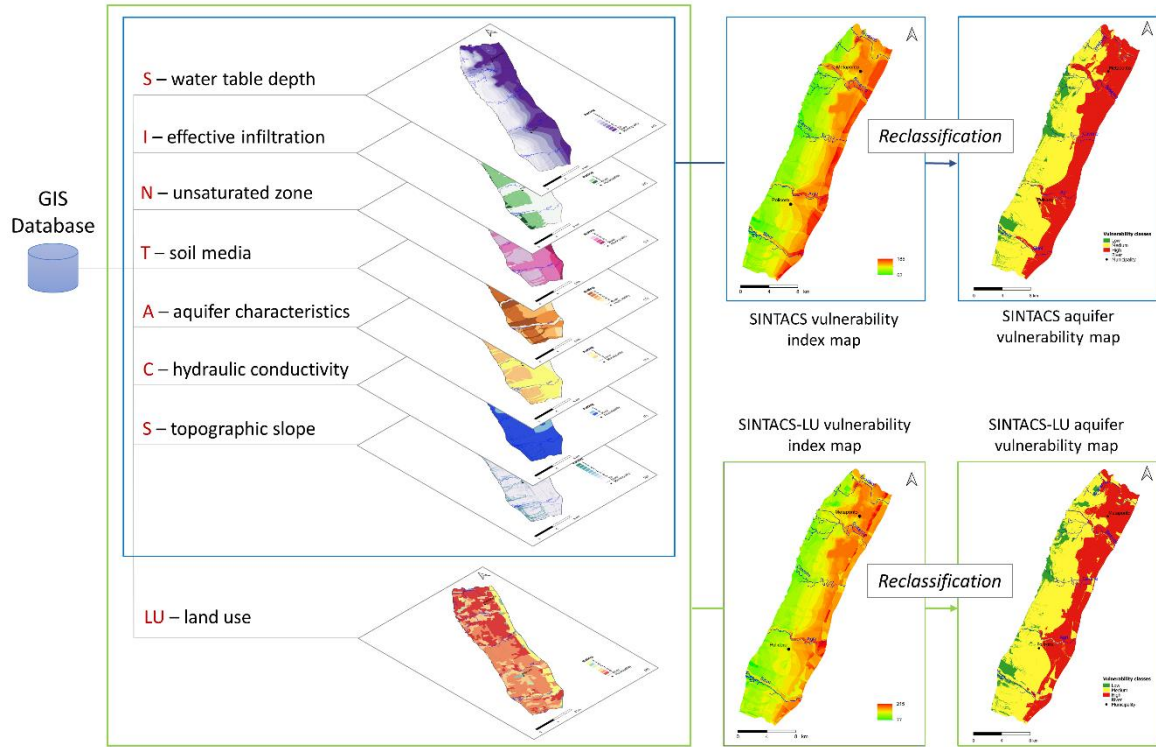
Fig. 12 *Methodology flow chart for SINTACS and SINTACS-LU methods (from Canora et al., 2022).*

Each parameter is evaluated depending upon its relative importance to the potential intrinsic vulnerability and indexed by attributing rating ranges from 1 to 10, according to **Tab. 4**.

Then each parameter is given a multiplier weight ranging from 1 to 5 (**Tab. 4**). The SINTACS method proposes six strings of weights related to the different hydrogeological and anthropogenic conditions to which the Land Use (LU) parameter was added (**Tab. 5**). The choice of the string of weights "Nitrates" was made considering the mainly agricultural vocation of the study area (Civita, 2010). The most relevant parameters are assigned a weight of 5, while the least important are assigned a weight of 2 (**Tab. 4**). Finally, vulnerability indices are calculated from Equations (10) and (11). The higher the resulting SINTACS index, the greater the inherent vulnerability to pollution.

Parameter	Normal	Severe	Seepage	Karst	Fissured	Nitrates
S	5	5	4	2	3	5
I	4	5	4	5	3	5
N	5	4	4	1	3	4
T	3	5	2	3	4	5
A	3	3	5	5	4	2
C	3	2	5	5	5	2
S	3	2	2	5	4	3
LU	5	5	5	5	5	5

Tab. 5 *Strings of multiplier weights given for SINTACS (from Canora et al., 2022).*

Data collection and surveys were carried out in the entire Metaponto plain. Processing and preparation of the SINTACS thematic layers were performed with QGIS software and rasterized with 5-m grids size, using the Kriging approach (Webster & Oliver, 2007) (**Fig. 12**). The Kriging technique provides an efficient method for interpolating a limited number of observations such as wells, rainfall, and temperature data for hydrogeological water balance and hydraulic conductivity determined in punctual sites, and for preserving the theoretical spatial correlation (De Marsily, 1984). The elaborated data were retrieved as follows.

The water table depth (S) is the distance between the ground surface and the water table and indicates the depth a contaminant must pass through to reach groundwater (Eftekhari & Akbari, 2020). It affects the contaminant in biological and chemical reactions and the time required to reach groundwater (Jesudhas et al., 2021). A low depth to groundwater leads to a higher vulnerability rating. This parameter originated from 42 selected monitored wells' water level measurements in the study area (**Fig. 1**). The layer was elaborated based on their localization, and the raster map of the water table spatial distribution was obtained through the Kriging interpolation technique.

The effective infiltration (I) is the amount of infiltration that penetrates from the ground surface and reaches the aquifer, and can transport contaminants to the water table through the unsaturated zone. If the effective infiltration increases, the potential contamination of groundwater also rises. The effective infiltration in the study area was evaluated by the estimation of the hydrogeological budget components applying the inverse hydrogeological water balance approach (Canora et al., 2018; Canora & Sdao, 2020). The effective infiltration results directly related to groundwater contamination. The hydrogeological water balance of the study area, due to the low hydraulic conductivity of the outcropping soils (Muzzillo et al., 2021a) and the unfavourable climatic conditions, shows low values of the effective infiltration rate.

Unsaturated zone (N) characteristics and thicknesses influence groundwater intrinsic vulnerability. The vadose zone between the bottom of the soil horizon and the water table controls the dilution and the contaminant rate that reach the saturated zone. The ratings assigned to the unsaturated zone classes are given in **Tab. 4**. This parameter was elaborated considering the lithological characteristics of geological formations and available stratigraphic data from wells.

Soil media (T) affects the transport mechanisms of the contaminant from the soil surface to the water table. Aquifer potential vulnerability depends upon soil characteristics such as soil organic materials percentage, texture, and permeability (Eftekhari & Akbari, 2020). Soil media plays a key role in assessing the vulnerability index of groundwater as it restricts the vertical flow of contamination into the subsurface. In addition, it has a significant impact on the amount of recharge that flows through the soil. Soil data were obtained from the regional pedological map (Regione Basilicata, 2006).

The aquifer media (A) parameter refers to the characteristics of the saturated zone, such as the porosity rate, particle types, and size (Eftekhari & Akbari, 2020). The relative layer was prepared using geological data, lithological maps, and stratigraphic borehole data available for the study area. The ratings assigned to the aquifer media parameter are reported in **Tab. 4**.

Hydraulic conductivity (C) measures the capability of the aquifer to transmit water and controls the rate at which the groundwater will move when subjected to a given hydraulic gradient. This parameter controls the transport and distribution of contaminants from the injection point inside the saturated zone (Eftekhari & Akbari, 2020). High permeability allows more infiltration rates and higher contaminants concentrations to reach the saturated zone. The high permeability of the aquifer system provides a high vulnerability index. The hydraulic conductivity values were obtained from many

pumping tests carried out in the study area in the last twenty years (Polemio et al., 2003). These values were used to elaborate the hydraulic conductivity map.

Topography (S) indicates the slope of the topographic surface and influences the vulnerability assessment in relation to the fact that water and pollutant can run off or stay on the surface long enough to infiltrate. For low topographic slope, the infiltration rate is higher, and, as a result, contaminants are more likely to infiltrate into the aquifer. With higher slopes, the infiltration capacity decreases, and the surface is less vulnerable to groundwater contamination. Thus, as the slope decreases, the vulnerability of the aquifer increases. The slope map was derived from the digital elevation model data downloaded from the Regional Spatial Data Infrastructure (RSDI) with a spatial resolution of 5 m and expressed as a percentage of the steepness.

Land use (LU) impact on vulnerability was considered by including the land use parameter in the SINTACS approach. The land use data were derived from Corine Land Cover 2018. In the study area, the groundwater quality is subject to degradation due to the anthropic impact of the urban, agricultural and industrial pressures. In particular, the Metaponto coastal plain aquifer system is affected by intensive agricultural activities and other pollution sources.

6.5.2 GALDIT method

As part of the relevant issue of SWI in the Metaponto coastal aquifer, the GALDIT method was applied (Chachadi & Lobo Ferreira, 2001; Chachadi & Lobo Ferreira, 2005; Lobo Ferreira et al., 2005), aimed at assessing the intrinsic vulnerability of groundwater. It considers the geological and hydrogeological conditions of a specific site regardless of the pollutant characteristics (Ducci & Sellerino, 2013; Medici et al., 2021). This approach involves, before the actual application, the creation of a geodatabase and the processing of the collected data in a Geographic Information System (GIS).

The development of GIS has made it possible to store, process, represent, and analyse a huge quantity of georeferenced data over large spatial scales (Jha et al., 2007). In this study, QGIS software (version 3.16.4) made it easier to process and overlay the data required by the GALDIT method. The developed approach is low-cost, needs low computational time, and provides reliable outcomes.

GALDIT is an overlay-index method based on six hydrogeological, topographic, and geomorphological parameters that influence the SWI phenomenon: groundwater occurrence (G), aquifer hydraulic conductivity (A), the height of groundwater level above the sea (L), distance from the shore (D), the impact of the existing status of SWI (I), and aquifer thickness (T) (**Fig. 13**). These conditioning factors of the aquifer give a time independent evaluation of its vulnerability to SWI. The relationship used for the calculation of the GALDIT index is expressed as follows:

$$GALDIT\ index\ =\ \frac{\sum_{i=1}^{6} R_i W_i}{\sum_{i=1}^{6} W_i} \tag{12}$$

where R_i is the rating and W_i is the relative weight assigned to each parameter, respectively. The range, rating, and weight of the parameters depend on the local aquifer characteristics.

The dataset was implemented in QGIS with information collected from the Regional Spatial Database and monitoring hydrogeological data of 42 wells. The study area was discretized with a 5 m resolution grid. In each cell, each factor was assigned a score based on the proposed classification and the influence on the vulnerability, ranging from 2.5 (lowest vulnerability) to 10 (highest vulnerability). To produce the final vulnerability index, the chosen scores were multiplied by the weights string. Following the procedure, the weight 1 is assigned to Groundwater occurrence and Impact of the existing status of SWI parameters, to Aquifer thickness the defined weight is equal to 2, the weight 3

is attributed to Aquifer hydraulic conductivity parameter, whereas to the last two parameters Height of the groundwater level above the sea and Distance from the shore is assigned the highest weight, equal to 4, that represents the heaviest impact on vulnerability (**Tab. 6**). The six products thus obtained are added together and then the result is divided by the sum of the weights, equal to 15. The GALDIT index has a minimum value of 2.5 and a maximum value of 10.

The increase in the GALDIT index values indicates that the aquifer vulnerability to SWI also increases. The GALDIT index is classified into three classes: low (<5), moderate (from 5 to 7.5), and high (>7.5).
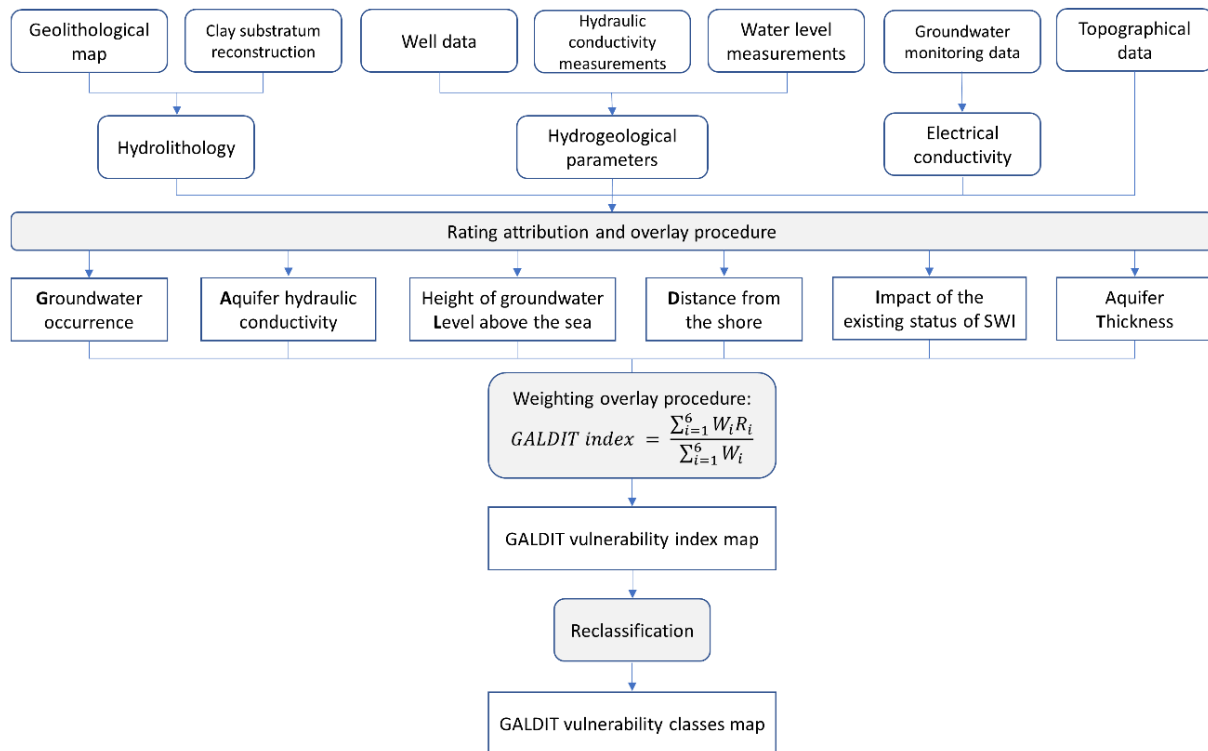
Fig. 13 *Flow chart of the GALDIT method (from Muzzillo et al., 2022).*

GALDIT parameters	Range	Rating	Weight
G – Groundwater occurrence	Bounded	2.5	1
	Leaky confined	5	
	Unconfined	7.5	
	Confined	10	
A – Aquifer hydraulic conductivity (m/day)	<5	2.5	3
	5-10	5	
	10-40	7.5	
	>40	10	
L – Height of the groundwater level above the sea (m)	>2	2.5	4
	1.5-2	5	
	1-1.5	7.5	
	<1	10	
D – Distance from the shore (m)	>1000	2.5	4
	750-1000	5	
	500-750	7.5	
	<500	10	
I – Impact of the existing status of seawater intrusion (µS/cm)	<1000	2.5	1
	1000-2000	5	
	2000-3000	7.5	
	>3000	10	
T – Aquifer thickness (m)	<5	2.5	2
	5-7.5	5	
	7.5-10	7.5	
	>10	10	

Tab. 6 Ranges, ratings, and weights of GALDIT parameters (from Muzzillo et al., 2022).

6.5.3 Sensitivity analysis

The selection of ratings given to the parameters of SINTACS, SINTACS-LU and GALDIT methods is inevitably related to subjectivity. Since this choice significantly impacts the final vulnerability maps, the sensitivity analysis was performed to understand the influence of the input parameters on the output, assess the consistency of the results, individuate which variables are more relevant and hence require more thorough information and accuracy (Napolitano & Fabbri, 1996). Map removal and single variable analysis were the two types of sensitivity analysis performed with a quick and low-cost GIS-based approach.

The goal of the map removal analysis is to understand if all the parameters are necessary for the computation of the vulnerability index, or if one or more of the parameters may be deleted without having a significant impact on the outcome. The analysis was performed for both SINTACS and SINTACS-LU methods by deleting one parameter at a time and assessing the effect on the output by calculating the following sensitivity measurement in each cell in which the study area was discretized (Lodwick et al., 1990; Babiker et al., 2005; Majandang & Sarapirome, 2013):

$$S = \frac{\left| \frac{V}{n} - \frac{V'}{n'} \right|}{V} \cdot 100 \tag{13}$$

where S is the sensitivity measurement expressed in terms of a variation index, V is the unperturbed vulnerability index obtained using all the parameters, V' is the perturbed vulnerability index computed using a lower number of input layers, n and n' are the number of parameters considered to calculate

V and V', respectively. The average variation index of all cells for each parameter can be used to identify which parameter could have less influence on the outcome if omitted (Babiker et al., 2005). Any parameter with a lower overall average index value has less influence. A cell with a high or low index for a removed parameter will consequently show a greater or smaller influence on the outcome.

The single-parameter sensitivity analysis is a cell-based process, too (Napolitano & Fabbri, 1996). The theoretical weight assigned by the SINTACS, SINTACS-LU and GALDIT methods to each parameter was compared to the "effective" or "actual" weight W, which was calculated as:

$$W = \frac{P_r P_w}{V} \cdot 100 \tag{14}$$

where P_r and P_w are the rating and weight of the P parameter, respectively, and V is the vulnerability index as computed in Equations (10), (11) or (12).

The objective of this analysis was to determine which parameter had the highest effective weight and therefore provided higher values of the vulnerability indexes when its spatial variation throughout the entire study area was considered (Napolitano & Fabbri, 1996; Majandang & Sarapirome, 2013).

6.6 Numerical modeling

Numerical hydrogeological models are increasingly being used to support water resources management. Among the various numerical models, MODFLOW (McDonald & Harbaugh, 1984), since its development in the early 1980s, is considered a standard code for aquifers' simulation. The United States Geological Survey (USGS) developed MODFLOW, a finite-difference groundwater flow modeling software, for producing a numerical representation of hydrogeologic environments. It is based on the finite-difference method to divide the groundwater flow model domain into rows, columns, and layers, defining a unique set of grid cells to represent the distribution of hydrogeologic properties and hydrologic boundaries within the model domain. Properties and boundaries are assigned to these model cells when creating a groundwater model, and MODFLOW uses the cell dimensions, property values, and boundary values to build a set of finite-difference equations that it solves to compute the hydraulic head at the centre of each model cell.

MODFLOW requires a set of text files to run a groundwater flow simulation, which specifies all the model domain's features, including cell-by-cell dimensions, properties, and boundaries. MODFLOW reads these text files and uses them to determine the hydraulic head in every active finite-difference cell. Because these input files are text files, using MODFLOW directly to generate a groundwater model can be complicated and time-consuming. This has resulted in the creation of Graphical User Interfaces (GUIs), such as Visual MODFLOW, that enable the creation of groundwater models graphically on-screen, using easily imported DXF, TXT, and SHP files. In Visual MODFLOW, cell size, property values, and boundary conditions are graphically assigned in a row, column, or layer view, and this information is then translated into the set of MODFLOW input text files that are run to generate a groundwater flow solution.

The benefit of utilizing MODFLOW as a hydrogeologic modeling tool is that once a groundwater model has been constructed and calibrated, it can be used to understand how the hydrogeologic system may respond to future design modifications. For example, groundwater design (such as pumping and injection wells, infiltration galleries, grout cut-off walls, seepage drains, etc.) can be added to the model to simulate their influence on the hydraulic heads and flow before they are built in the field. In Visual MODFLOW, the findings are shown as 2D and 3D images, making it easier to visualize the influence of these designs on the hydrogeologic system and, as a result, modeling becomes an indispensable tool in the design process.

In this research activity, groundwater flow was simulated using Visual MODFLOW (VMOD) Flex 7.0, a software package that provides the tools for building three-dimensional groundwater conceptual and numerical models using raw GIS data objects.

VMOD Flex supports SEAWAT (Guo & Langevin, 2002; United States Geological Survey, 2012), a three-dimensional variable density flow and multi-species solute transport model developed by the USGS, based on a combination of MODFLOW and MT3D-MS.

Model calibration, under steady-state and transient conditions, was performed in Visual MODFLOW Flex through the interface to PEST, the parameter estimation and predictive analysis program.

The portion of the aquifer selected for modeling was discretised into a finite difference grid with square cells of 200 m resolution, consisting of 60 rows and 43 columns. The cell size was chosen considering the extent of the model domain, the spatial variability, and data availability of hydrogeological parameters, and at the same time to ensure the stability and convergence of the numerical solution.

Information on heads, hydraulic conductivity, hydrochemical data, and electrical conductivity data were provided by CNR's Research Institute IRPI and taken from the literature. Spatial data (such as DTM and hydrography) were downloaded from the Regional Spatial Data Infrastructure (RSDI).

The active domain covered an area of about 41 km^2 with 1018 active cells. The 5 m resolution DTM (maximum and mean elevation equal to 11.71 m and 3.24 m, respectively) was used to define the surface morphology of the model.

7. The inverse hydrogeological water balance

The recharge of the studied aquifer was estimated by applying the GIS-based distributed inverse hydrogeological water balance method (Celico, 1988; Lerner et al., 1990; Civita & De Maio, 2001; Canora et al., 2018), which provided the distribution of all components of the hydrogeological water balance in the above-described hydrogeological basin (**Fig. 14**, **Fig. 15** and **Fig. 15**). These values are averaged over the reference periods of observations 1925-1979 and 2000-2015 (**Tab. 7**).

As described previously, the spatial distribution of corrected temperature and precipitation in the study area was estimated using the linear correlation of thermal and rainfall data with altitude q by defining linear regression functions $T_c = f(q)$ and $P = f(q)$.

For the period 1925-1979 the obtained equations are:

$$T_c(°C) = -0.0025 \cdot q(m\,a.s.l.) + 14.526 \qquad r^2 = 0.3523 \quad (15)$$

$$P(mm) = 0.5149 \cdot q(m\,a.s.l.) + 555.62 \qquad r^2 = 0.7533 \quad (16)$$

For the period 2000-2015 the obtained equations are:

$$T_c(°C) = -0.0034 \cdot q(m\,a.s.l.) + 14.727 \qquad r^2 = 0.8582 \quad (17)$$

$$P(mm) = 0.5149 \cdot q(m\,a.s.l.) + 507.22 \qquad r^2 = 0.8711 \quad (18)$$
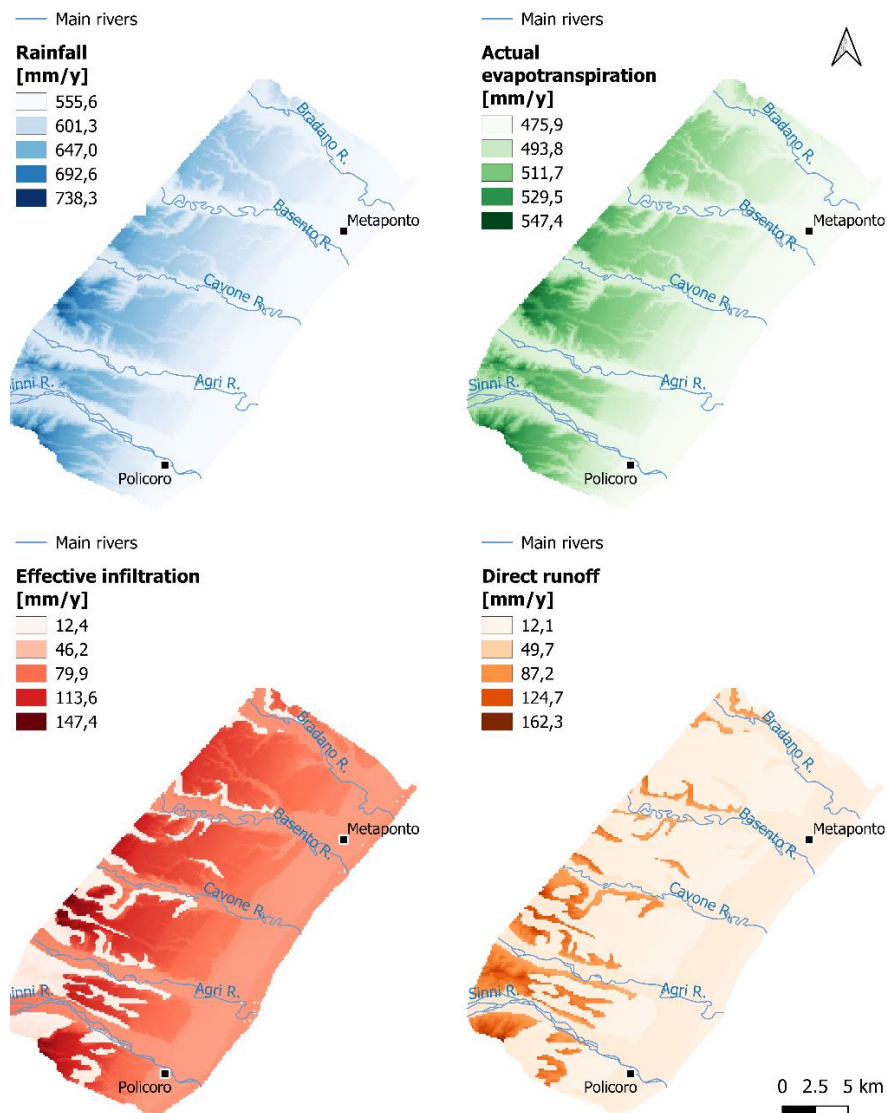
Fig. 14 *Spatial distribution of the annual mean amount of the inverse hydrogeological water balance variables from 1925 to 1979.*
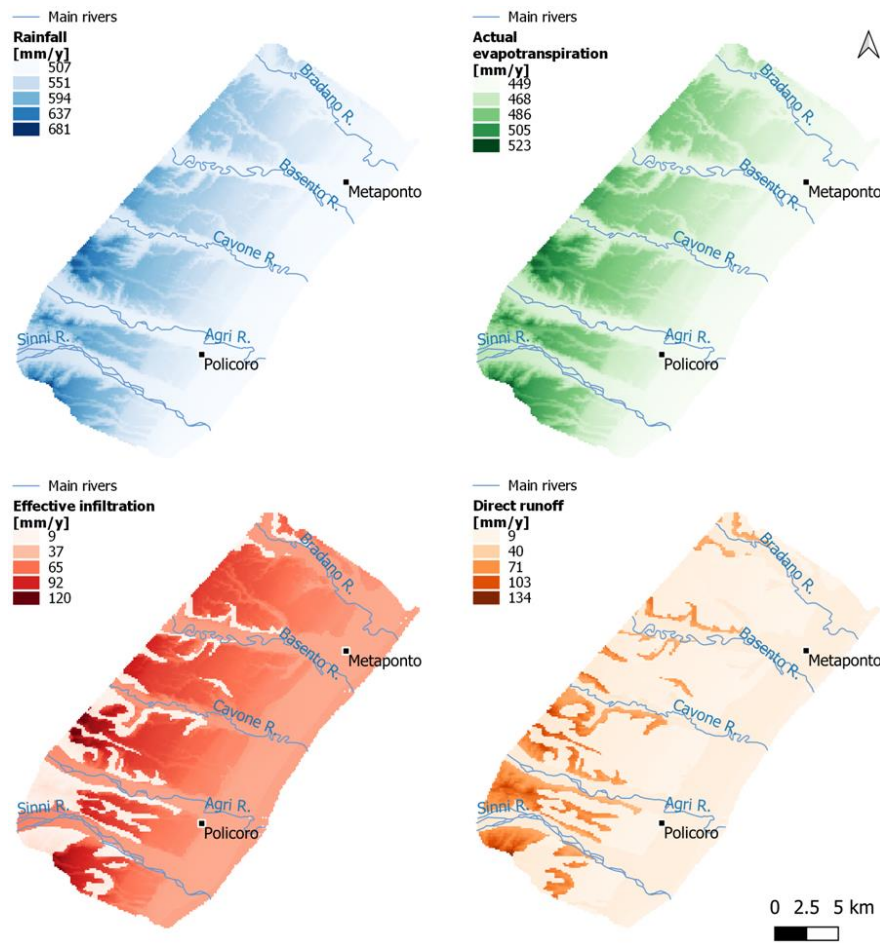
Fig. 15 *Spatial distribution of the annual mean amount of the inverse hydrogeological water balance variables from 2000 to 2015 (from Muzzillo et al., 2021a).*

Variable	mm/y (1925-1979)	mm/y (2000-2015)
Rainfall (P)	588	538
Actual evapotranspiration (ET_r)	491	465
Effective infiltration (I)	69	52
Direct runoff (R)	29	21

Tab. 7 *Annual mean amount of the inverse hydrogeological water balance variables for the periods 1925-1979 and 2000-2015.*

In the hydrogeological basin, with an extension of about 655 km^2, the mean annual rainfall changes from 588 mm (1925-1979) to 538 mm (2000-2015). The results of the inverse hydrogeological water balance show that the effective evapotranspiration, equal to 491 mm (1925-1979) and 465 mm (2000-2015), provides an effective infiltration rate of 69 mm/year and 52 mm/year, equivalent to about 1433 l/s and 1080 l/s for the periods 1925-1979 and 2000-2015, respectively. The mean annual value of direct runoff changes from 29 mm/year (1925-1979) to 21 mm/year (2000-2015).

The groundwater recharge is about 10%-12% of the total amount of rainfall, a low rate due to the unfavourable climatic conditions and the low hydraulic conductivity of the topsoil (Polemio et al., 2003; Muzzillo et al., 2021b). The spatial distribution of the mean annual effective infiltration shows changing behaviour throughout the entire basin due to the different infiltration capacities of the geological formations. In particular, the lowest infiltration values are found in the Sub-Apennine Clays Formation, where direct recharge is essentially interdicted by a silty and clayey surficial layer (Polemio et al., 2003). The main water supply of the aquifer comes from the points at higher altitudes of the marine terraced deposits, where the highest rainfall and infiltration values are found. Except

for areas where the Sub-Apennine Clays Formation outcrops, direct infiltration tends to decrease from the inland toward the coastline, with values below 50 mm/y. The direct natural recharge of the shallow coastal aquifer is extremely low, both because of low actual rainfall and especially because of the low hydraulic conductivity of the topsoil. The recharge is mainly provided by discharge from the upward aquifers of marine terraced deposits and the river leakage.

The amount of aquifer active recharge plays an important role in achieving adequate management of groundwater resources, which may be affected by future climate trends.

8. Hydrochemical characterization of groundwater

The descriptive statistics for groundwater samples reported in **Fig. 9** are provided in **Tab. 8**. The charge balance errors for the analyses were <5%. The chemical groundwater classification can be obtained from the Langelier-Ludwig diagram (Custodio & Llamas, 1996).

Value	EC	T	pH	Na$^+$	K$^+$	Cl$^-$	HCO$_3^-$	Ca^{2+}	Mg^{2+}
	µS/cm at 25 °C	°C	-				meq/L		
Minimum	649	16.00	6.70	1.49	0.07	0.80	2.13	0.59	0.75
Mean	1732	18.14	7.36	7.82	0.48	5.97	6.68	3.63	4.59
Maximum	4630	21.00	7.98	40.46	1.84	38.47	14.19	10.39	12.62
SD	870	1.26	0.42	7.31	0.38	6.20	3.29	1.93	2.74

*Tab. 8 Descriptive statistics for the physical-chemical parameters of groundwater samples reported in **Fig. 9** (from Muzzillo et al., 2021b).*

The chemical facies of groundwater are shown using the Langelier-Ludwig diagram (**Fig. 16**). The first group of samples (right-bottom) shows a Ca-Mg-HCO$_3^-$ composition, the second group shows a Ca-Cl-SO$_4^{2-}$ composition, and the third group shows a Na-Cl-SO$_4^{2-}$ composition. Sample 2 was the only one that showed a Na-HCO$_3^-$ composition.

The theoretical pure mixing line was plotted and compared to the whole dataset (**Fig. 16**). It shows that the hydrochemical variability can be mainly explained in terms of fresh-saline water mixing or SWI. The rest of the variability seems to be due to other geochemical phenomena, indicating the role of the different aquifer types to the recharge, the relationships with soil cover, the deep drainage system of the reclamation works, and the surface water system (Polemio et al., 2003; Polemio et al., 2005). The hydrochemical results showed that SWI affects groundwater quality in the Metaponto coastal plain, with significant effects closer to the coast.
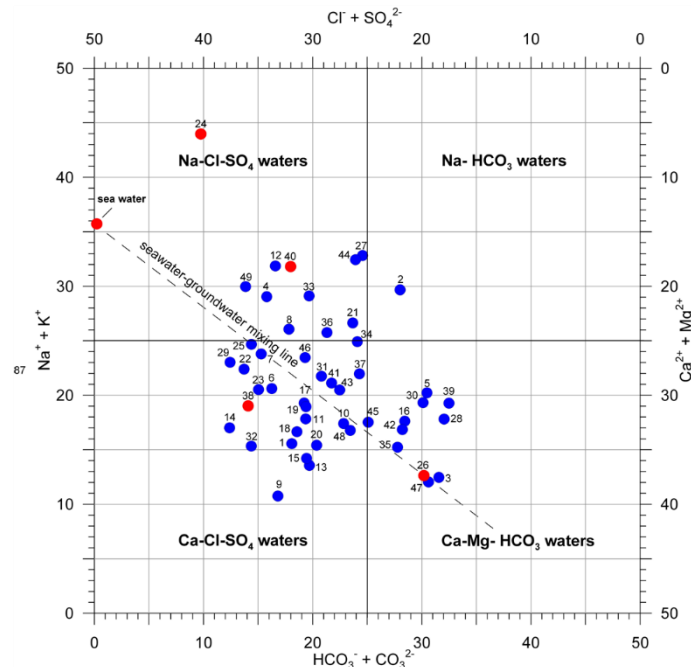
Fig. 16 Langelier-Ludwig diagram of the sampled waters (red dots mark cited wells) (from Muzzillo et al., 2021b).

The mixing ratio was calculated and is plotted in **Fig. 9**. The minimum and the mean value of the fraction of seawater (f$_{sea}$%) were 0.04 and 0.80, respectively. The highest values were observed near the coast, specifically in wells 24 (f$_{sea}$% = 6.2), 38, and 40. The f$_{sea}$% trend increased moving from inland coastward, confirming the role of SWI. Focusing on the ERT area, the f$_{sea}$% results are shown

in **Tab. 9**. The fresh-saline groundwater mixing ratio was between 0.3% and 0.8% near the three ERT profiles.

These results are in good agreement with other similar international experiences. In the case of the main USA coastal aquifers, the mean $f_{sea}\%$ values observed close to the coast generally ranged from 8 to 10 (Lotfata & Ambinakudige, 2020). In the case of the coastal springs of Taranto, located in the Ionian Sea not far from Metaponto, the $f_{sea}\%$ range was from 5 to 7 (Zuffianò, et al., 2015).

Sample	$f_{sea}\%$	Na^+_{mix}	Na^+_{react}	Ca^{2+}_{mix}	Ca^{2+}_{react}	Mg^{2+}_{mix}	Mg^{2+}_{react}	$HCO_3^-_{mix}$	$HCO_3^-_{react}$
13	0.26	2.9	-0.7	1.3	-0.1	0.9	0.3	3.7	-0.5
14	0.83	5.8	-1.9	1.4	-0.4	1.3	0.8	3.8	-0.8
35	0.62	4.7	10.9	1.4	1.1	1.2	0.7	3.7	4.4
37	0.54	4.3	13.3	1.3	0.5	1.1	1.8	3.7	6.1

Tab. 9 Fraction of seawater, mixing, and reacting (from Muzzillo et al., 2021b).

These values showed that the fresh-saline mixing was not negligible so far from the coast, confirming the negative role of the paleovalley on the groundwater salinization risk.

The whole study area is subject to SWI, not only very close to the coastline, as shown by previous researches based only on geophysical tools (Satriani et al., 2011; Satriani et al., 2012; Imbrenda et al., 2018). SWI can be considered the main source of salinization risk in the Metaponto coastal plain.

However, as for the investigated area between the Cavone and Bradano Rivers (Muzzillo et al., 2021a), **Tab. 10** provides a statistical outline, listing the minimum, the maximum, the mean, and the standard deviation values of each chemical parameter for the samples reported in **Fig. 11**.

Value	EC	pH	Na^+	K^+	Ca^{2+}	Mg^{2+}	F^-	Cl^-	NO_3^-	SO_4^{2-}	HCO_3^-
	μS/cm at 25 °C	-					meq/L				
Minimum	337.00	6.69	0.63	0.07	0.49	0.53	0.01	0.45	0.02	0.07	1.07
Mean	1522.90	7.50	7.59	0.47	3.66	3.84	0.04	6.03	0.31	3.29	6.25
Maximum	8697.34	9.64	73.95	2.17	8.78	12.62	0.12	76.16	1.84	20.05	14.19
SD	1245.17	0.68	10.60	0.48	2.33	2.58	0.03	10.46	0.38	3.95	2.92

Tab. 10 Descriptive statistics for the physical-chemical parameters of groundwater (from Muzzillo et al., 2021a).

The concentrations of the major ions estimated for each sample are plotted in the Piper diagram (**Fig. 17**), used to show the geochemical facies and water types. Three dominant groundwater types were distinguished: the HCO_3-Ca, SO_4-Cl-Na, and a mixed Ca-Mg-Cl water type. Most of the HCO_3-Ca (bicarbonate-alkaline earthy) type samples are representative of groundwater flowing in the Marine terraces and Alluvial deposits, whereas most of the SO_4-Cl-Na (sulfate-chlorinated-alkaline) type is characteristic of samples taken in the coastal plain deposits. The peculiarities of each aquifer domain are reflected in the type of water; significant dispersion is observed in **Fig. 17**, which means that other processes can be identified.
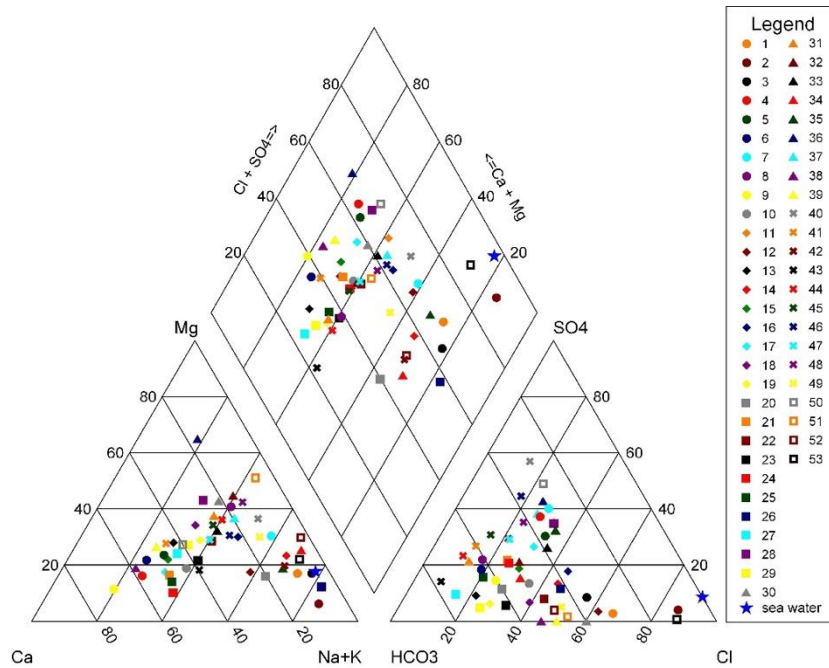
Fig. 17 *Piper diagram of sampled groundwater (Muzzillo et al., 2021a).*

In addition to the anthropogenic role in the worsening of groundwater quality along the path from the inland recharge areas to the outflow coastal area (Polemio & Limoni, 2006), the natural phenomenon of ion exchange processes occurring in coastal aquifers due to SWI or displacement of seawater by freshwater (freshening) was considered.

Ca^{2+} and HCO_3^- ions, resulting from calcite dissolution, are predominant in the composition of fresh groundwater in coastal areas, whereas Na^+ and Cl^- are the dominant ions in seawater. If groundwater samples from a coastal aquifer show a Ca^{2+} surplus compared to the conservative mixture, this could be due to the effects of SWI, whereas an excess of Na^+ could indicate aquifer freshening (Appelo & Postma, 2005).

As shown in **Tab. 11**, where only water samples with significant changes are listed, water samples 3, 14, 26, 31, 34, 35, and 52 show an enrichment of Na^+ and HCO_3^- together with a depletion of Ca^{2+} ions, which are indicative of aquifer. The remaining samples show enrichment of Ca^{2+} along with a depletion of Na^+ and K^+ ions, indicative of a progressive mixing with saline water potentially due to lateral and/or upconing effects of SWI.

According to the hydrochemical analysis of the groundwater samples, the ion exchange processes are dominant in this coastal aquifer, demonstrating the impacts of SWI and seawater displacement by freshwater (Muzzillo et al., 2021a). SWI affects groundwater quality, with higher effects closer to the coast (Muzzillo et al., 2021b).

The trend of the fraction of seawater increased moving from inland to the shore, indicating the significance of SWI. These data suggested that the fresh-saline mixing was not negligible so far from the coast, confirming the negative role of the paleo valley on the groundwater salinization risk. The whole study area is vulnerable to SWI, not just the portion closest to the coast (Muzzillo et al., 2021a).

Sample location	f_{sea} %	Na^+_{react}	K^+_{react}	Ca^{2+}_{react}	Mg^{2+}_{react}	$SO_4^{2-}_{react}$	$HCO_3^{2-}_{react}$
3	2.22	5.69	-0.13	-1.02	1.91	0.77	4.80
4	0.40	-1.19	-0.22	4.88	0.68	3.12	-0.26
5	0.74	-1.46	-0.26	5.39	2.28	3.66	1.63
6	0.29	-0.76	-0.25	4.27	1.41	1.34	3.38
9	0.33	-1.97	-0.14	5.17	-0.03	0.61	1.94
10	0.81	-0.80	-0.23	4.21	1.28	1.06	3.57
12	2.53	-2.38	1.28	3.70	1.80	-0.54	4.74
13	0.30	-1.17	0.34	2.35	1.80	0.14	3.26
14	1.21	2.43	0.25	-0.58	2.24	1.25	3.23
15	0.60	-1.12	-0.25	4.23	1.62	1.64	2.90
16	1.26	-1.13	0.40	1.43	3.41	2.07	2.47
17	0.79	-0.84	-0.25	6.43	1.49	3.59	3.29
18	0.50	-1.94	-0.21	0.61	1.68	-0.29	0.72
19	0.53	-0.29	-0.01	2.22	2.47	-0.06	4.84
21	0.49	-0.11	-0.27	4.45	0.88	2.08	3.18
22	0.97	-1.40	-0.20	2.07	2.49	0.15	3.06
23	0.71	-0.24	-0.13	3.21	1.64	-0.12	4.93
24	0.11	-0.68	-0.31	0.43	-0.58	0.12	-1.77
25	0.19	-0.30	-0.32	1.62	-0.07	0.41	0.85
26	0.92	1.09	-0.39	-1.87	-0.44	0.51	1.36
28	0.63	-0.71	-0.36	1.57	5.02	3.58	0.13
29	0.27	-1.40	-0.33	0.07	0.44	-0.42	1.71
31	0.07	0.66	-0.31	-0.14	2.07	0.59	0.05
34	0.38	3.16	-0.34	-1.81	1.36	0.49	0.47
35	0.52	1.81	-0.35	-0.98	0.49	2.51	-0.60
41	0.06	-0.91	-0.24	0.30	0.50	0.90	-0.32
47	0.34	-0.30	0.82	1.36	2.16	2.47	1.47
50	0.44	-1.13	0.66	3.02	2.27	6.04	-0.01
52	1.71	2.67	0.28	-1.87	4.25	-0.33	6.61

Tab. 11 *Fresh-saline mixing and effects of cation exchange (from Muzzillo et al., 2021a).*

9. Groundwater vulnerability

9.1 SINTACS and SINTACS-LU

The parameters conditioning the assessment of intrinsic aquifer vulnerability by SINTACS and SINTACS-LU methods are discussed below.

The depth of the water table (S) appears to be one of the parameters that most significantly impacts groundwater vulnerability. Commonly, shallow aquifers are more vulnerable than deep aquifers, where infiltrating contaminants require a longer interaction time with unsaturated media, and biogeochemical reactions can reduce their impact. The data on the groundwater level were acquired from 42 wells utilized for agricultural and domestic supply and monitoring aims (**Fig. 1**). These data were elaborated to determine water table depth (S). The observed data highlight that the water table is relatively shallow, and the water depth ranges from 1.5 to 8 m. Kriging method was used for interpolating the punctual data. The depth of the water rasterized layer was ranked by assigning four classes of ratings, listed in **Tab. 4**, and its spatial distribution is shown in **Fig. 18(a)**. It is evident that a shallow aquifer is subject to higher potential intrinsic vulnerability, whereas a deep aquifer is relatively less impacted by contamination. In the investigated area, the south eastern sector shows high intrinsic vulnerability due to the higher rating of this parameter.
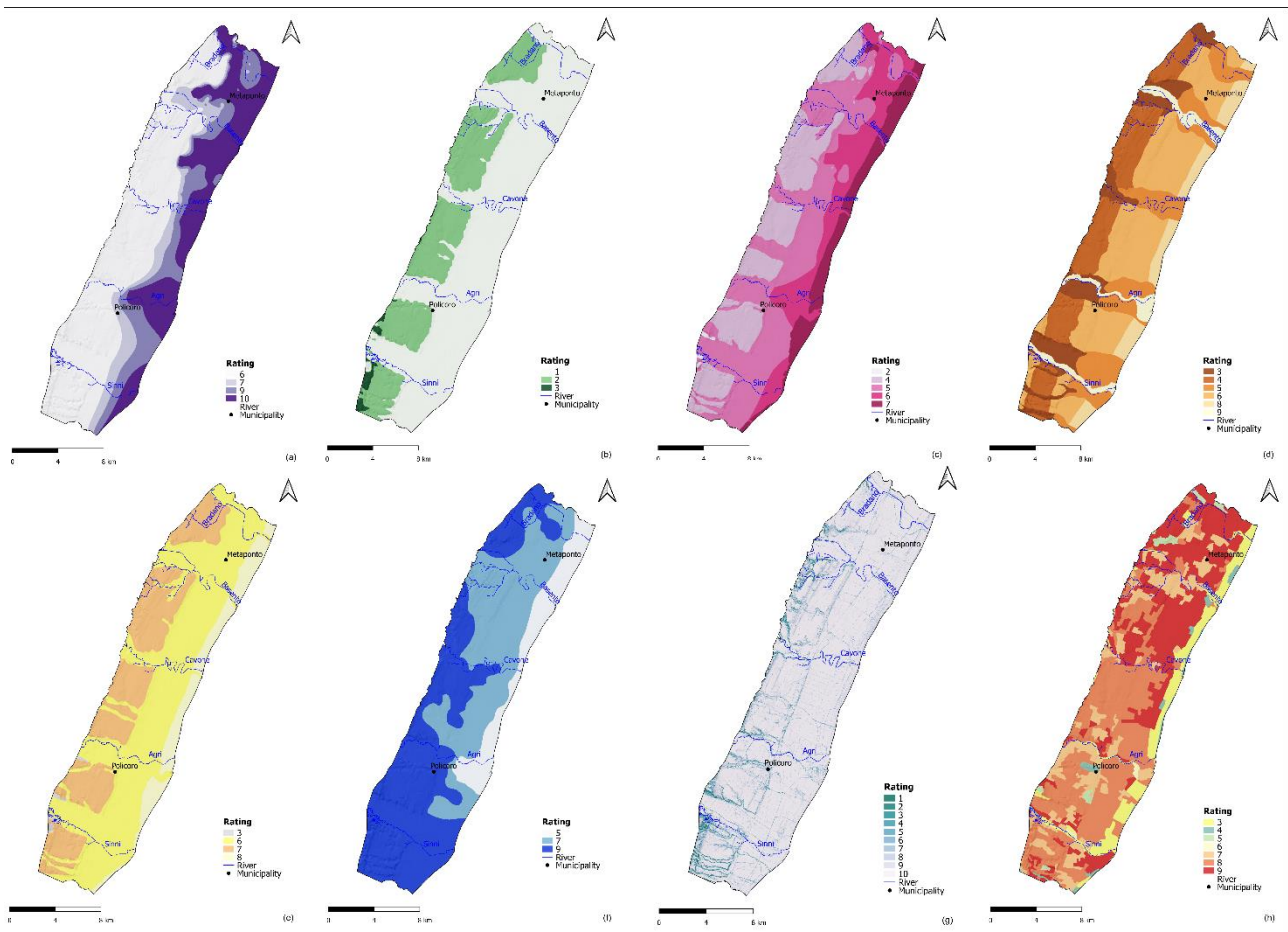
***Fig. 18** The thematic maps for SINTACS and SINTACS-LU methods: (a) water table depth; (b) effective infiltration; (c) unsaturated zone; (d) soil media; (e) aquifer media; (f) hydraulic conductivity; (g) topography; (h) land use.*

Effective infiltration (I) is the amount of water infiltrating through the unsaturated zone and reaching the aquifer. The infiltration was estimated using the inverse hydrogeological water balance (Celico, 1988; Civita, 2005). This methodology consists of estimating infiltration from the analysis of climatic

data, such as rainfall and temperature, topographic parameters, such as altimetry, and the characteristics of the hydrogeological complexes in the study area. The GIS-based method makes it possible to obtain the spatial distribution of the effective infiltration rate in the hydrogeological basin (Canora et al., 2018; Canora & Sdao 2020). In QGIS software, daily rainfall and air temperature series were elaborated for 2000-2015. In the hydrogeological basin, the mean annual rainfall is about 538 mm. The GIS-based distributed inverse hydrogeological water balance showed that the actual evapotranspiration (equal to 465 mm) provides an effective infiltration rate of 52 mm/year, which is equivalent to about 1080 l/s. The mean annual value of direct runoff is 21 mm/year (Muzzillo et al., 2021a) (**Fig. 18(b)**).

The unsaturated zone (N) or vadose zone represents the thickness defined by the soil horizons and the groundwater table. The attenuation capacity of the contaminants is strongly affected by the unsaturated media properties that influence many processes, such as biodegradation, diffusion, and chemical reactions. The possibility of groundwater contamination can increase with small thicknesses of the vadose zone and high permeability, consequently enhancing the intrinsic vulnerability of the aquifer. The values of the parameter N were obtained from well stratigraphic profiles integrated with geological maps and geophysical surveys (Muzzillo et al., 2021b). The N parameter ratings range from 2 to 7 (**Tab. 4**). The results highlighted that among the vadose zone classes: Medium-fine alluvial deposits (rating 5), Fine alluvial deposits (rating 4), Coarse alluvial deposits (rating 6), Sand coastal deposits (rating 7), and Clay deposits (rating 2) cover around 42%, 26%, 20%, 11% and 1% of the total study area, respectively (**Fig. 18(c)**).

Soil media (T) is the uppermost vadose layer where biological activities are significant. Soil characteristics condition the behaviour and amount of contaminants that can reach the water table (Ckakraborty et al., 2007). The presence of organic components, the thickness of soil media, and the grain size can significantly impact the contaminant's attenuation mechanisms. Different textures of soil media (coarse sand, sand, sandy loam, loam, silty clay loam, and clay loam) are present throughout the study area (**Fig. 18(d)**).

Aquifer media (A) describe the components' characteristics of the saturated zone, such as the porosity rate, particle types, grain size, and the processes that take place below the piezometric level. These processes are essentially hydrodynamic dispersion, dilution, absorption, and chemical reactions between the aquifer media and the contaminants (Polemio et al., 2005). The aquifers of the study area are mainly unconfined. The results showed that the medium-fine alluvial complex covers 59% of the study area. Alluvial, sandy, and fine sand complexes cover 29.5%, 11%, and 0.5%, respectively (**Fig. 18(e)**). The analysis of the thematic layer suggests that the south eastern portion of the study area (closest to the coast) is under high intrinsic vulnerability.

Hydraulic conductivity (C) is defined as the ability of the fluid to pass through the aquifer media. This physical property expresses the groundwater flow and mobile contaminants rate that can reach the water table (Aller et al., 1987). High hydraulic conductivity gives higher potential groundwater contamination and, thus, greater intrinsic vulnerability. The hydraulic conductivity of the study area ranges from 10^{-5} to 10^{-3} m/s (**Tab. 4**, **Fig. 18(f)**).

Topography (S) is expressed by the variability of a land surface slope as a percentage. This study used DEM data for extracting the slope information. Low-slope areas can be more vulnerable to pollution as they retain water longer and contaminants are more likely to infiltrate. More than 70% of the study area has a slope class of 0-2%, corresponding to flat areas, which are given the highest rating and, therefore, have a significant impact on intrinsic vulnerability (**Fig. 18(g)**).

The study area land use (LU) is characterized by urban, industrial, and vegetation land cover (CORINE Land Cover, 2018). The quality of groundwater resources in the Metaponto coastal plain is threatened mainly due to population growth and intensive agricultural, industrial and urban activities. The development of agricultural activities has resulted in a general increase in the size of cultivated areas. The vegetation covers areas largely characterized by agricultural crops. Forests and pastures are located mainly in the southeastern part of the plain. Along the coast, the Mediterranean maquis takes on the prevailing vegetational characteristics. The Mediterranean maquis is replaced by the garrigue, a low, soft-leaved scrubland, in areas with unfavorable climatic and soil conditions and where anthropogenic pressures, such as fire and grazing, are heavier (Canora et al., 2015; CORINE Land Cover, 2018). Some areas are characterized by parcels allocated to permanent crops, mainly vineyards, olive trees, and sown land. Permanent crops are found throughout the plain; the coastal area is mainly covered by orchards. Inadequate or intensive farming practices have aggravated the ongoing degradation phenomena, especially in the study area characterized by unfavorable climatic conditions (Canora et al., 2015; CORINE Land Cover, 2018). The impact of land use on the vulnerability was considered by adding the LU parameter to the SINTACS method (**Tab. 4**).

The SINTACS and SINTACS-LU indexes were determined using Equations (10) and (11), and the resulting intrinsic vulnerability indexes are represented in **Fig. 19** and **Fig. 20**.

According to the procedure (Civita & De Maio, 1997), the results of the SINTACS parameters elaboration show that the groundwater vulnerability index ranges from 62 to 185; it was classified into low (<105), moderate (106–140), and high (>140) vulnerability classes (**Fig. 19**). The results also indicated that the low, moderate, and high groundwater vulnerability zones cover 7%, 51%, and 42% of the study area, respectively. The application highlights that more than half of the study area is at moderate vulnerability in terms of intrinsic susceptibility to pollution (**Fig. 21**).

The SINTACS-LU intrinsic vulnerability index was calculated combining the eight thematic layers in the GIS-based application of the method. The elaboration considering the LU parameter shows that the vulnerability index ranges from 77 to 215 (**Fig. 20**).

Since the SINTACS and SINTACS-LU indexes do not vary in the same range, they were normalized to allow the vulnerability zonation. The normalization of the SINTACS and SINTACS-LU indexes of the single cells was performed based on the following equation (Civita & De Maio, 1997; Civita & De Maio, 2004; Civita, 2010):

$$I_{norm} = \left(\frac{I - I_{min}}{I_{max} - I_{min}} \right) \cdot 100 \qquad (19)$$

where I_{norm} is the normalized index, and I_{min} and I_{max} are the minimum and the maximum values of the indexes, respectively.

The groundwater vulnerability map resulting in the application and normalization of the SINTACS-LU classifies the majority of the plain (56%) as moderate vulnerability, 7% is classified as low, and 37% as high vulnerability (**Fig. 22**).
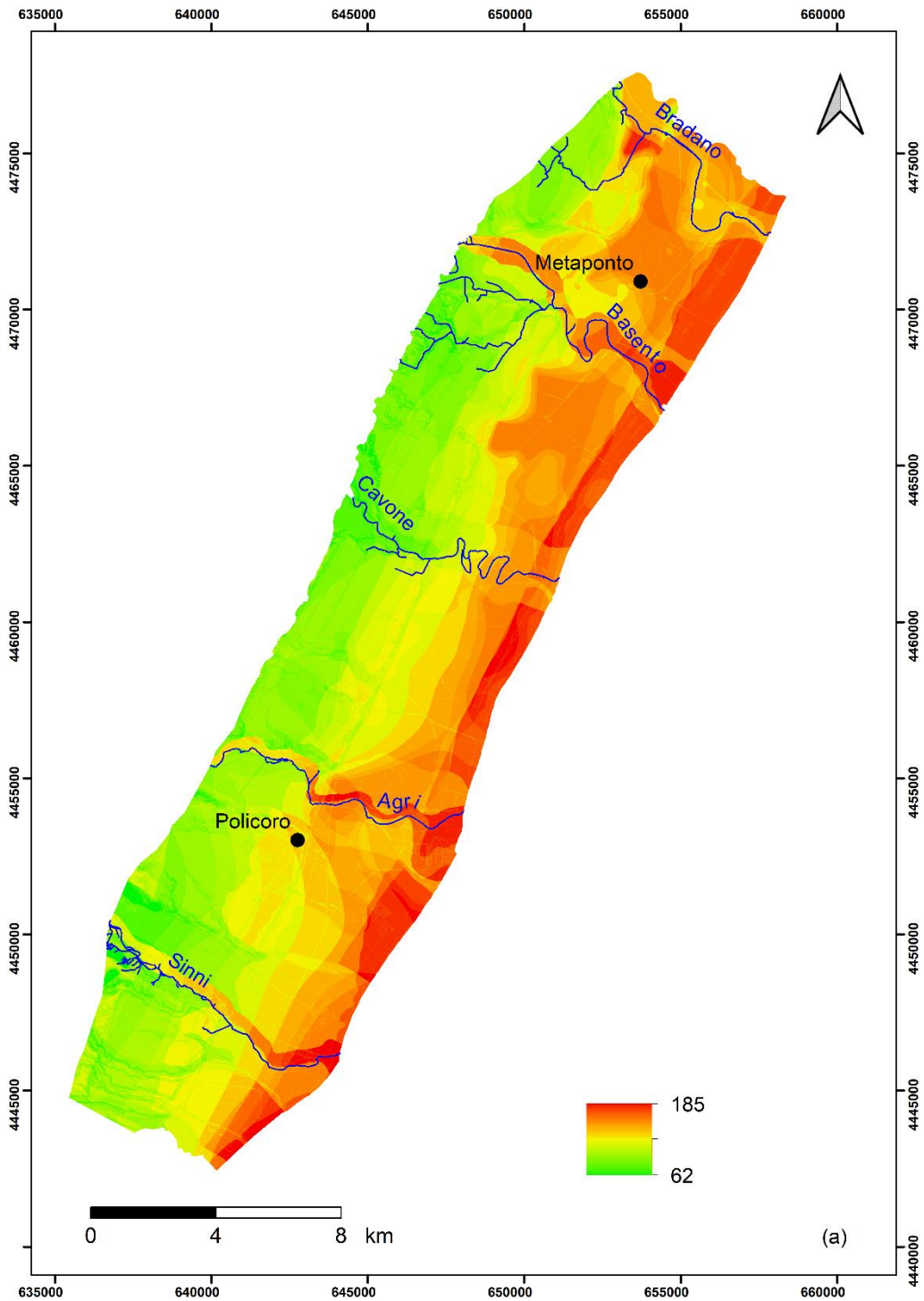
Fig. 19 *Groundwater vulnerability index elaborated with SINTACS method (from Canora et al., 2022).*
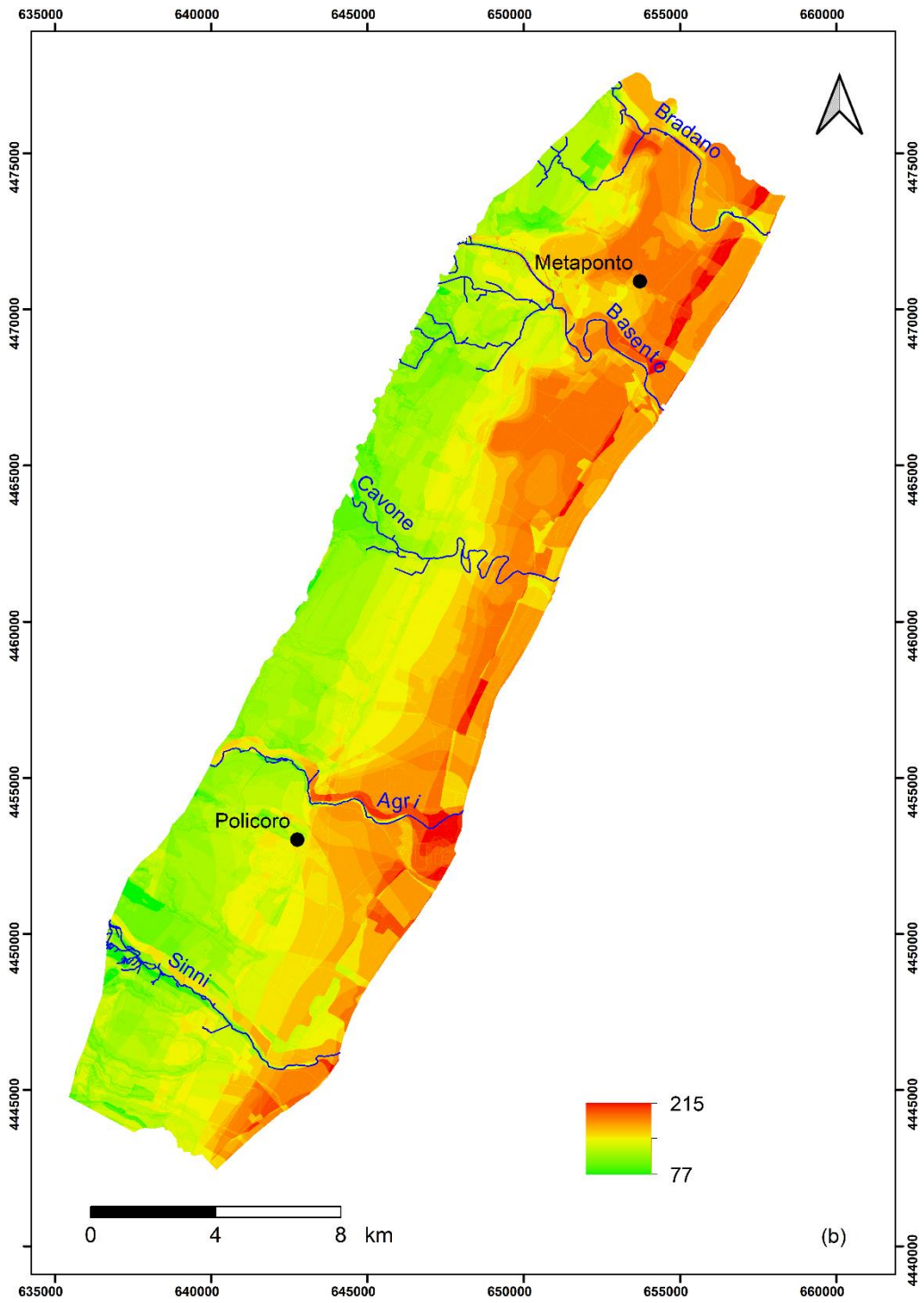
Fig. 20 *Groundwater vulnerability index elaborated with SINTACS-LU method (from Canora et al., 2022).*
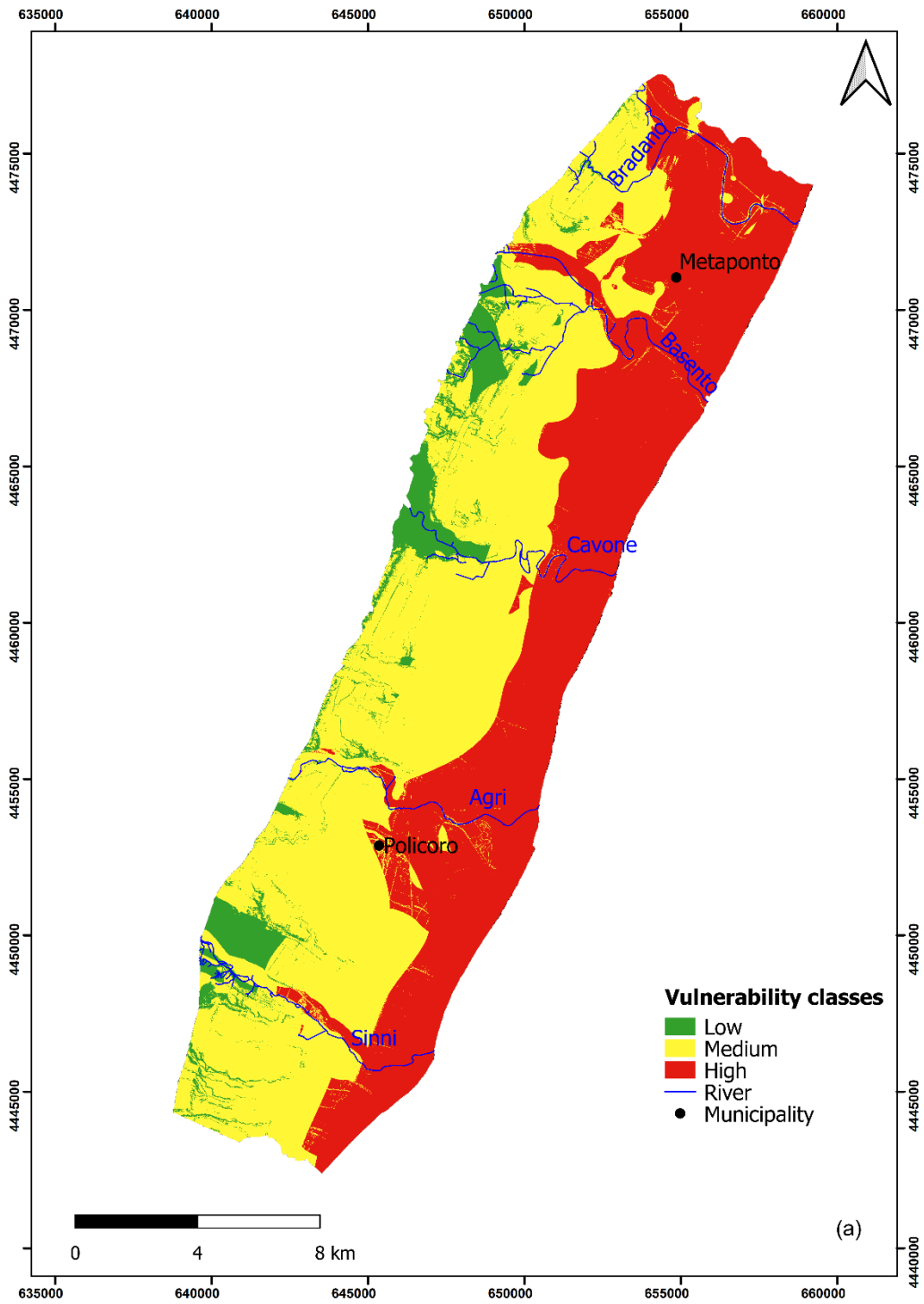
Fig. 21 *Groundwater vulnerability map derived from SINTACS method (from Canora et al., 2022).*
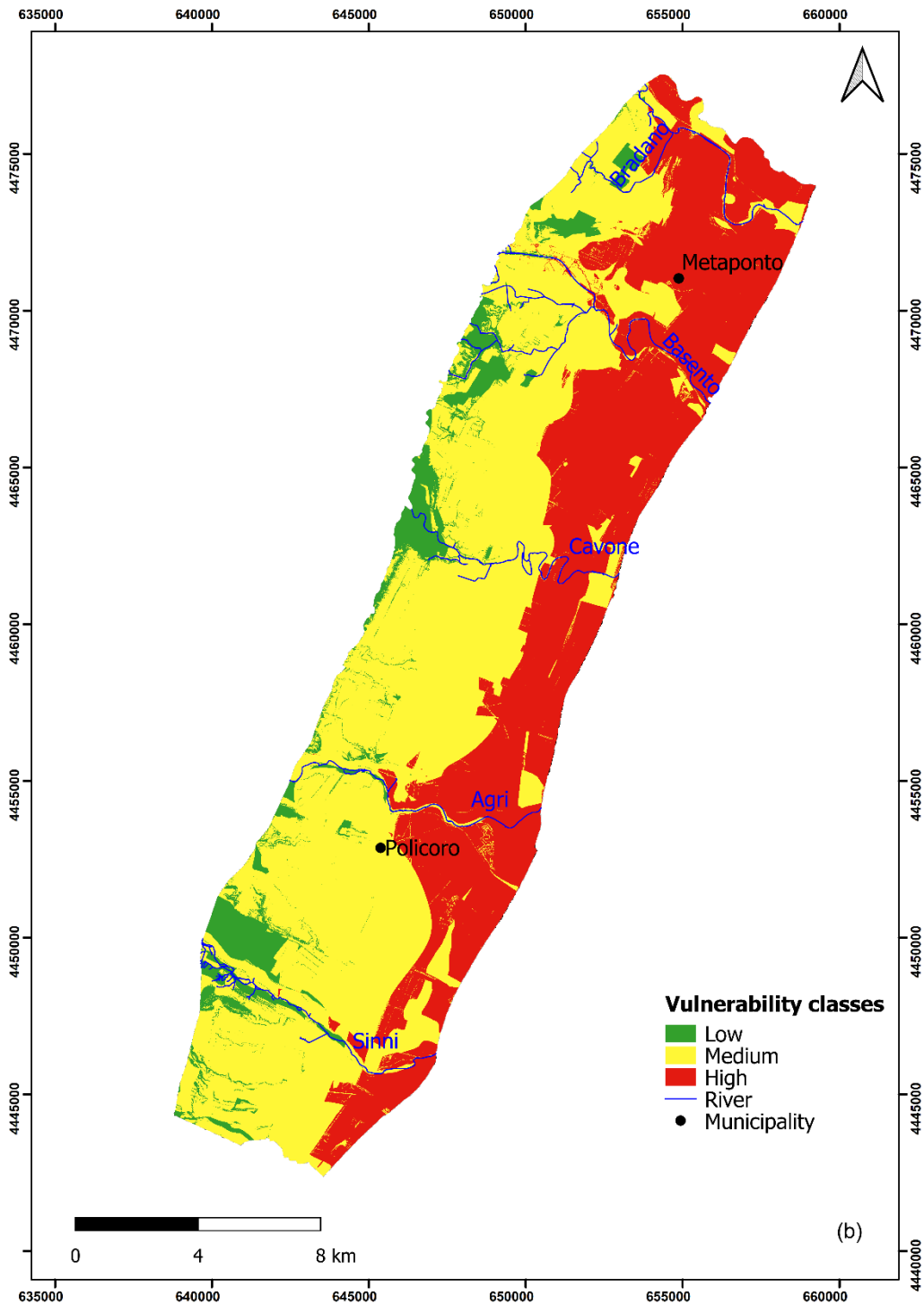
Fig. 22 *Groundwater vulnerability map derived from SINTACS-LU method (from Canora et al., 2022).*

No part of the study area is classified in the very high vulnerability class by the SINTACS and SINTACS-LU methods.

Low vulnerability areas, situated at a small scale in the upper part of the hydrogeological basin, showed low ratings of the water depth and soil media, despite high ratings of the hydraulic conductivity and effective infiltration. Part of the northwestern and the central sides show diffuse moderate vulnerability. The southeastern side shows high vulnerability due to the effects of the shallow water table, the small thicknesses of the unsaturated zones and the soil media typologies.

The vulnerability classes of both methods have a comparable pattern. In the SINTACS-LU approach, land use has a great impact due to the high weight assigned to it.

Fertilizer use in agricultural activities can be recognized as a source of nitrate contamination in the study area. Hence, the consideration of the land use as a vulnerability conditioning parameter and the choice of the "Nitrates" string of weight are significantly representative of the actual land use condition and implies the actual suitability of SINTACS-LU for assessing groundwater vulnerability in the study area. The comparison between SINTACS and SINTACS-LU findings highlights that the SINTACS-LU method considers the specific characteristics of the land use, which plays an essential role in groundwater vulnerability evaluation.

The southeastern part is classified as highly vulnerable on both maps. The lowest vulnerable portions, located in the north-western and southern zones of the study area, are similarly distributed in both maps. The intensive agricultural, industrial and other anthropogenic activities with the peculiar hydrogeological characteristics of the aquifer system favor the high vulnerability to contamination. In the SINTACS-LU map, some areas classified as highly vulnerable in the SINTACS method show a minor vulnerability class. These areas are located in natural and forest sectors of the Metaponto plain, which are less populated, and where human impact on the groundwater is limited.

In the map removal sensitivity analysis, each SINTACS and SINTACS-LU parameter was removed one at a time to see how it affected the output. The effect is expressed in terms of the variation index (Babiker et al., 2005) calculated in each cell of the study area by Equation (13). **Tab. 12** and **Tab. 13** give a statistical overview of the variation index resulting from the removal of each parameter. For each variable, the mean of the variation index in all cells was used to evaluate the sensitivity of that variable if omitted.

Variation index (%)	Variable removed						
	S	I	N	T	A	C	S
Mean	1.44	2.99	1.37	1.22	2.23	1.90	0.78
Minimum	0.00	0.74	0.00	0.00	0.00	0.00	0.00
Maximum	4.56	8.01	7.38	5.92	7.80	5.30	7.76
SD	0.82	1.02	1.28	1.13	1.08	0.96	0.82

Tab. 12 Statistical summary of the SINTACS map removal sensitivity analysis (from Canora et al., 2022).

Variation index (%)	Variable removed						
	S	I	N	T	A	C	S	LU
Mean	1.08	1.26	0.27	0.46	0.78	0.58	0.46	2.03
Minimum	0.30	0.14	0.00	0.00	0.12	0.00	0.00	0.01
Maximum	2.98	1.48	1.08	2.47	1.31	1.16	1.55	5.41
SD	0.52	0.22	0.17	0.38	0.14	0.27	0.22	1.01

Tab. 13 Statistical summary of the SINTACS-LU map removal sensitivity analysis (from Canora et al., 2022).

For the SINTACS method, removal of the effective infiltration (I) parameter resulted in the largest variation index, with a mean of 2.99%. Aquifer media (A) and hydraulic conductivity (C), with mean values of 2.23% and 1.90%, respectively, were the other parameters with higher variation indexes. In descending order, the other parameters are the depth of the water table (S), unsaturated zone (N), and soil media (T). With a variation index of 0.78%, Topography (S) had the lowest means.

In the SINTACS-LU approach, the removal of the land use (LU) parameter caused the highest variation index, with a mean of 2.03%. In descending order, the other parameters are the effective infiltration (I), depth of the water table (S), aquifer media (A), hydraulic conductivity (C), soil media (T), and topography (S). The unsaturated zone (N), with a variation index of 0.27%, had the lowest mean.

Tab. 14 and **Tab. 15** show for each variable the statistics of the single-parameter sensitivity analysis: the theoretical weight originally assigned by SINTACS and SINTACS-LU methods, the same weight

normalized to 100, the average effective weight computed on the entire study area, the standard deviation and the minimum and maximum values.

Parameter	Theoretical weight	Theoretical weight (%)	Average effective weight (%)	Standard deviation (%)	Minimum value (%)	Maximum value (%)
S	5	19.23	27.17	3.33	19.87	48.39
I	5	19.23	5.17	2.55	2.63	15.63
N	4	15.38	14.99	1.74	8.42	24.10
T	5	19.23	19.36	4.12	9.26	39.13
A	2	7.69	9.70	1.84	5.36	16.28
C	2	7.69	11.69	3.39	5.62	29.03
S	3	11.54	20.71	4.30	2.10	37.50

Tab. 14 *Statistical summary of the SINTACS single-parameter sensitivity analysis (from Canora et al., 2022).*

Parameter	Theoretical weight	Theoretical weight (%)	Average effective weight (%)	Standard deviation (%)	Minimum value (%)	Maximum value (%)
S	5	16.13	23.35	3.19	16.85	50.85
I	5	16.13	4.41	2.10	2.30	16.13
N	4	12.90	12.89	1.67	6.90	25.00
T	5	16.13	16.69	3.99	7.94	40.18
A	2	6.45	8.31	1.50	4.48	16.87
C	2	6.45	10.00	2.83	4.61	30.51
S	3	9.68	17.74	3.48	1.76	32.88
LU	5	16.13	23.95	6.40	8.02	47.62

Tab. 15 *Statistical summary of the SINTACS-LU single-parameter sensitivity analysis (from Canora et al., 2022).*

In both methods, almost all parameters showed an effective weight higher than the theoretical one. The effective infiltration (I) showed effective weight was significantly lower than theoretical one whereas the unsaturated zone (N) and soil media (T) showed the lowest differences between the effective and theoretical weights.

For the SINTACS method, the depth of water table (S) had the greatest influence on the final vulnerability index, with an average weight of 27.17%, in agreement with the highest theoretical weight of 19.23%. On the contrary, the effective infiltration (I), which had the highest theoretical weight together with the depth of water table (S) and soil media (T), had the lowest effective weight with an average value of 5.17%.

In the SINTACS-LU approach, the land use (LU) was the most effective parameter on the final vulnerability index (average weight 23.95%), coherently with the highest theoretical weight of 16.13%, in agreement with the results of the map removal sensitivity analysis. On the other hand, as for the SINTACS method, the effective infiltration (I), which together with the depth of the water table (S), soil media (T), and land use (LU) had the highest theoretical weight and had the lowest effective weight with an average value of 4.41%.

9.2 GALDIT

The groundwater vulnerability to SWI was assessed by applying the GALDIT method. The collected data and the thematic layers were implemented, elaborated, and represented in the QGIS environment. All GALDIT parameters were evaluated, rated, and weighted (**Tab. 6**) according to the methodology above-described (**Fig. 13**). The spatial distribution of the GALDIT parameters was elaborated using the Kriging interpolation technique (**Fig. 23**).
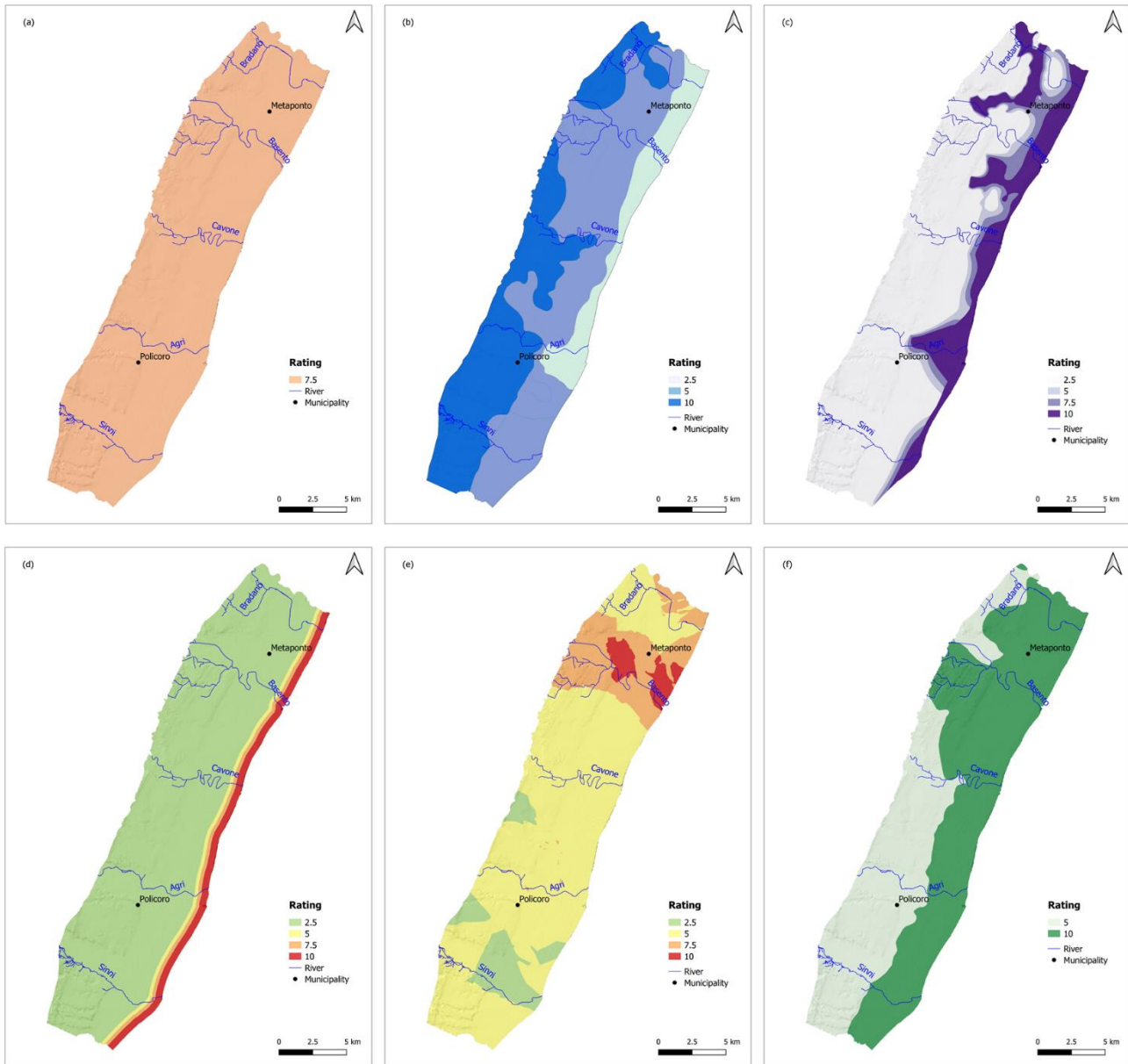
Fig. 23 Thematic layers of the GALDIT parameters: (a) groundwater occurrence; (b) aquifer hydraulic conductivity; (c) groundwater table above sea level; (d) distance from shore; (e) impact of the existing seawater intrusion; (f) aquifer thickness (from Muzzillo et al., 2022).

G – Groundwater occurrence is related to confined and unconfined conditions of the aquifer and can influence the extent of SWI. The confined aquifer rating is higher (more vulnerable) because, during pumping, the depression cone is commonly larger than the unconfined aquifer. A large portion of the investigated aquifer system occurs in unconfined conditions, so a rating of 7.5 was given (**Tab. 6**, **Fig. 23(a)**).

A – High hydraulic conductivity implies an increase in the magnitude of seawater front movement and, consequently, higher vulnerability to SWI. For the study area, the hydraulic conductivity values were derived from several pumping tests conducted in the study area over the previous twenty years (Polemio et al., 2003). The hydraulic conductivity thematic layer was elaborated using these values. The study area's hydraulic conductivity varies from 10^{-5} to 10^{-3} m/s. The hydraulic conductivity expressed in m/day, with rating that ranges from 2.5 to 10, is shown in **Tab. 6** (**Fig. 23(b)**).

L – Groundwater table above sea level is a crucial factor in determining the extent of SWI due to its control of the hydraulic pressure to drive the seawater's front back. As the height of water above sea level increases, the possibility of undergoing the intrusion phenomenon decreases. This parameter was derived from measurements taken at 42 monitoring wells in the study area, used for agricultural and household consumption (**Fig. 8**). The height of groundwater level above the sea was rated following the four classes shown in **Tab. 6**. The maximum impact of SWI is observed near the coast, and the impact decreases moving inland (**Fig. 23(c)**).

D – Generally, the influence of SWI decreases moving inland from the shore, whereas the greatest influence is along the coast. Chachadi & Lobo Ferreira (2005) indicated the perpendicular distance inland from the coast and the height of the groundwater level above sea level as the factors with the greatest influence on potential SWI, assigning them the maximum weight equal to 4. The distance from the shore was calculated using the four buffer zones tool of QGIS (500 m, 750 m, 1000 m, >1000 m) (**Fig. 23(d)**).

I – To consider the effect of the existing SWI, firstly, Chachadi & Lobo Ferreira (2001) proposed using the groundwater $Cl^-/(HCO_3^- + CO_3^{2-})$ ratio. Then, Dörfliger et al. (2011) presented groundwater electrical conductivity as an alternative indicator of groundwater salinity, and this parameter has been used in literature for the computation of the GALDIT index (Luoma et al., 2017; Chang et al., 2019). The rates attributed to parameter I by Chang et al. (2019) were used in this study. The impact of the current status of SWI was expressed in terms of measured groundwater electrical conductivity (**Tab. 6**) (**Fig. 23(e)**).

T – The extent and magnitude of SWI are heavily influenced by the aquifer thickness or saturated thickness, where the aquifer is unconfined. Aquifer with high thickness values is more prone to SWI than aquifer with lower ones. In this study, the aquifer thickness was defined with reference to the top of the Sub-Apennine Clays Formation, which represents the bottom of the aquifer. The thickness of the coastal aquifer is generally higher than 10 m and increases from inland to the coast (Polemio et al., 2003) (**Tab. 6**, **Fig. 23(f)**).

The final vulnerability index to SWI was elaborated using Equation (12) by the GIS-based procedure. The GALDIT index ranges from 3.3 to 8.5. The final map, showing the spatial distribution of the vulnerability to SWI, was obtained by reclassifying the GALDIT index defined in the study area. Three vulnerability classes are depicted: low (GALDIT index <5), moderate (5-7.5), and high (>7.5) (**Fig. 24**). The results of the GALDIT application agree with the hydrogeological characteristic of the investigated area. Low vulnerability covers most of the study area (70.40%), in areas more than 1000 m away from the coast, where both the groundwater level above the sea and the groundwater electrical conductivity have the lowest values. 22.65% of the area is characterized by moderate vulnerability, extending on average up to 4 km at the Agri and Cavone Rivers and up to about 7 km in the area between the Basento and Bradano Rivers, where the aquifer thickness is greater than 10 m and the highest values of electrical conductivity, greater than 2000 μS/cm, were measured. The high vulnerability to SWI class was detected along the coastal strip, within a distance of 500 m from the coastline, and covers 6.95% of the investigated territory, with an extent of about 20 km^2. On the coastline, this result is primarily due to the proximity of the detected area to the shore and the freshwater-seawater interface. Another highly impacting factor on the final result is the aquifer thickness, which shows the highest value along the coast. As highlighted below, this phenomenon seems to be accentuated from SW towards NE, moving along the coast since the top of the grey-blue clay formation gently slopes from the Sinni to the Bradano Rivers.
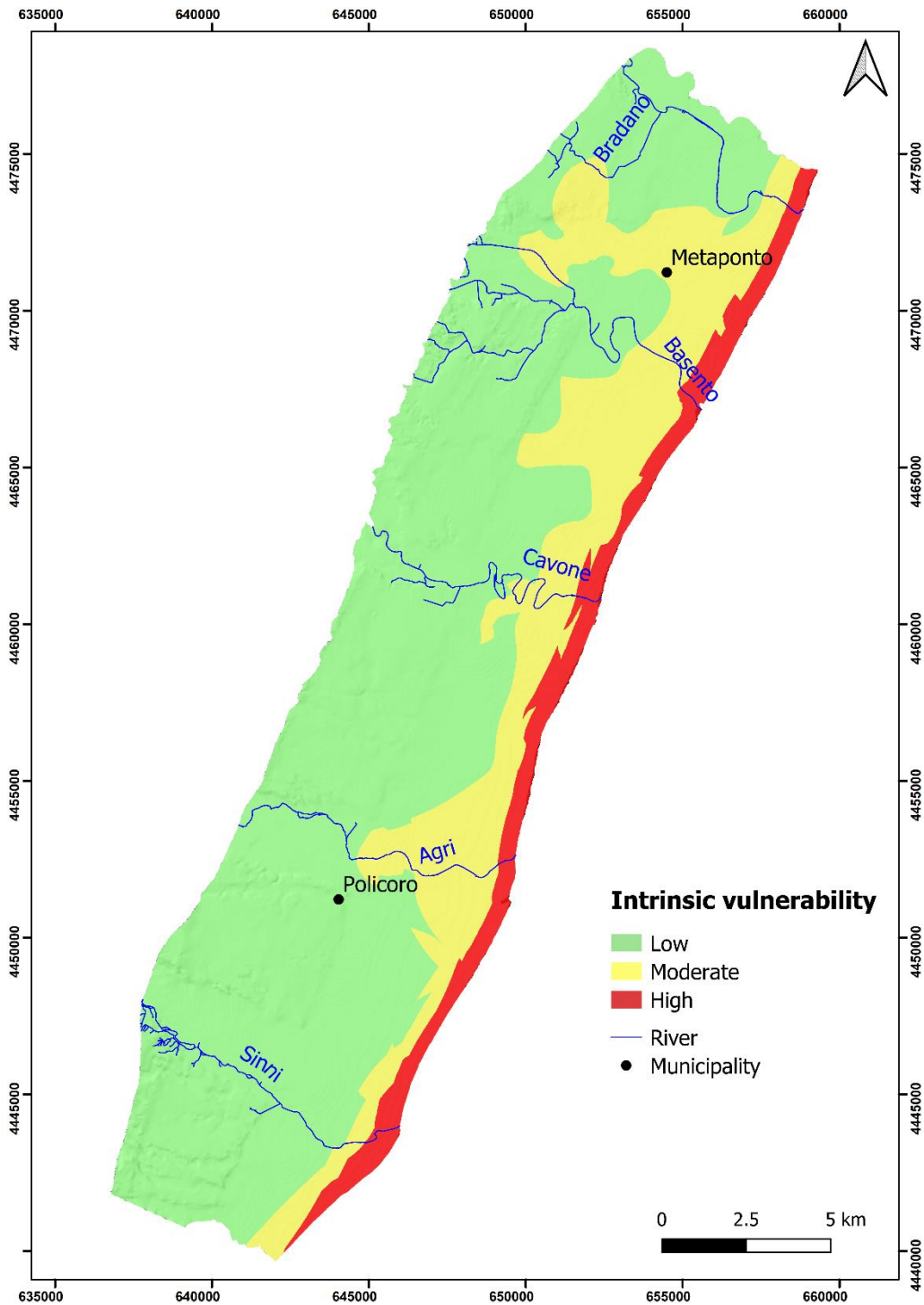
Fig. 24 *Map of the groundwater vulnerability to seawater intrusion (from Muzzillo et al., 2022).*

The statistics of the single-parameter sensitivity analysis were computed for each parameter (**Tab. 16**). The original theoretical weight provided by the GALDIT method, the theoretical weight normalized to 100, the average effective weight calculated over the entire study area, the standard deviation, and the minimum and maximum values are reported (**Tab. 16**). The analysis shows that for almost all factors the theoretical weights are lower than the effective ones.

The Distance from the shore and the Impact of the existing status of SWI parameters showed the highest and lowest differences (in absolute value terms) between the effective and theoretical weights, respectively. The Aquifer hydraulic conductivity, with an average weight of 26.63%, has the greatest influence on the final vulnerability index. On the contrary, the Impact of the existing status of SWI

has the lowest effective weight, equal to 6.90%, confirming the lowest value of the theoretical one (6.67%).

Parameter	Theoretical weight	Theoretical weight (%)	Average effective weight (%)	Standard deviation (%)	Minimum value (%)	Maximum value (%)
G	1	6.67	9.84	1.72	5.88	15.00
A	3	20.00	26.63	12.23	6.00	42.86
L	4	26.67	20.67	9.94	10.26	50.00
D	4	26.67	15.71	5.73	8.51	42.11
I	1	6.67	6.90	2.02	2.00	16.00
T	2	13.33	20.25	6.46	9.30	33.33

Tab. 16 Statistical summary of the GALDIT single-parameter sensitivity analysis (from Muzzillo et al., 2022).

A statistical overview of the variation index obtained from the map removal sensitivity analysis was provided (**Tab. 17**). The removal of the parameter Distance from the shore, with a mean value of 6.32%, has the highest variation index. In descending order, Groundwater level above the sea, Impact of the existing status of SWI, Aquifer hydraulic conductivity, and Groundwater occurrence are the other factors showing lower values (**Tab. 17**). Aquifer thickness showed the lowest mean value, with a variation index of 1.93%.

Variation index (%)	Variable removed					
	G	A	L	D	I	T
Mean	2.65	3.10	5.09	6.32	3.28	1.93
Minimum	1.55	0.23	0.04	0.22	1.33	0.04
Maximum	3.50	6.83	7.81	8.28	4.33	4.26
Standard deviation	0.37	1.59	2.47	1.55	0.43	1.23

Tab. 17 Statistical summary of the GALDIT map removal sensitivity analysis (from Muzzillo et al., 2022).

Assessing groundwater vulnerability to SWI represents a significant step to preventing and controlling the degradation process of the resources. Indeed, identifying areas more subject to SWI is useful and important for water resources managers that can define appropriate and proper prevention actions, such as SWI monitoring, engineering planning, regulatory or legislative approaches.

10. Numerical modeling

Since it was unthinkable to carry out numerical modeling of groundwater flow for the entire coastal plain due to the lack of data and excessive computational burden, the research activity focused on the area that, from the assessment of intrinsic vulnerability to SWI using the GALDIT method, is found to be potentially most affected by this phenomenon. This area, selected at the mouth of the Basento River, extends on average for about 3.6 km inland and 11.6 km along the coast, covering an area of about 42 km^2 (**Fig. 25**).
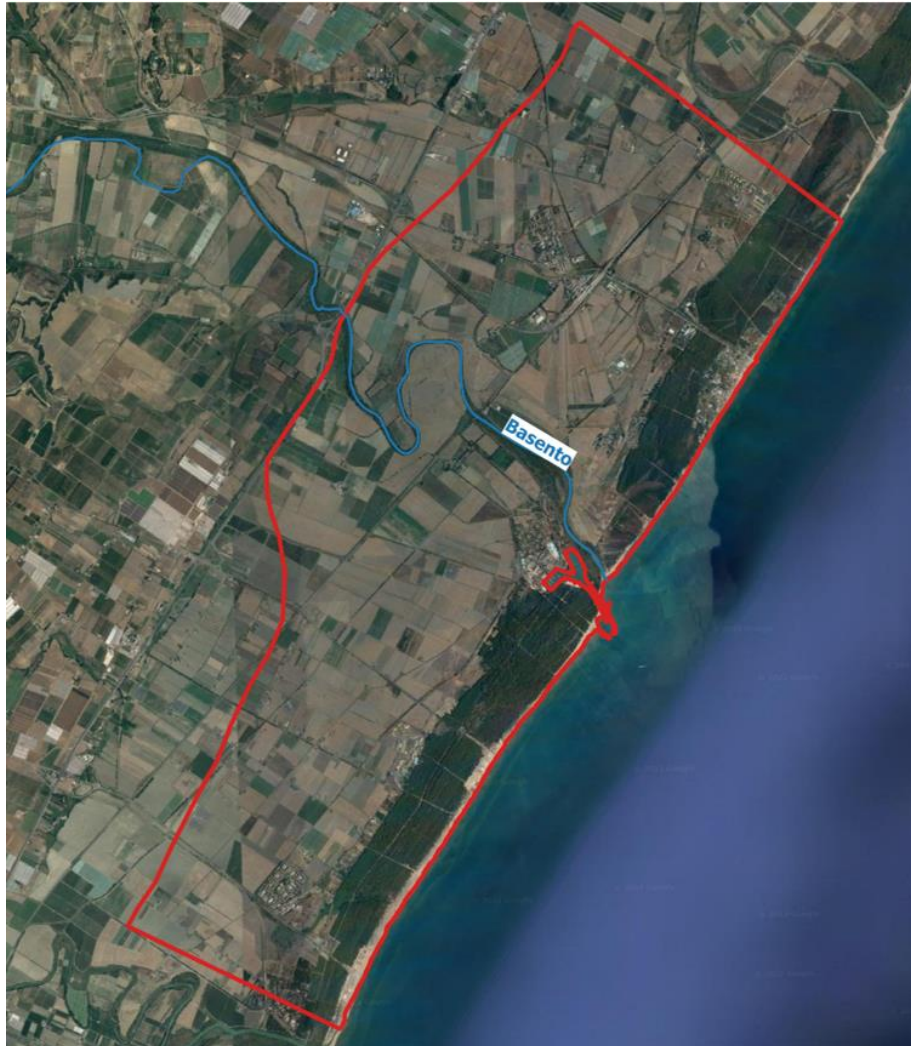
Fig. 25 Area selected for numerical modeling (outline in red).

The choice of the area to be modelled and the consequent definition of the polygon imported into the software to delineate it, took into account several considerations:

- a nearly homogeneous area was considered from an altimetric point of view (with an average elevation of about 3.24 m);
- the lateral edges were defined to exclude the Bradano and Cavone riverbeds;
- the lower edge coincides with the coastline.

Geologically, the area is mainly characterized by the presence of two main formations: coastal deposits and alluvial, transitional, and marine deposits.

The modeling started with the definition of the conceptual model of the hydrogeological system, which formed the basis for numerical modeling. Inputs were defined using raw data objects (surfaces,

polylines, polygons, etc.). The grid was introduced only when the numerical model was launched. This made it possible to:

- – convert the conceptual model to multiple numerical model grids for different analyses during the modeling process (coarse models for quick runs, refined models with more detail and resolution, scenario and uncertainty analysis);
- – easily update corresponding numerical models as conceptualization changes.

The steps followed to build the conceptual model are summarized below:

- – definition of the modeling objectives;
- – collection of the data objects and definition of the conceptual model of the area;
- – definition of the geological model of the subsurface;
- – definition of the structural zone properties;
- – definition of the grid (horizontal and vertical discretization);
- – conversion to the numerical model;
- – definition of the boundary conditions;
- – modeling execution;
- – results visualization.

The first step was to define the modeling objectives, which involved the selection of the desired flow and transport simulation options. The selected combination of flow (in the present case, saturated groundwater flow) and transport options narrows the list of available flow and transport engines and generates associated input variables. This phase's goal is to develop the inputs needed to build the model based on the understanding of the relevant physical processes present within the study area.

At this stage of the workflow, the data needed to define the conceptual model were collected. At least the following data objects are necessary to build a conceptual model:

- – two surfaces: one for the top and one for the bottom of a geological unit;
- – a polygon representing the area of the model.

The GIS shapefiles of the model area and the Basento River were imported as polygon and polyline data objects, respectively. The DTM .GRD file was imported as surface data object to simulate the ground surface.

The geological structure of the conceptual model was then defined, providing the geological surfaces representing the top and bottom of the geological model. These were then converted into Horizons. Horizons are stratigraphic layers that define the upper and lower boundaries of the structural zones in a conceptual model. When horizons are created, the Structural Zones are automatically generated by VMOD Flex between the horizons. They can be used later to define property zones.

In addition to the DTM, the surfaces representing the top and bottom of the clayey formation were loaded into the software and converted into horizons (**Fig. 26**). Reconstruction of the clay basement of the aquifer was done from studies conducted in the Metaponto coastal plain (Pescatore, et al., 2009; Cilumbriello, et al., 2010; Tropeano, et al., 2011). The Sub-Apennine Clays Formation represents the confining unit of the aquifer, which was considered monolayer because, although multilayer portions were found, the overlying aquifers are almost homogeneously all interconnected. Previous studies (Tropeano, et al., 2011) made it possible, through the application of the Horizontal-to-Vertical Spectra Ratio survey (HVSR) geophysical method, to model the base of the aquifer. From the integration of these findings with the previously-published lithostratigraphic interpretation of the subsurface of the

Metaponto coastal plain (Cilumbriello, et al., 2010), it was possible to hypothesize the trend of the top of the clay substrate, the depth of which was measured up to 120 m (Pescatore, et al., 2009). During the process of horizon creation, VMOD Flex automatically generates the structural zones between the defined horizons.
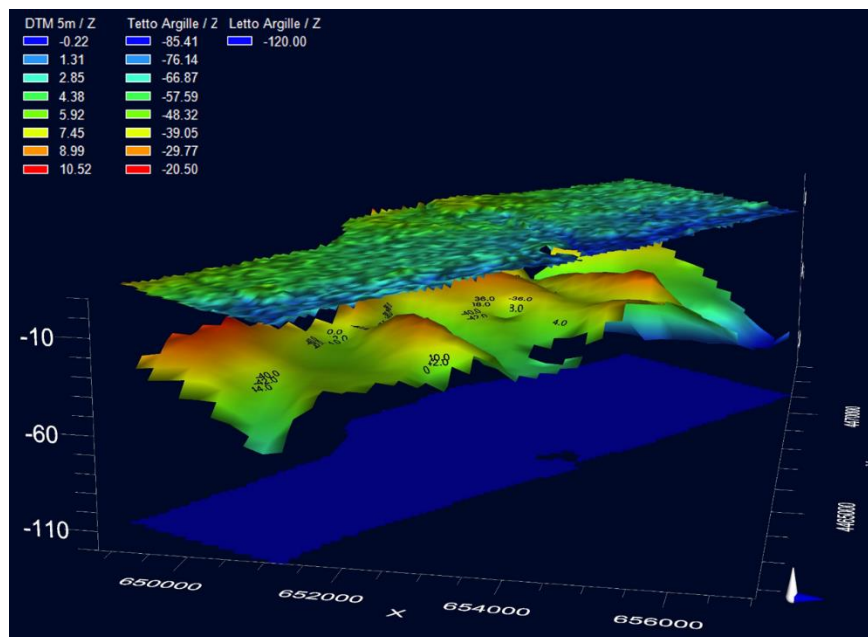

***Fig. 26** Surfaces imported into VMOD Flex for subsurface geological model definition.*

At this step, the Property Zones were defined for the conceptual model. In VMOD Flex, a property zone is a specified 3D volume whose geometry is defined from the existing structural zones, with user-defined hydrogeologic attributes. As such, the property zones can be generated only after horizons have been defined. In this case, we focused on the structural zone between the DTM and the surface of the clay substrate top (**Fig. 27**), to which the following hydraulic conductivity values, taken from the literature (Polemio et al., 2003), were assigned:

- conductivity in the horizontal/x-direction (K_x) and in the horizontal/y-direction (K_y) = 6.53 * 10^{-5} m/s;
- conductivity in the vertical/z-direction (K_z) = 10^{-6} m/s.

The conceptual model was discretized using the finite difference method, which involves fitting the conceptual model to one or more finite difference grids. The horizontal grid resolution (200 m * 200 m) and the vertical layering type and resolution were specified. The Deformed grid type was chosen, in which the tops and bottoms of the model layers conform to the horizons' elevation. For the simulation of groundwater flow under steady-state and transient conditions, only one layer was considered. The study area was thus discretized into a grid consisting of 60 rows and 43 columns (**Fig. 28**).

The conceptual model was then translated into a numerical model to run in a groundwater modeling engine within the VMOD Flex environment. During translation, the software automatically populates the specified grid with the defined geological formations and property zone attributes and creates the necessary input files for loading into the desired simulator. Separate workflows are generated every time a conceptual model is converted into a numerical model. In the numerical modeling workflow, the properties of the numerical grid can be viewed and edited, groundwater modeling engines can be run, and the results can be visualized.
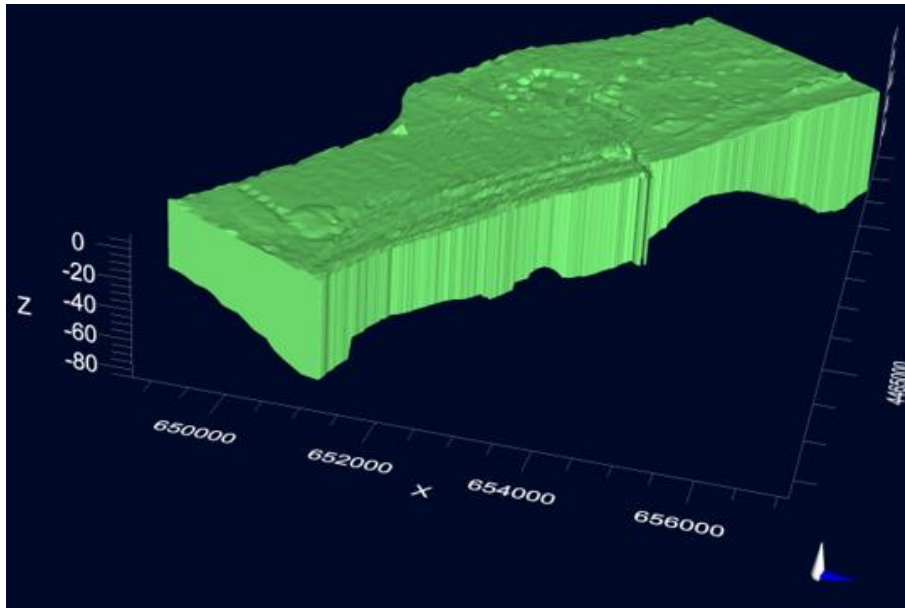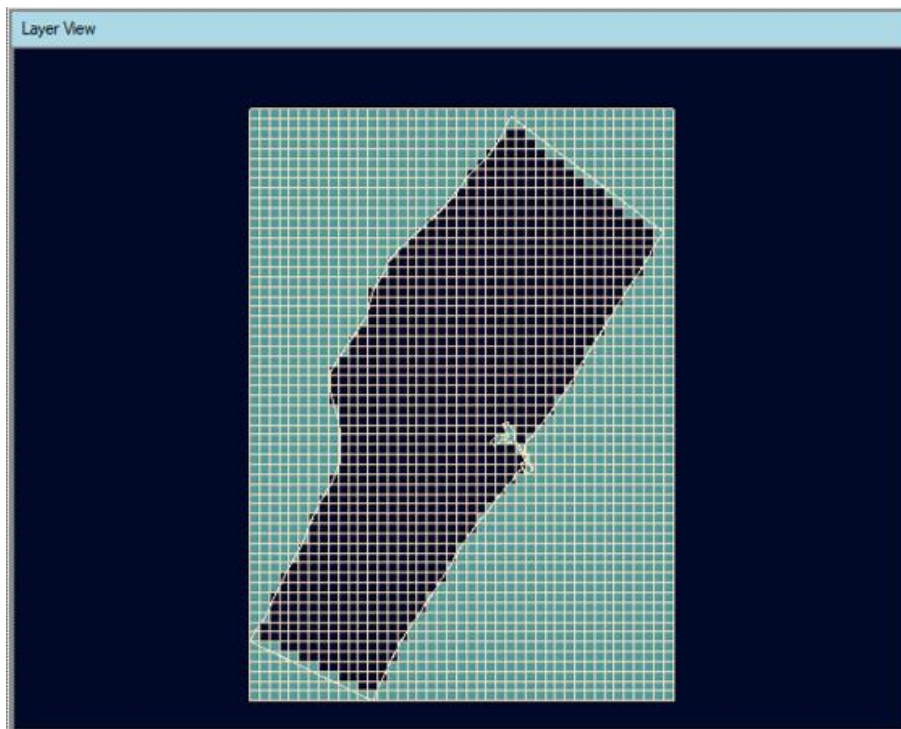
Fig. 27 *Structural zone.*

Fig. 28 *Finite difference grid.*

Every conceptual model needs a suitable set of boundary conditions to represent how the system interacts with the surrounding environment. In the case of the groundwater flow model, boundary conditions describe the flow exchange between the model and the external system. The boundary condition types are divided into the following groups in VMOD Flex:

- Boundary Conditions (standard) (Constant Head, Rivers, Drains, General Head, Recharge, EVT, etc.);
- Wall (Horizontal Flow Barrier);
- Pumping Wells.

10.1 Steady-state conditions

The boundary conditions assigned under steady-state flow conditions are described below (**Fig. 29**).

Cells at the lateral edges of the modeling domain were defined as inactive (no flow).

The Constant Head boundary condition fixes the head value in selected grid cells regardless of the system conditions in the surrounding cells. As a result, it acts as a potentially infinite source of water entering the system or as an infinite sink for water leaving the system. This boundary condition was applied along the shoreline to simulate the sea (assigning a head equal to zero) and along the upper edge of the modeling domain (assigning a head of 4 m). In particular, the groundwater flow conditions described by Polemio & Ricchetti (1991) were considered. They were obtained by reconstructing the piezometric surface trend using data from 26 stations of the National Hydrographic Service present in the Metaponto coastal plain and active on average for about 30 years between 1927 and 1976.

The River boundary condition is a conceptualization of surface water features used to simulate the influence of a surface water body on the groundwater flow system. The conceptualization of rivers is represented by a seepage layer of bed sediments that is assumed to have a flat bottom, with no seepage through the sides of the channel. The Basento River has a variable water pull. According to data from the hydrological annals of the National Hydrographic Service available for the hydrometric stations of Mercuragno and Torremare (shown in **Fig. 29**) for 1925-1938, the river stage is lower than 0.55 m on average. Therefore, the River boundary condition was assigned to Basento River cells up to the Mercuragno station, since the observed river stages were found to be significant up to this station.

The Recharge boundary condition simulates the superficially-distributed recharge to the groundwater system. Climate data and the results of the previously described inverse hydrogeological water balance for 1925-1979 were used for the recharge assessment, considering it to be free of the relevant effects of climate change. For the area chosen for numerical modeling, recharge was estimated to be 27 mm/year and assigned to the entire domain.
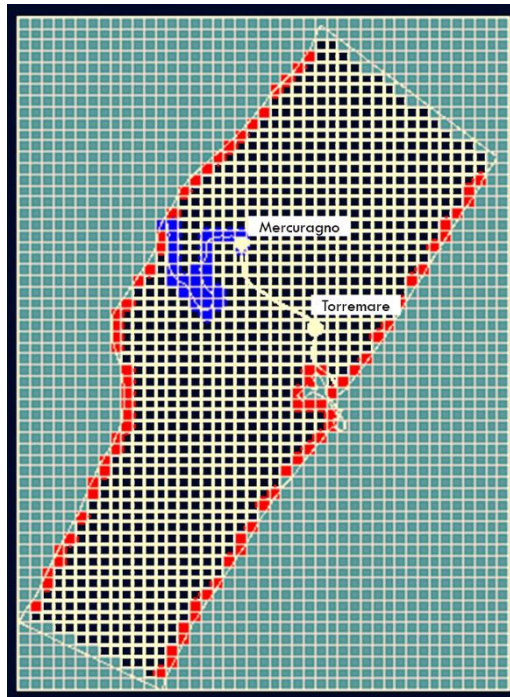

Fig. 29 *Assigned boundary conditions under steady-state flow conditions - inactive cells (in blue), Constant Head (in red), River (in blue), Recharge (in black) - and location of Mercuragno and Torremare hydrometric stations.*

After defining the boundary conditions, seven observation wells were added to the numerical model for calibration (**Fig. 31**), against which to compare the calculated results. Data of measured values of heads provided by CNR's Research Institute IRPI were loaded in the software and included for calculating the objective function. To aid in the calibration of the model, PEST is tasked with minimizing an objective function Φ, which is ultimately a function of the defined parameters (p_j) and consists of the sum of the weighted squared deviations between the calculated (X_{calc}) and observed (X_{obs}) system responses. For a groundwater model, these system responses are typically the head at a point in space. The residual r_i is the difference between the calculated and observed values:

$$r_i = X_{obs} - X_{calc} \tag{20}$$

In the simplest PEST run, the objective function Φ is computed using the equation:

$$\Phi = \sum_1^n \min(r_i) = f(p_j) \tag{21}$$

Horizontal conductivity K_x was selected as the parameter to include in the PEST run. A transformation option can be also specified for the parameter sensitivity derivatives. The Parameter Transformation field controls how the parameter value will be transformed during the optimization process. By default, all conductivity parameters are set to Log transformation: instead of using the parameter's "actual" value, the log value is optimized. Many studies mentioned in the groundwater literature that consider hydraulic conductivity as a regionalized variable show that a log variogram is better than a variogram based on native property values to describe its distribution.

Bounds of the values can be specified. In this simulation, $1,29*10^{-5}$ m/s and $1,71*10^{-4}$ m/s were entered as the minimum and maximum values of K_x, respectively. These data were provided by CNR's Research Institute IRPI.

Pilot points were defined and used as a means of characterizing the spatial distribution of the aquifer hydraulic conductivity. Pilot points are XY points with an initial value for the parameter that PEST must estimate. Examples include points where data concerning pumping/slug test data are available. For all other points, their initial value is taken from the property zone in which they lie. The use of pilot points to characterize the spatial distribution of a hydraulic property is accompanied by a mechanism whereby hydraulic property values assigned to pilot points are spatially interpolated to the cells of the finite difference grid. The Kriging algorithm is employed for such spatial interpolation (Webster & Oliver, 2007). General tips on using pilot points can be followed[3]:

- use more pilot points in areas of the model domain with a high spatial density of information (e.g., where there are more observation wells);
- place pilot points between head measurement wells in the direction of groundwater flow where they indicate hydraulic conductivity.
- place hydraulic conductivity pilot points between measurement wells and any downstream boundary, since the hydraulic conductivity of the material between these wells and the boundary determines the heads in those wells.
- avoid leaving any large gaps in the final pilot points pattern.

---

[3] https://pesthomepage.org/frequently-asked-questions

A set of 35 pilot points was imported into the software trying to comply with the described suggestions. Twenty points whose conductivity values were provided by CNR's Research Institute IRPI, were specified as fixed. For the others, instead, their initial values were taken from the property zone in which they lay.

The kind of regularization to use in the PEST analysis was chosen. Regularization introduces new information into the model's objective function in the form of "prior information equations". Regularization is used in the calibration process for two reasons. Firstly, it greatly improves the numerical stability of the parameter estimation problem. Secondly, if regularization constraints are properly defined, model calibration can proceed with a "homogeneous unless proven otherwise" philosophy. In other words, PEST will make each zone within the model domain as uniform as it can in terms of the distribution of the estimated hydraulic property, introducing heterogeneity into a zone only where this is necessary in order to allow a good of fit between model outputs and field data to be achieved, despite it has a variety of parameters at its disposal. In this model, the Preferred Homogenous Tikhonov Regularization was chosen, which introduces only enough heterogeneity into the system as necessary in order to achieve numerical stability. Tikhonov Regularization can induce PEST to prefer a more homogeneous solution (i.e., pilot points close together should have similar values) or to prefer parameter values that are as close to their initial values as possible. The new information added by the Tikhonov regularization approach to the overall problem helps to guide PEST toward reasonable parameter estimates based on the user's knowledge of the modelled domain and to avoid 'overfitting' solutions.

After the PEST run was completed, the results were analysed. The graph showing the observed and calculated head values and the table with the residuals obtained for each well are presented below (**Fig. 30** and **Tab. 18**). The coefficient of determination R^2 is equal to 0.82, and the absolute value of the maximum residual is 1.30 m for well n. 54.
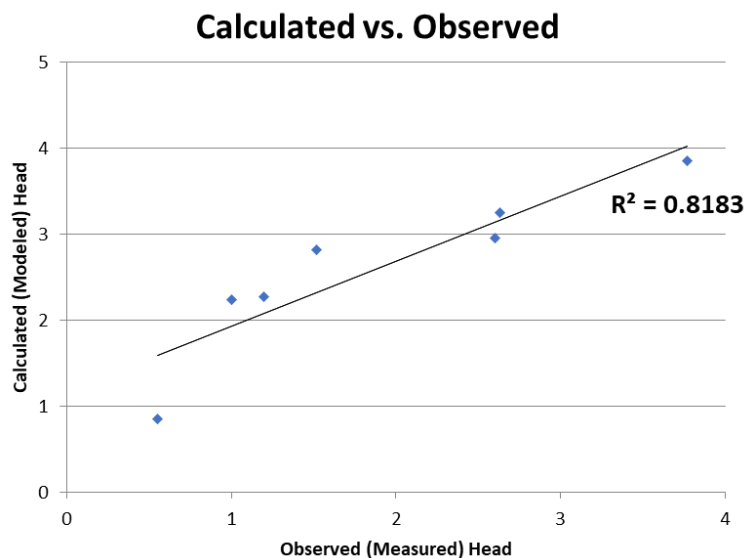

Fig. 30 Observed and calculated head values under steady-state conditions, before calibration.

Observation well	Head Measured (m)	Head Modeled (m)	Residual (m)
54	1.52	2.82	-1.30
72	2.63	3.26	-0.63
73	2.60	2.95	0.35
123	3.77	3.86	-0.09
129	1.00	2.24	-1.24
142	0.55	0.85	-0.30
143	1.20	2.28	-1.08

Tab. 18 Observed and calculated head values with residuals.

The adjusted K_x parameter zonation obtained after reviewing the PEST run outputs was saved as inputs for a new model run (**Fig. 31**). VMOD Flex saved the adjusted model parameters in a new model run within the same project. This new model run was translated and run in order to see the updated MODFLOW results using the adjusted K_x parameter from PEST.
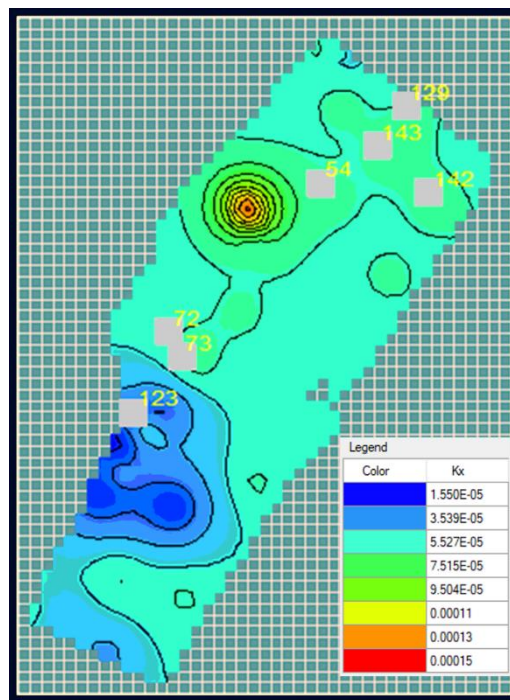
Fig. 31 K_x values obtained after calibration performed with PEST and location of the observation wells.

The obtained results are shown in the figures below, which depict the head trend in the modeling domain (**Fig. 32**) and the new graph with the observed and calculated head values (**Fig. 33**). The correlation coefficient is equal to 0.91, the absolute value of the maximum residual is 1.34 m for well n. 129. Groundwater flow modeling under steady-state conditions confirms the reconstruction of the spatial trend of the piezometric surface (**Fig. 8**).
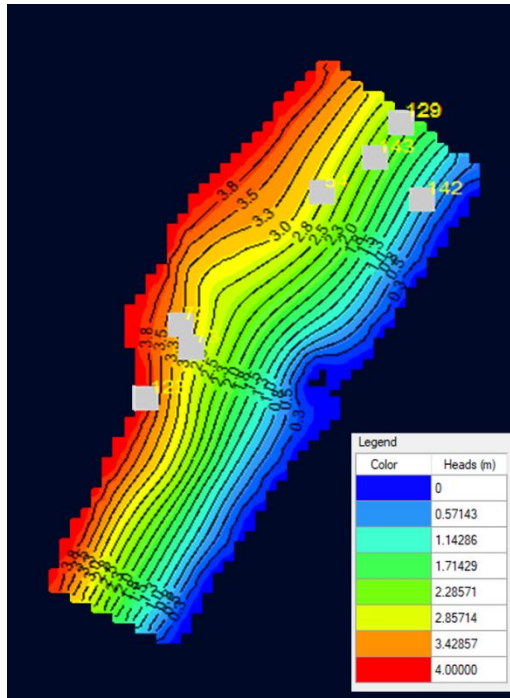
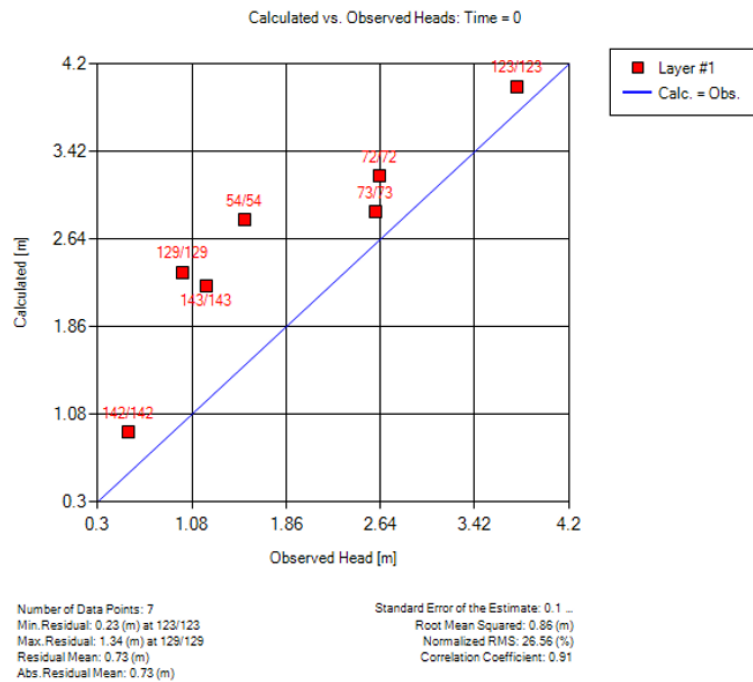***Fig. 32*** *Head trend in steady-state conditions after the calibration.*

Fig. 33 *Observed and calculated head values after calibration.*

10.2 Transient conditions

For groundwater flow modeling under transient conditions, the only boundary condition that differs from the steady-state conditions is the Constant Head at the top edge of the modeling area. The schedule was set as transient, and the starting heads and ending heads were specified. Since data were available for some wells of the PRISMAS network (**Fig. 34**) between the winter of 1997 (hereinafter I97) and the winter of 1999 (I99), an end time of 730 days was assigned. Interpolated heads from the I97 and I99 data were assigned as starting head and ending head, respectively. The results of the first run are shown in the figures below for each time step (**Fig. 35**).
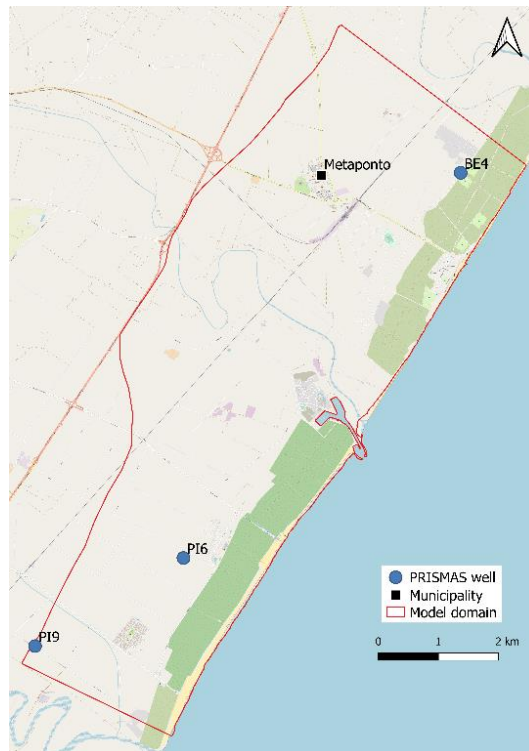
Fig. 34 *Location of PRISMAS network wells used for calibration under transient conditions.*
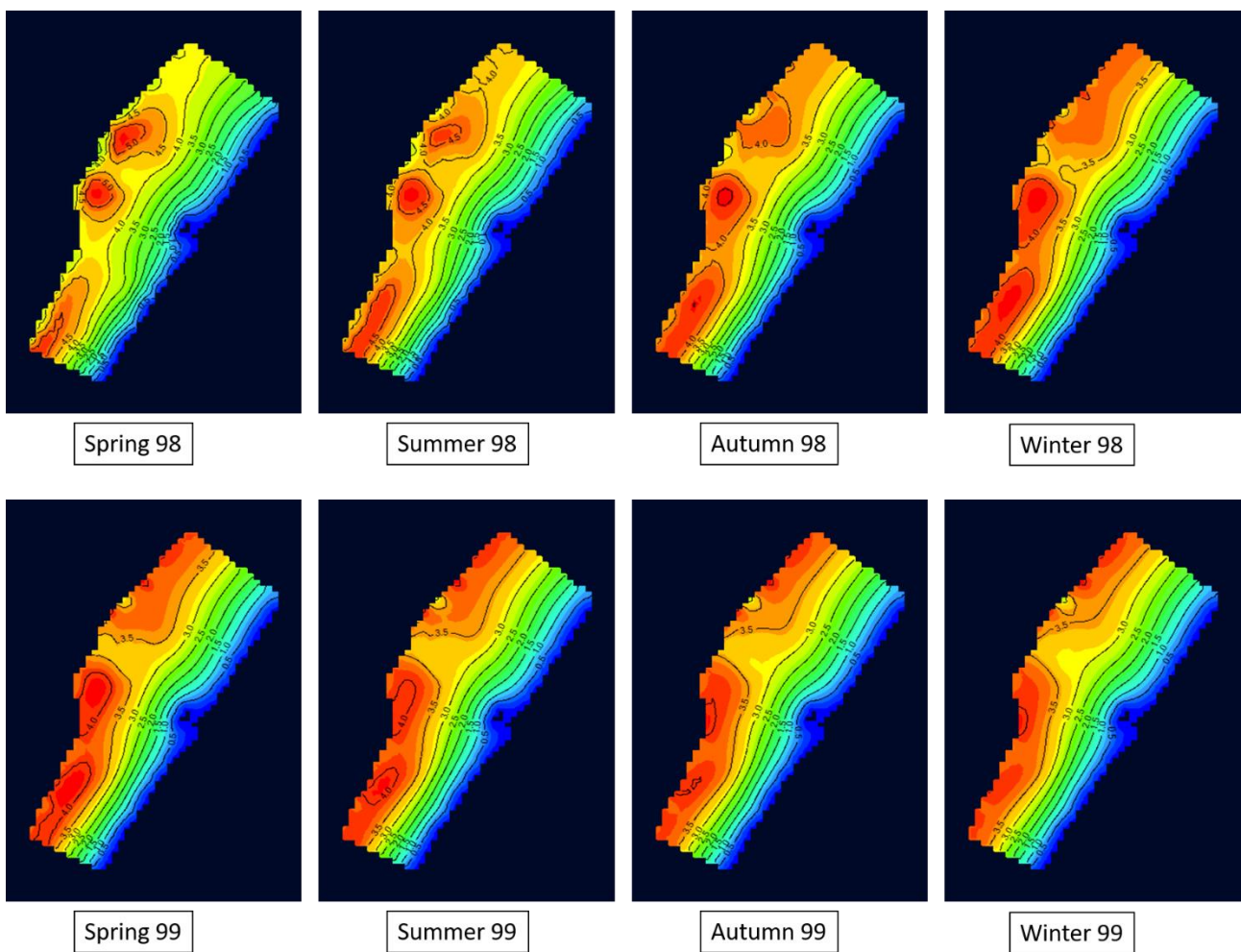

Fig. 35 *Results of the first run under transient conditions, before calibration.*

Specific storage S_s and specific yield S_y are the parameters included in the PEST run for the calibration of the simulation in transient conditions. They are only used in the transient run. These parameters were assigned default values: $S_s = 1 * 10^{-5} m^{-1}$ and $S_y = 0.2$. After the PEST run was completed, the results were analysed. The graph showing the observed and calculated head values is presented below (**Fig. 36**). The coefficient of determination R^2 is equal to 0.28.
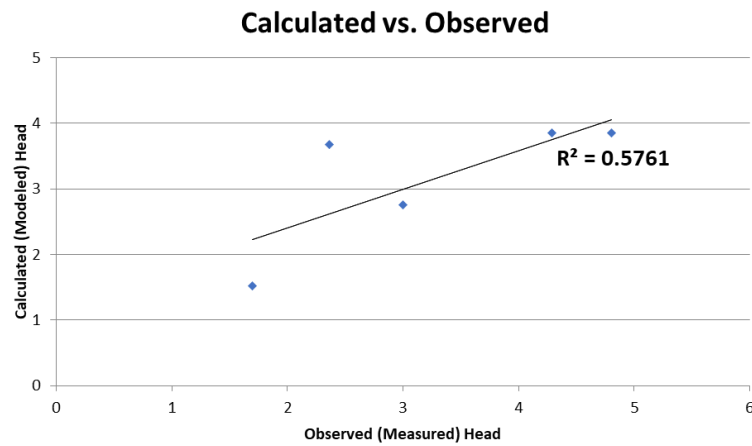
Fig. 36 Observed and calculated head values under transient conditions, before calibration.

The adjusted S_s and S_y zonation obtained after the PEST run was saved as inputs for a new model run. This new model run was translated and run in order to see the updated results using the adjusted S_s and S_y parameter from PEST.
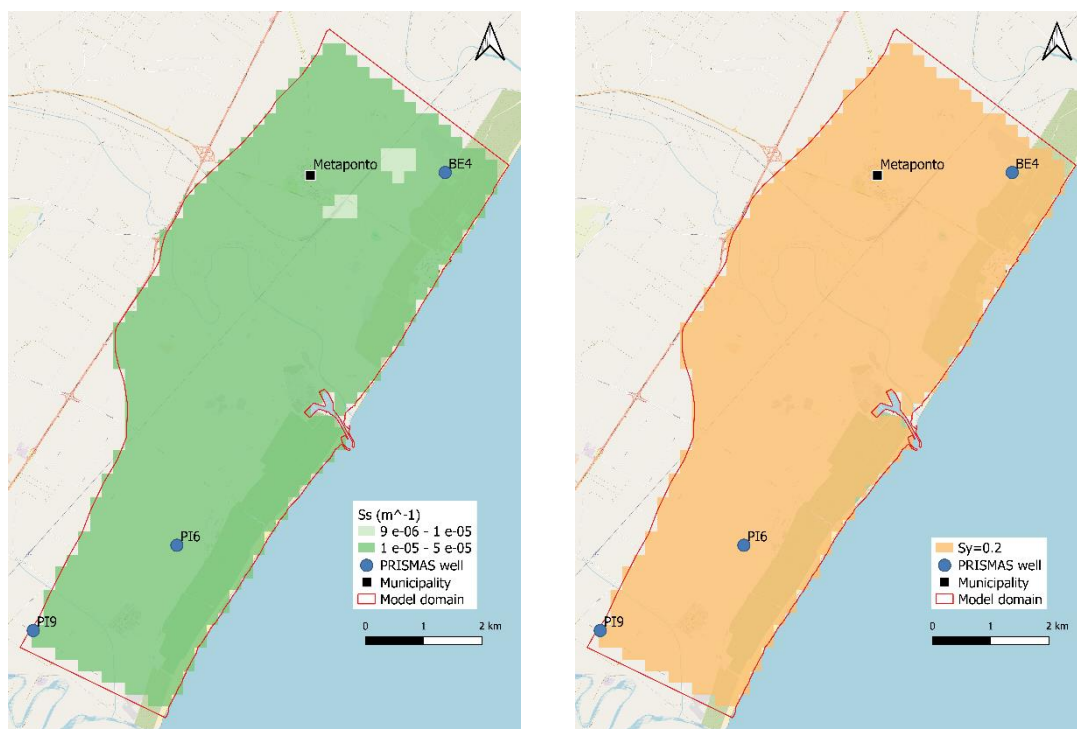

Fig. 37 Ss and Sy values obtained after the calibration performed with PEST, and location of the PRISMAS network wells.

The obtained results are shown in the figures below, which depict the graph with the observed and calculated head values and the head trend in the modeling domain (**Fig. 38** and **Fig. 39**), and in **Tab. 19** with the residuals of each well. The coefficient of determination R^2 is equal to 0.60, the absolute value of the maximum residual is 1.25 m for well PI6 in spring 1998.
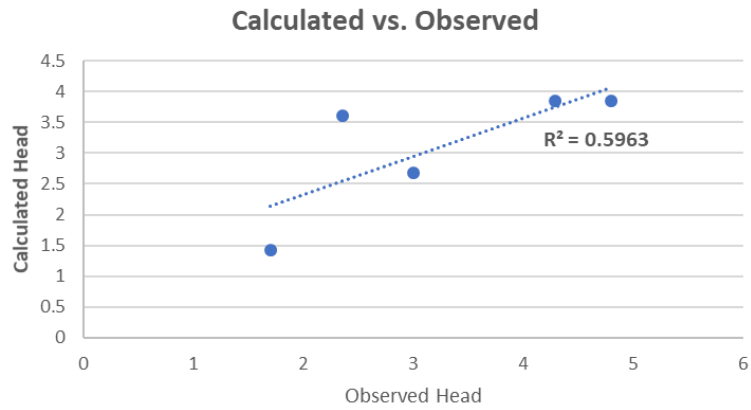
Fig. 38 *Observed and calculated head values under transient conditions, after the calibration.*
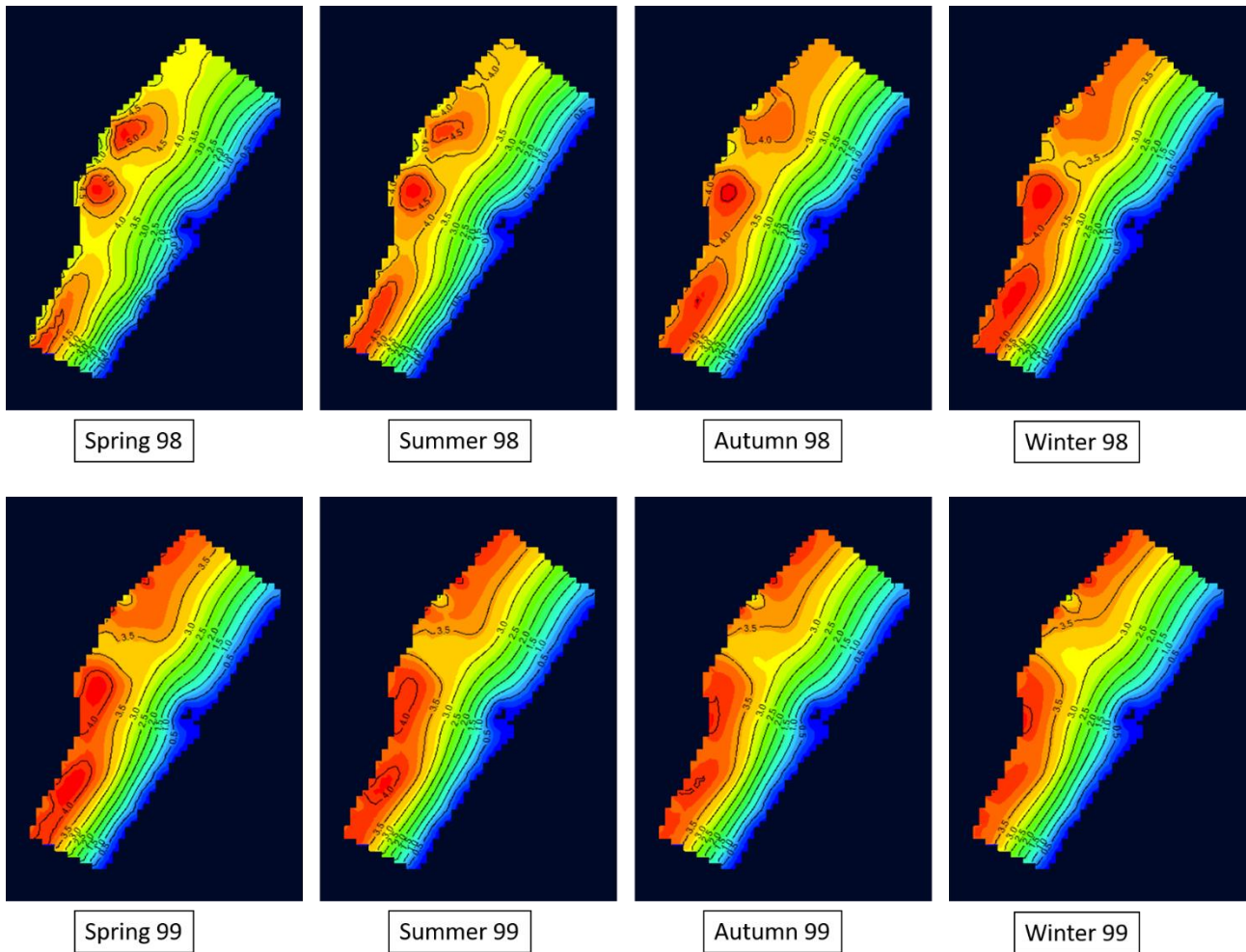

Fig. 39 *Results after calibration under transient conditions.*

Well	Observation	Head Measured (m)	Head Modeled (m)	Residual (m)
PI6	Spring 98	2.36	3.61	-1.25
PI9	Spring 98	4.29	3.85	0.44
BE4	Autumn 98	1.70	1.43	0.27
PI6	Winter 99	3.00	2.68	0.32
PI9	Winter 99	4.80	3.85	0.95

Tab. 19 *Observed and calculated head values with residuals under transient conditions after the calibration.*

11. Seawater intrusion numerical modeling

Seawater intrusion (SWI) phenomenon often occurs along coastlines worldly. Since seawater is denser than freshwater, it consequently tends to move inland underlying freshwater zones when groundwater resources are depleted or in areas where the water table is low. When the freshwater discharge force balances the buoyancy force due to density, a static equilibrium is reached.

VMOD Flex includes SEAWAT v.4.00.05 to simulate SWI. SEAWAT software (Guo & Langevin, 2002; United States Geological Survey, 2012) was developed by the USGS, based on a combination of MODFLOW and MT3D-MS. It is used for simulating three-dimensional, transient, variable-density groundwater flow and multi-species solute transport in porous media.

SEAWAT was selected as the numerical engine for the simulation and the saturated (variable density) flow type was specified. The concentration of total dissolved solids (TDS) expressed in mg/l was selected as the chemical indicator of SWI. For the vertical discretization, the model was divided into ten layers, each with an average thickness of 4.86 m.

Since direct data on TDS concentration in the model area weren't available, groundwater electrical conductivity values measured for selected samples were considered (**Fig. 11**). Changes in conductivity are closely related to the fixed residue, which can be calculated with good approximation by means of the following formula (Rodier, 1975):

$$RF = \alpha \delta_{20} \tag{22}$$

where RF is the fixed residue in (mg/l), α is a transformation coefficient, and δ_{20} is the conductivity at 20 °C. The **Tab. 20** shows the transformation coefficient values for conductivity ranges (Richard & Nguyen Van Cu, 1961).

conducibilità a 20 °C (μS/cm)	< 50	50 ÷ 166	167 ÷ 333	334 ÷ 833	834 ÷ 10.000	> 10.000
coefficiente (α)	1,365079	0,947658	0,769574	0,715920	0,758544	0,850432

Tab. 20 Coefficient for calculating water mineralization (Richard & Nguyen Van Cu, 1961), from (Celico, 1988).

In the study case, electrical conductivity values measured at 25 °C were available for the selected samples. Therefore, the following formula was applied to calculate the electrical conductivity at the standard temperature of 20 °C δ_{20} (Celico, 1988):

$$\delta_{20} = \delta_T c \tag{23}$$

where δ_T is the conductivity at the measurement temperature and c is a coefficient taken from **Tab. 21**.

Results are shown in **Tab. 22**. The average value of 669 mg/l was derived from the obtained TDS concentrations. This value was assigned as Initial Concentration property everywhere in the model domain, except in cells in contact with the sea, where the Constant Concentration boundary condition was applied. These cells were assigned the Ionian Sea salinity (in terms of TDS), equal to 39500 mg/l (Grauel & Bernasconi, 2010). The same concentration was assigned to the cells at the fresh water/salt

water interface, calculated using the head outputs obtained from simulation under steady-state conditions, by means of the Ghyben-Herzberg relationship (Ghyben, 1888; Herzberg, 1901):

$$\rho_s z = \rho_f z + \rho_f h \tag{24}$$

where: ρ_s is the density of salt water, equal to 1030.7 kg/m³ for the Ionian Sea (Cotecchia, 2014); z is the depth of fresh water below sea level; ρ_f is the density of freshwater, equal to 1000 kg/m³; h is the thickness of the freshwater zone above sea level.

Cells at the Basento River were assigned a TDS concentration of 575 mg/l, calculated from sampled electrical conductivity values reported in the Basilicata Region Water monitoring plan (2017)[4].

gradi centigradi	decimi di grado									
	0	1	2	3	4	5	6	7	8	9
5	1,490	1,488	1,483	1,479	1,477	1,468	1,464	1,459	1,455	1,449
6	1,445	1,440	1,436	1,432	1,428	1,424	1,418	1,414	1,410	1,404
7	1,400	1,396	1,392	1,388	1,385	1,379	1,375	1,371	1,368	1,362
8	1,358	1,353	1,349	1,347	1,342	1,340	1,335	1,331	1,328	1,324
9	1,319	1,316	1,312	1,308	1,305	1,300	1,297	1,293	1,288	1,285
10	1,282	1,279	1,277	1,273	1,269	1,265	1,261	1,257	1,254	1,250
11	1,246	1,244	1,242	1,239	1,234	1,231	1,227	1,224	1,219	1,216
12	1,213	1,210	1,207	1,204	1,202	1,199	1,194	1,191	1,189	1,184
13	1,182	1,180	1,176	1,173	1,169	1,166	1,164	1,160	1,157	1,154
14	1,152	1,149	1,146	1,144	1,141	1,138	1,135	1,132	1,129	1,127
15	1,123	1,121	1,118	1,116	1,112	1,109	1,107	1,103	1,101	1,099
16	1,096	1,094	1,091	1,088	1,086	1,084	1,081	1,078	1,075	1,073
17	1,070	1,069	1,067	1,064	1,061	1,059	1,056	1,053	1,050	1,048
18	1,046	1,044	1,043	1,039	1,037	1,035	1,033	1,029	1,027	1,025
19	1,023	1,022	1,019	1,016	1,014	1,012	1,010	1,008	1,004	1,002
20	1,000	0,999	0,996	0,994	0,992	0,990	0,988	0,985	0,983	0,981
21	0,979	0,977	0,975	0,973	0,970	0,969	0,967	0,965	0,962	0,960
22	0,958	0,956	0,954	0,952	0,950	0,947	0,946	0,943	0,941	0,940
23	0,938	0,937	0,934	0,933	0,931	0,929	0,926	0,926	0,923	0,921
24	0,919	0,918	0,916	0,915	0,912	0,910	0,908	0,907	0,905	0,902
25	0,902	0,899	0,897	0,896	0,893	0,891	0,889	0,888	0,885	0,885

Tab. 21 Correction factors (c) for homogenization at 20 °C of water conductivity (Rodier, 1975), from (Celico, 1988).

Sampled well	Electrical conductivity at 25 °C (µS/cm)	Electrical conductivity at 20 °C (µS/cm)	TDS (mg/l)
4	1240	1118	848
13	890	803	575
15	1130	1019	773
24	517	466	334
25	627	566	405
29	980	884	671
30	1284	1158	879
31	1268	1144	868

*Tab. 22 TDS values obtained from electrical conductivity measured in sampled wells (see **Fig. 11** for location)*

The following figures (from **Fig. 40** to **Fig. 49**) show the TDS concentrations in the modeling domain from layer 1 to layer 10 for the eight time steps considered for the simulation under transient conditions.

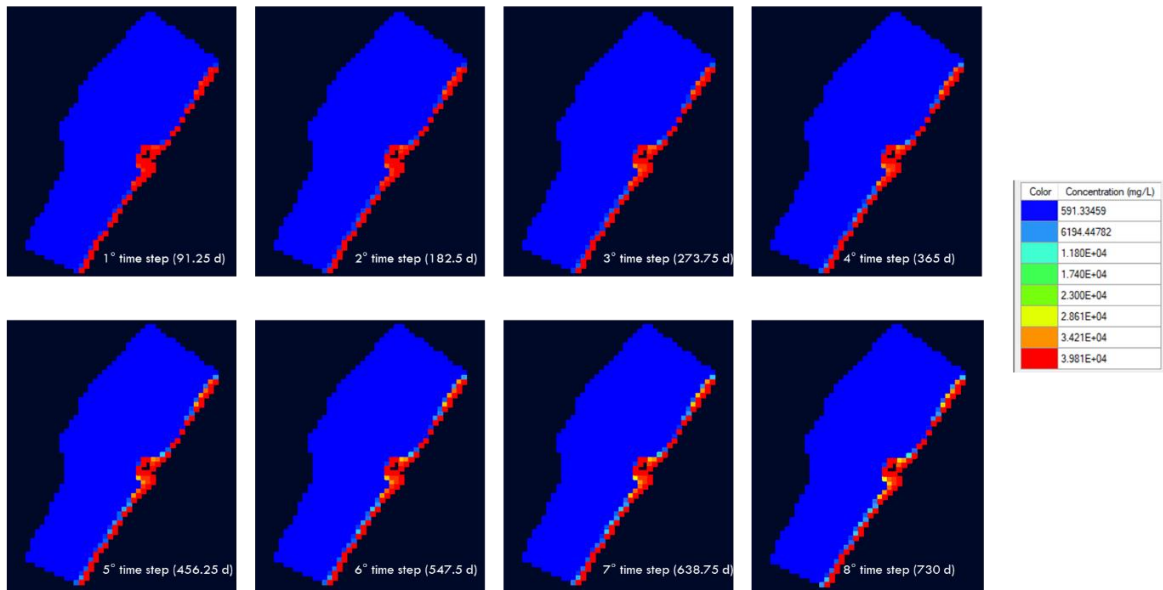[4] Piano di Monitoraggio Acque (regione.basilicata.it)

Fig. 40 *TDS concentrations for the layer 1 (elevation 0.79 m).*
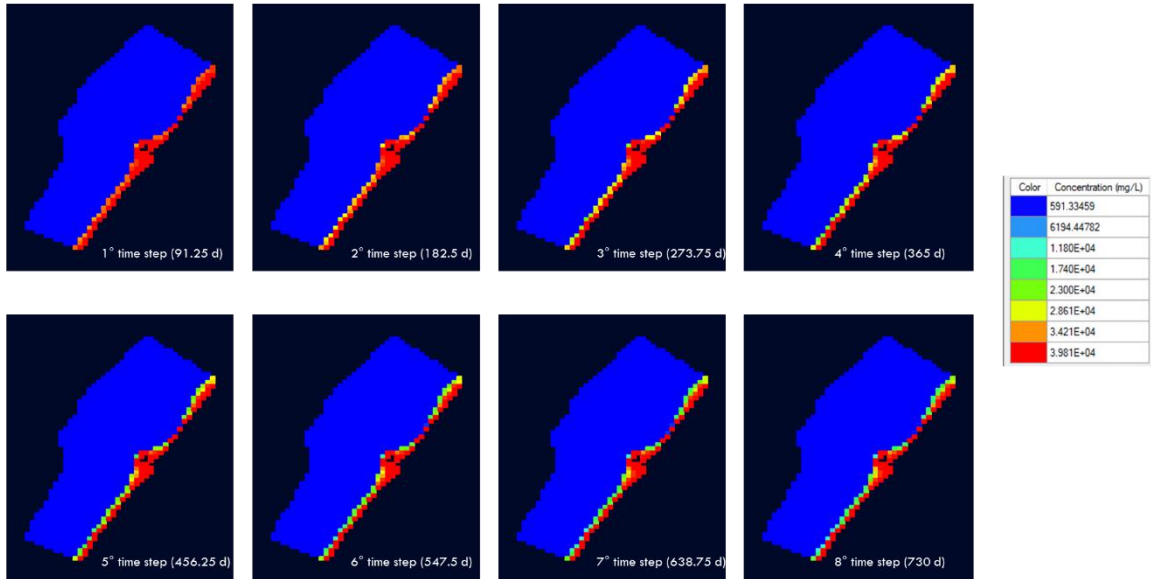

Fig. 41 *TDS concentrations for the layer 2 (depth 4.08 m).*
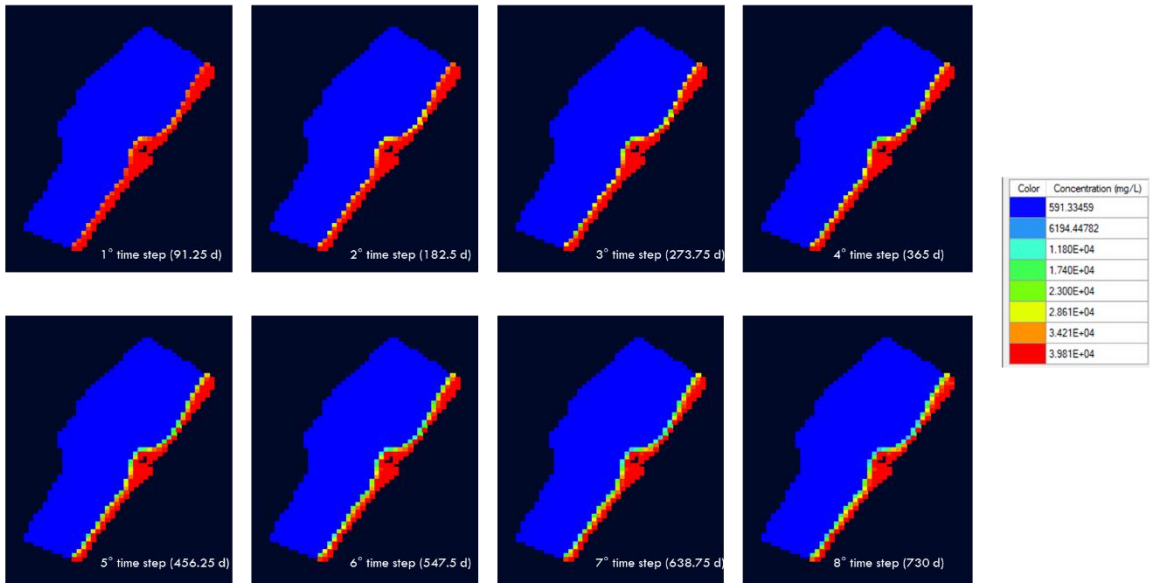
Fig. 42 *TDS concentrations for the layer 3 (depth 8.95 m).*
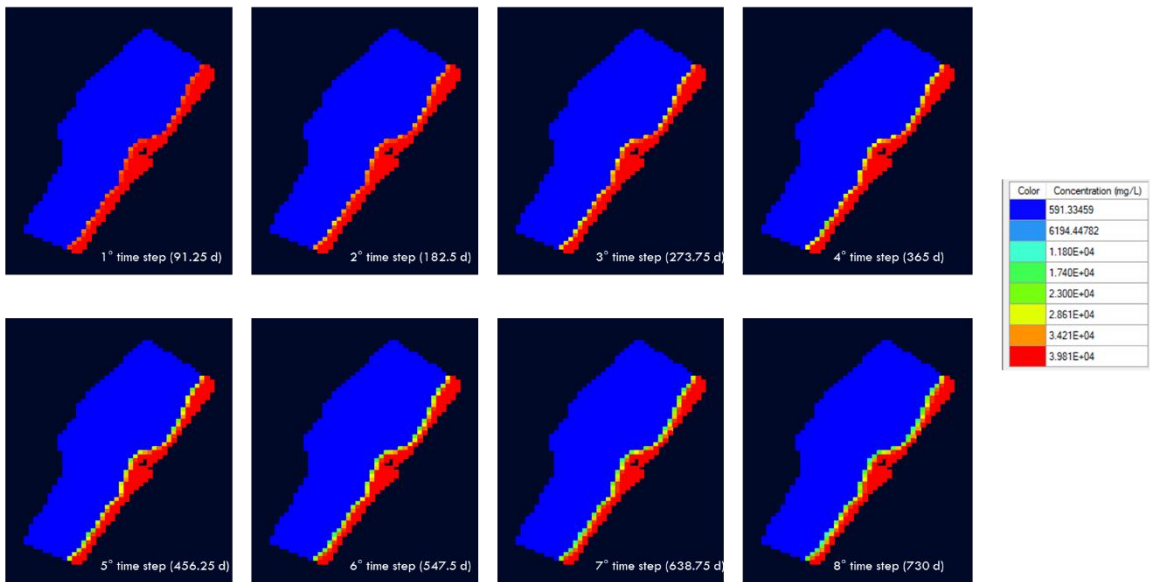

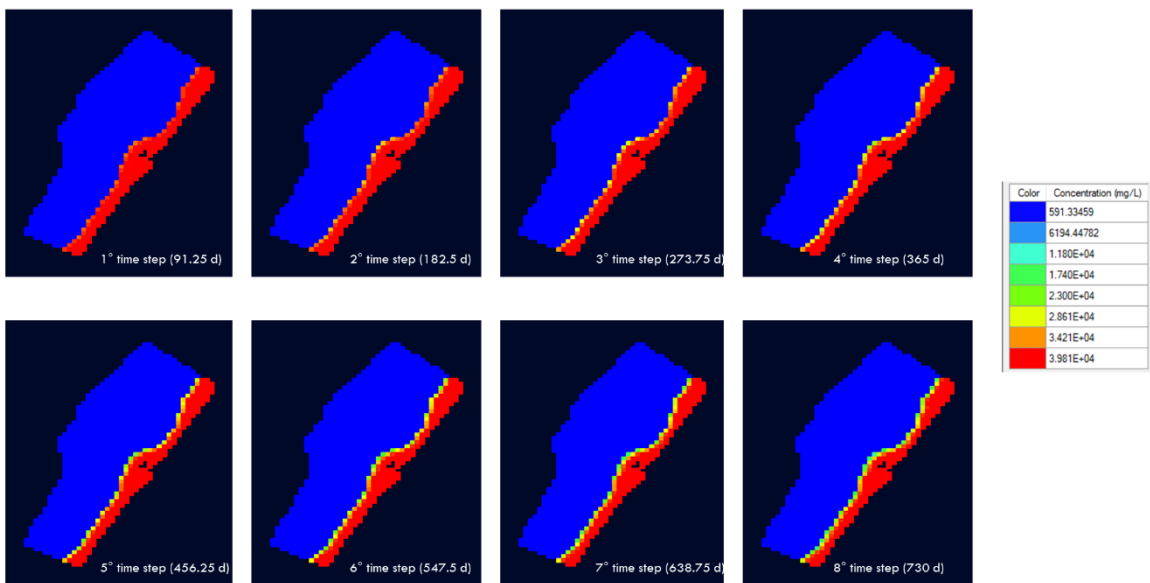**Fig. 43** *TDS concentrations for the layer 4 (depth 13.83 m).*

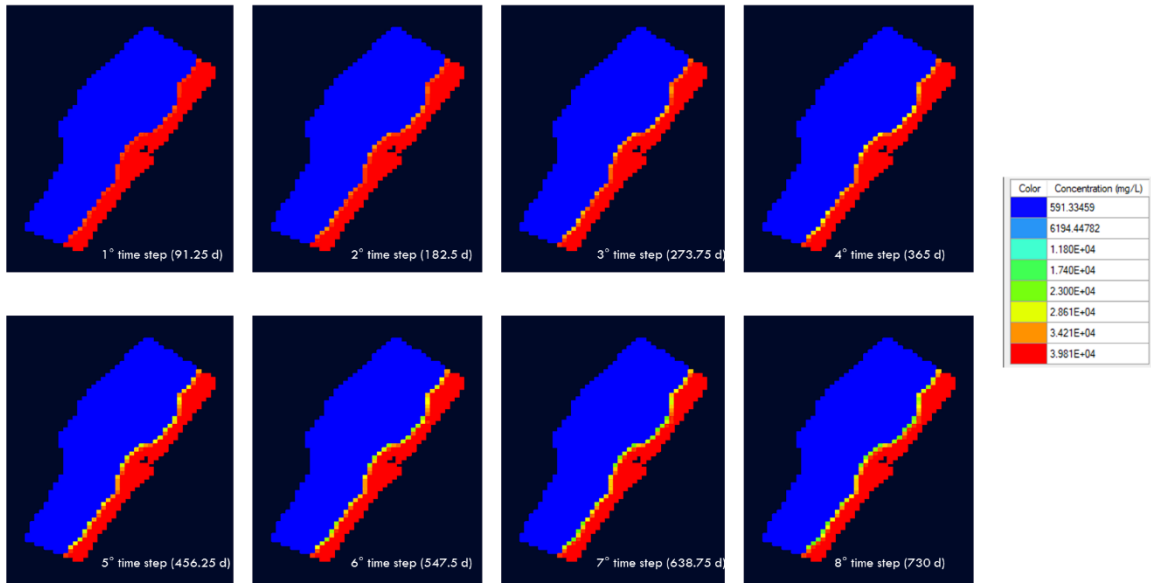**Fig. 44** *TDS concentrations for the layer 5 (depth 18.70 m).*

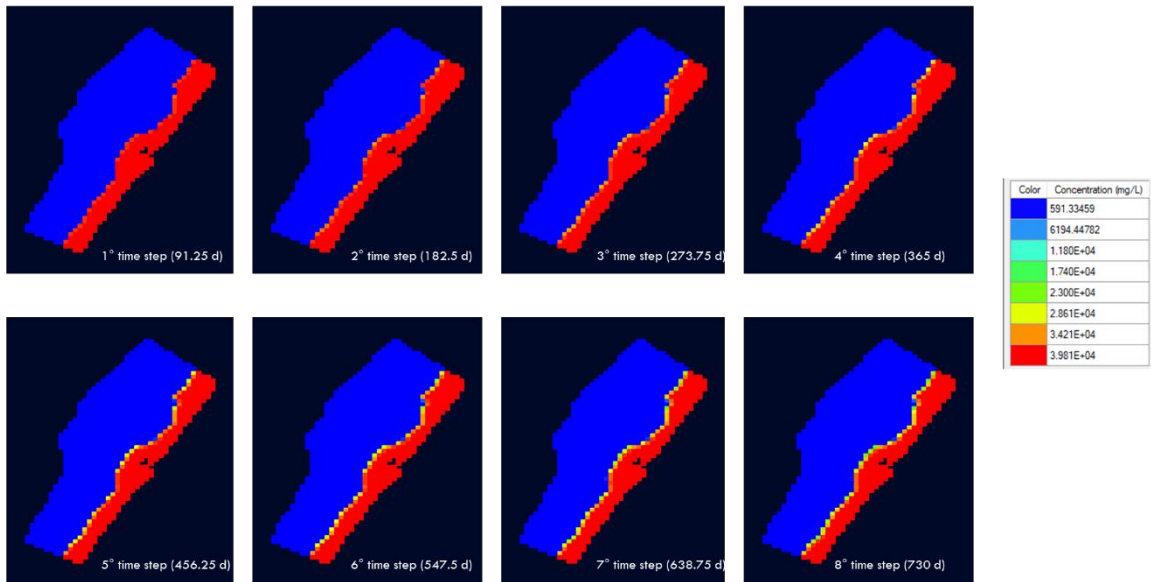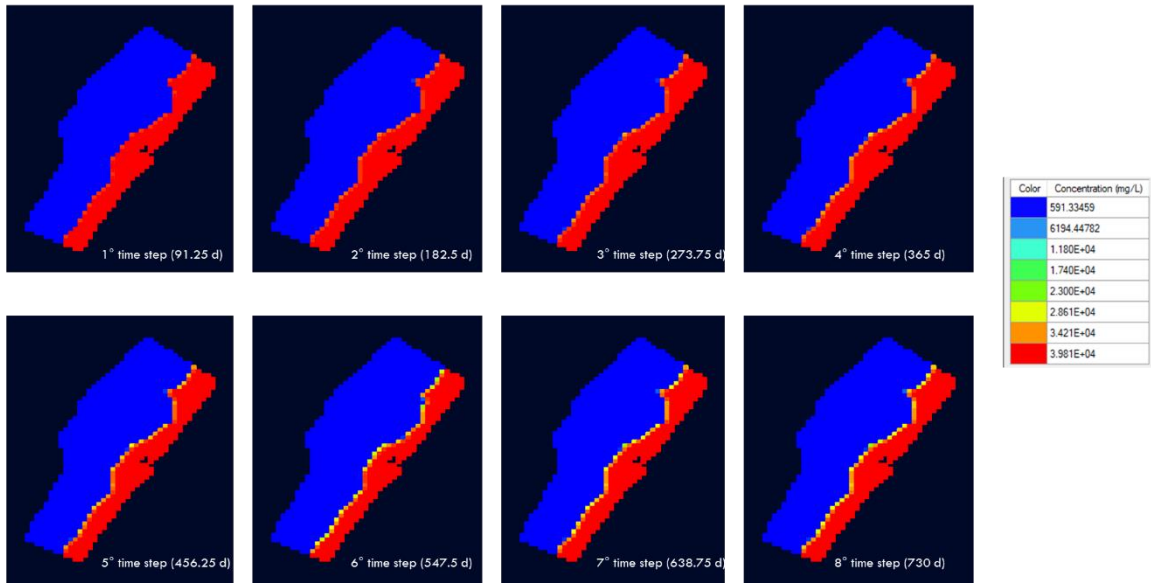**Fig. 45** *TDS concentrations for the layer 6 (depth 23.57 m).*

Fig. 46 *TDS concentrations for the layer 7 (depth 28.45 m).*

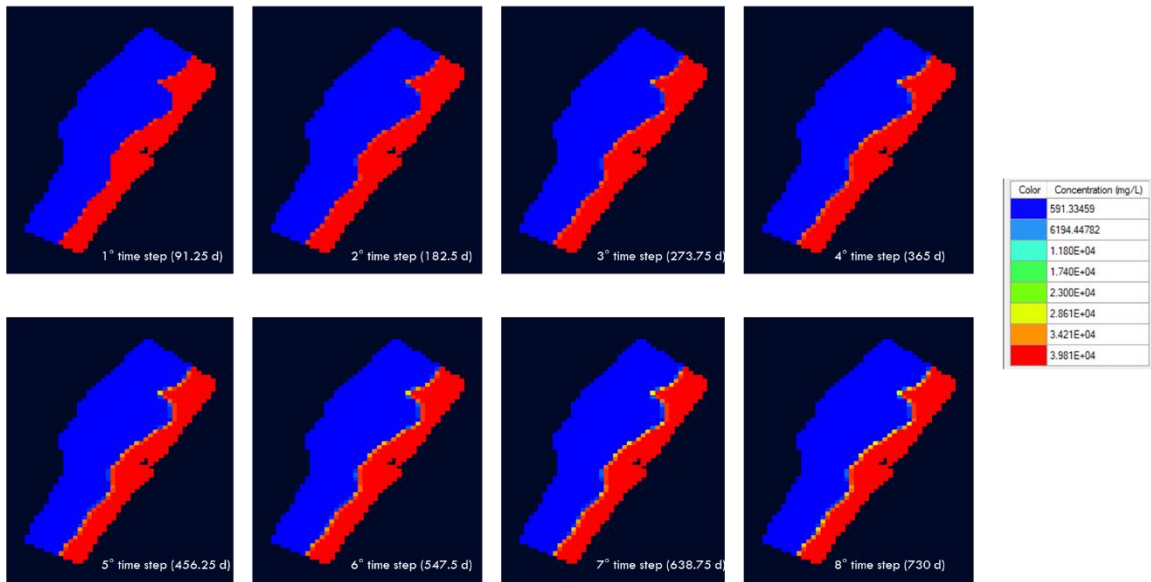**Fig. 47** *TDS concentrations for the layer 8 (depth 33.32 m).*

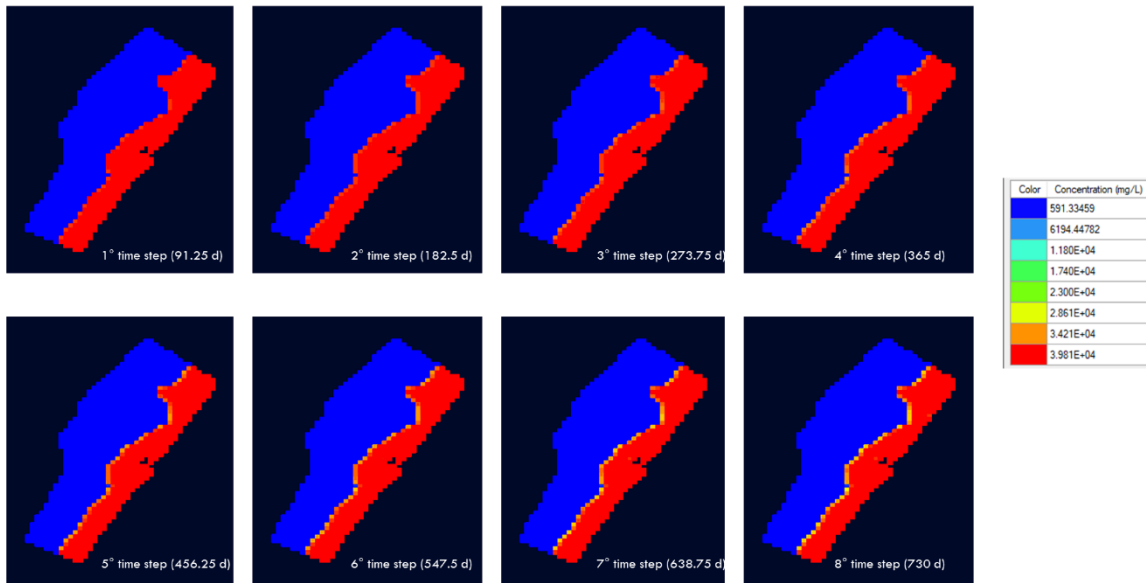**Fig. 48** *TDS concentrations for the layer 9 (depth 38.19 m).*

Fig. 49 *TDS concentrations for the layer 10 (depth 43.06 m).*

11.1 Effects of climate change

According to the latest IPCC report on climate change (IPCC, 2022), the Mediterranean region has warmed and will continue to warm more than the global average, particularly in summer. This is true for the terrestrial and marine environments, for average temperatures and heat waves. The region will become drier due to the combined effect of decreased precipitation and increased evapotranspiration. At the same time, extreme precipitation will increase in some areas. To assess the impact of climate change on the study area, the rainfall and temperature trends predicted by the A1B scenario of the Multi Global Model Ensemble (MGME) were considered (Giorgi & Lionello, 2008). This model makes predictions for the period 2001-2100 about temperature (i.e., the rise in Celsius degrees) and the change in precipitation in percent with respect to the mean values measured during the period 1961-1980, for which data were available. For temperature, in 2001-2020, an average rise for the entire Mediterranean basin of +0.9 °C was considered. For precipitation, a decrease of 3.9% was considered, compared to 1960-1980 (Romanazzi et al., 2015).

By redoing the inverse hydrogeological water balance with these variations of temperature and rainfall input, direct recharge (already extremely low, equal to 27 mm/year) is practically zero because evapotranspiration increases significantly.

It can be seen from the following results (from **Fig. 50** to **Fig. 59**) that there are no significant changes to the SWI phenomenon. Indeed, the aquifer recharge is provided by groundwater supply from upstream areas at higher elevations.
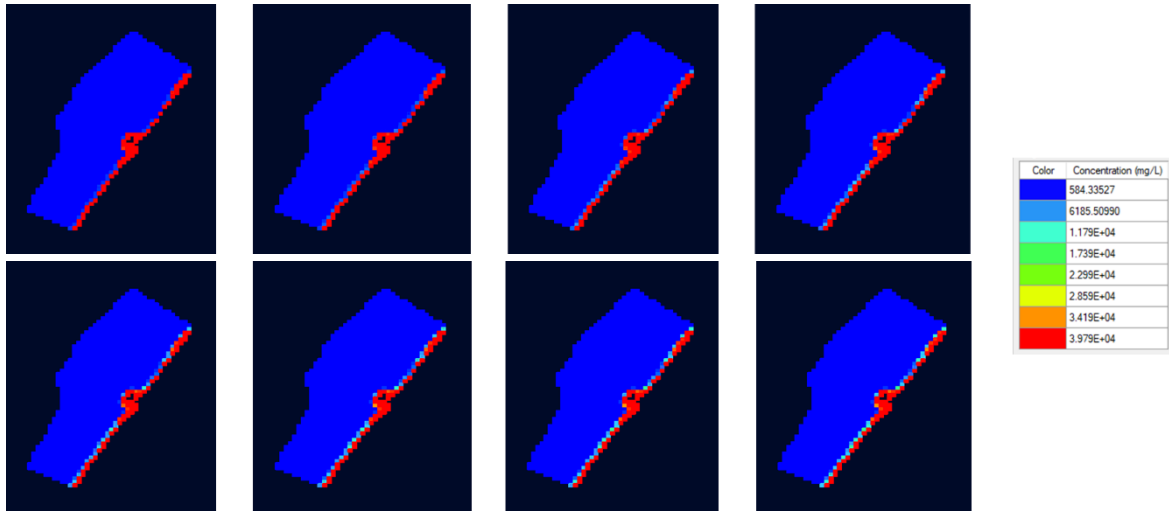
Fig. 50 *TDS concentrations for the layer 1 considering no recharge for the effects of climate change (the legend is also the same for the following figures).*
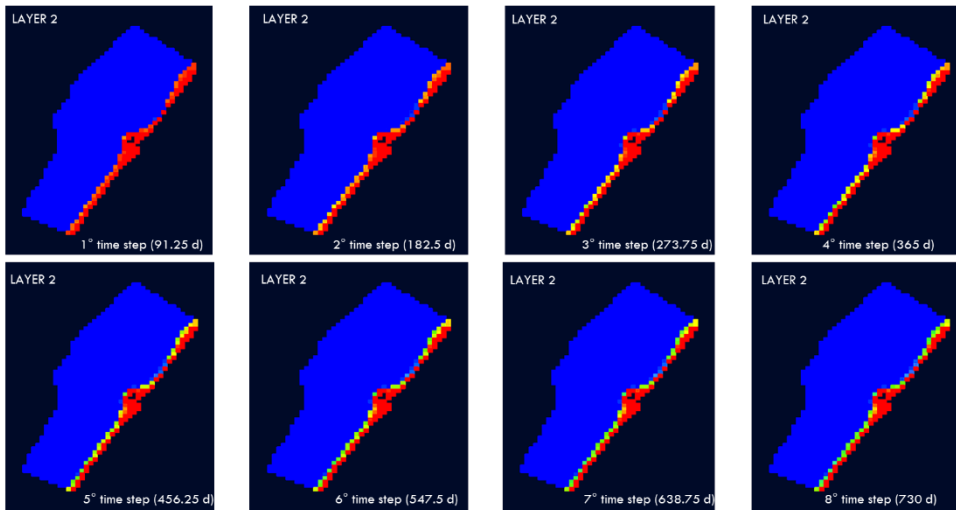

Fig. 51 *TDS concentrations for the layer 2 considering no recharge for the effects of climate change.*
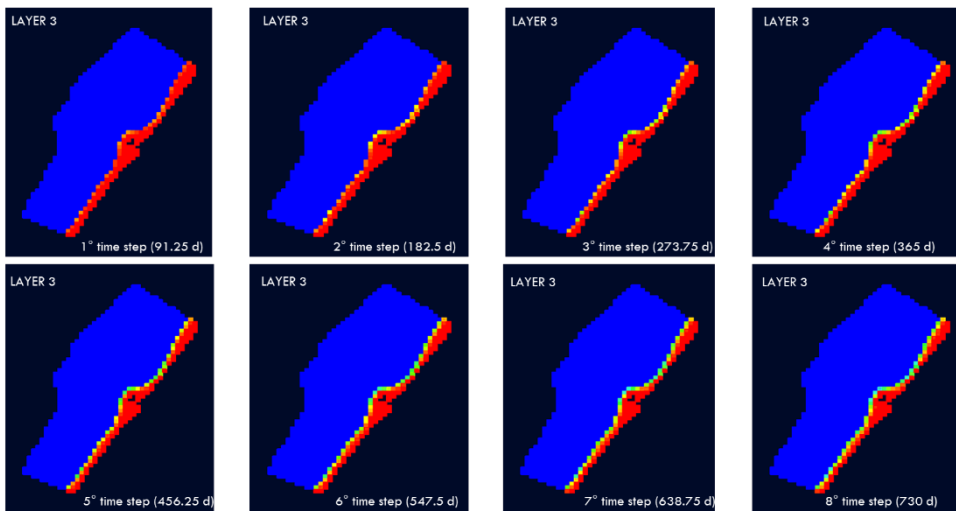

Fig. 52 *TDS concentrations for the layer 3 considering no recharge for the effects of climate change.*

82

Fig. 53 *TDS concentrations for the layer 4 considering no recharge for the effects of climate change.*

Fig. 54 *TDS concentrations for the layer 5 considering no recharge for the effects of climate change.*
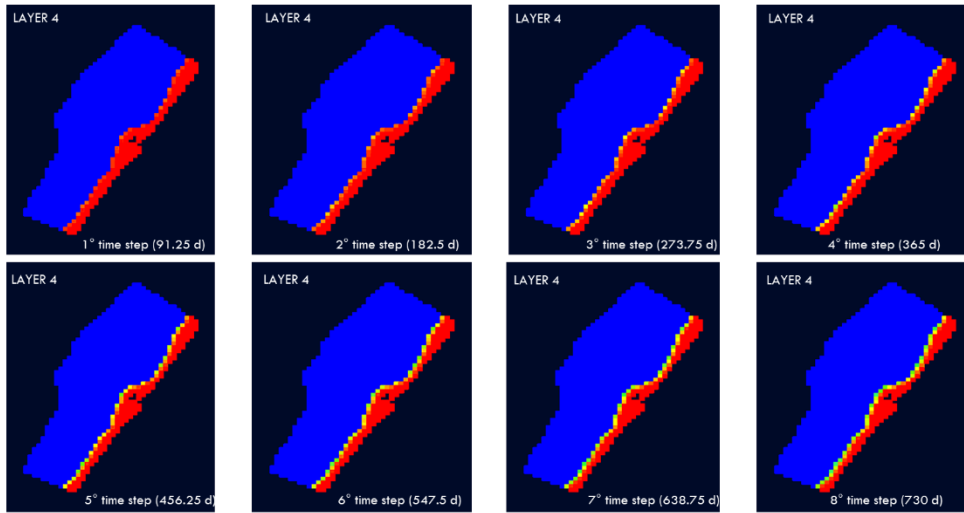

Fig. 55 *TDS concentrations for the layer 6 considering no recharge for the effects of climate change.*

Fig. 56 *TDS concentrations for the layer 7 considering no recharge for the effects of climate change.*

Fig. 57 *TDS concentrations for the layer 8 considering no recharge for the effects of climate change.*

Fig. 58 *TDS concentrations for the layer 9 considering no recharge for the effects of climate change.*
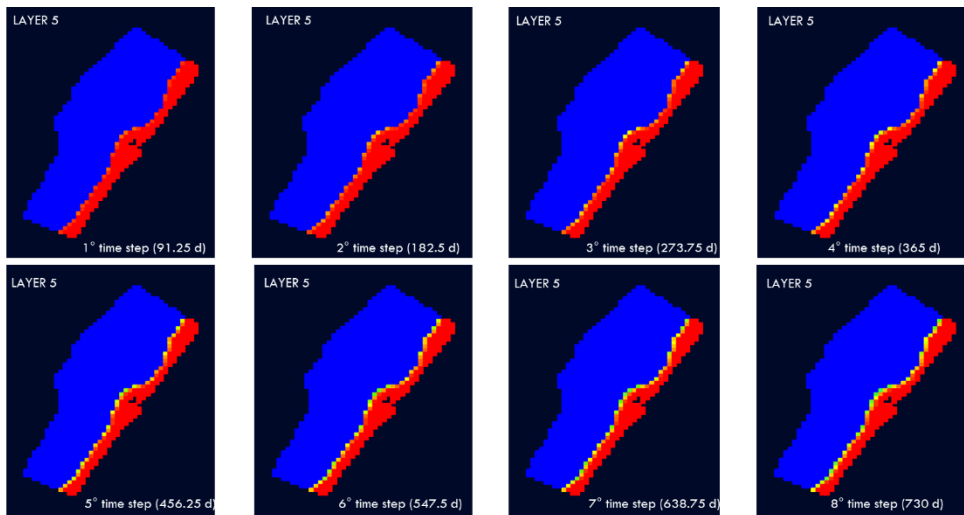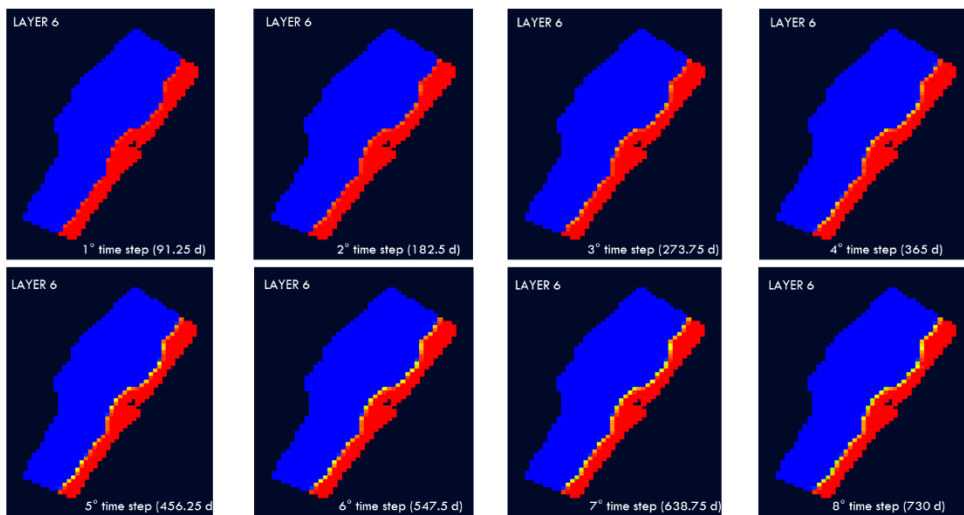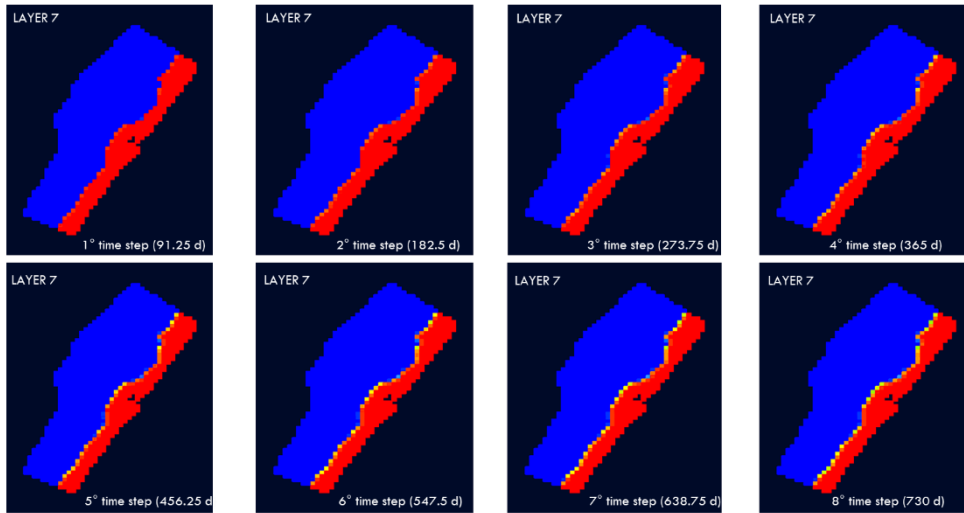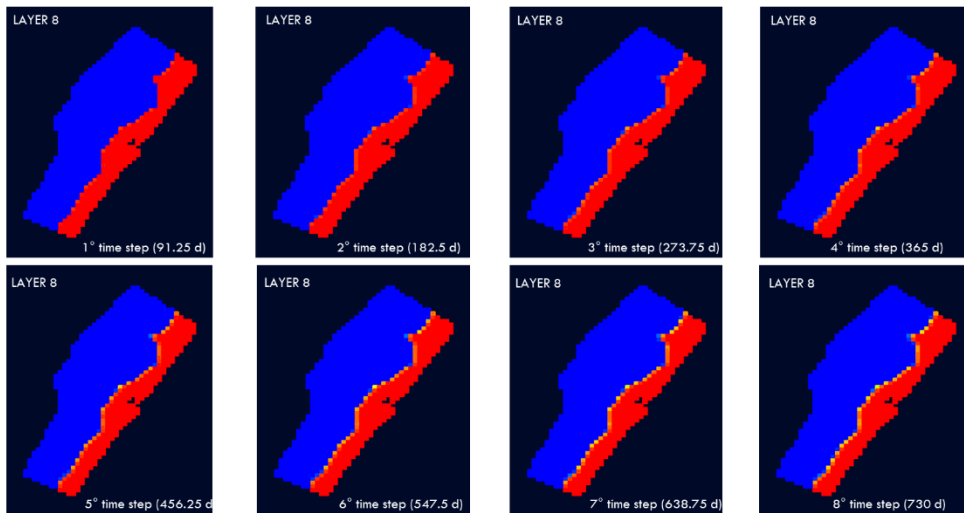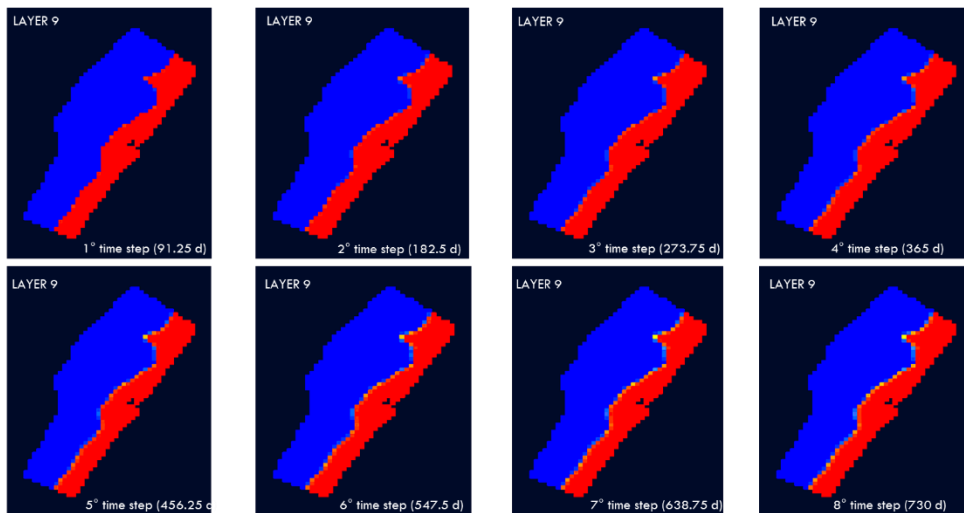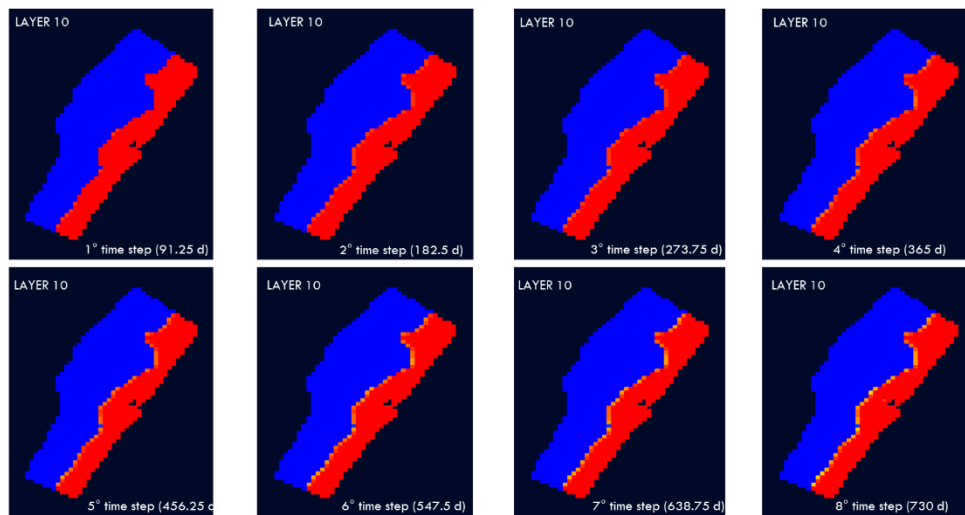
Fig. 59 *TDS concentrations for the layer 10 considering no recharge for the effects of climate change.*

11.2 Pumping wells scenarios

Further modeling was carried out by simulating two hypothetical pumping scenarios from five wells located in the study area. Three of these (BE4, PI6, PI9) are the wells used for calibration of the simulation under transient conditions, whereas the remaining two (2579 and 2586) were identified from the Basilicata Region's list of surveyed and authorized wells[5] (see **Fig. 60** and the following ones for well locations). Keeping the same characteristics of the modeling domain used for the simulation of SWI under transient conditions, a Pumping Well boundary condition was added to simulate the two scenarios. Two different pumping rates were assumed: one equal to 10 l/s, which is the average value obtained for the surveyed and authorized wells present in the entire coastal plain, and one of 100 l/s, to consider an extreme exploitation of the aquifer. Well data objects were imported in the model, and the pumping rates were kept activated and constant during the first two time steps, corresponding to the spring and summer seasons when water availability for irrigation of the numerous crops in the area decreases.

The following figures show the TDS concentration values obtained in each layer of the model domain, considering a pumping rate of 10 l/s.

---

[5] https://www.regione.basilicata.it/giunta/files/docs/DOCUMENT_FILE_3032152.pdf

Fig. 60 *TDS concentrations for the layer 1 considering a 10 l/s pumping rate (the legend is also the same for the following figures).*

Fig. 61 *TDS concentrations for the layer 2 considering a 10 l/s pumping rate.*

Fig. 62 *TDS concentrations for the layer 3 considering a 10 l/s pumping rate.*

Fig. 63 *TDS concentrations for the layer 4 considering a 10 l/s pumping rate.*

Fig. 64 *TDS concentrations for the layer 5 considering a 10 l/s pumping rate.*

87

Fig. 65 *TDS concentrations for the layer 6 considering a 10 l/s pumping rate.*

Fig. 66 *TDS concentrations for the layer 7 considering a 10 l/s pumping rate.*

Fig. 67 *TDS concentrations for the layer 8 considering a 10 l/s pumping rate.*

88

Fig. 68 _TDS concentrations for the layer 9 considering a 10 l/s pumping rate._

Fig. 69 _TDS concentrations for the layer 10 considering a 10 l/s pumping rate._

The following figures show the TDS concentration values obtained in each layer of the model domain considering a pumping rate of 100 l/s.

The results obtained by simulating a pumping rate of 10 l/s show no significant differences from what was obtained in previous simulations. On the other hand, comparing these results with those obtained by simulating a considerably larger pumping rate of 100 l/s shows an in-landward progression of cells with TDS concentrations above 15,000 mg/l.

Although this numerical value is not representative of the phenomenon of fresh groundwater salinization, it does make us realize that uncontrolled groundwater pumping could increase the risk.
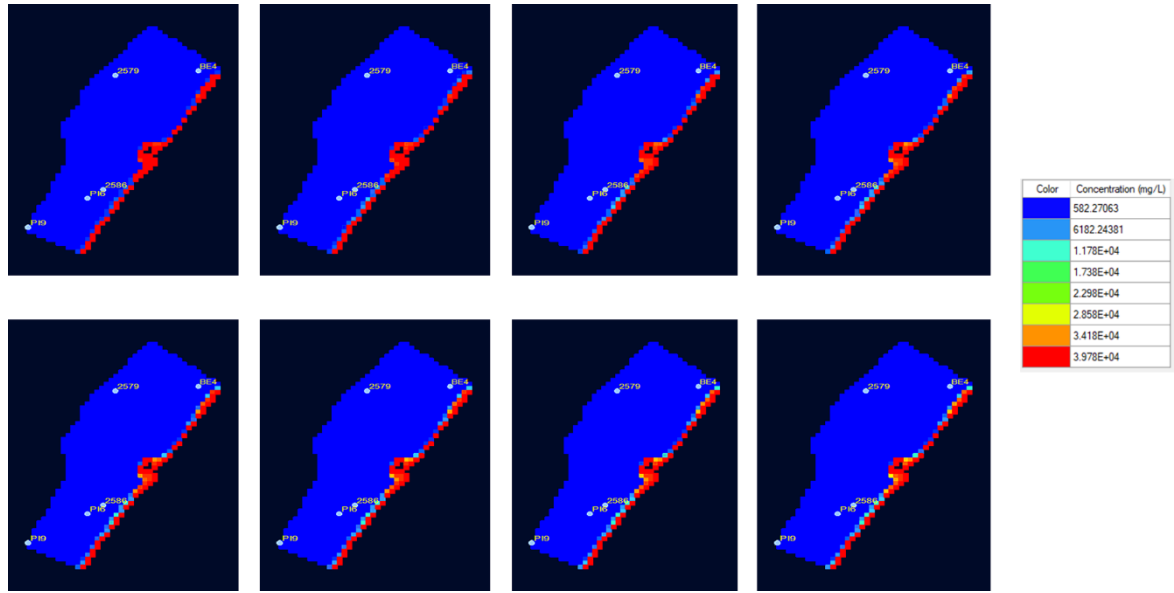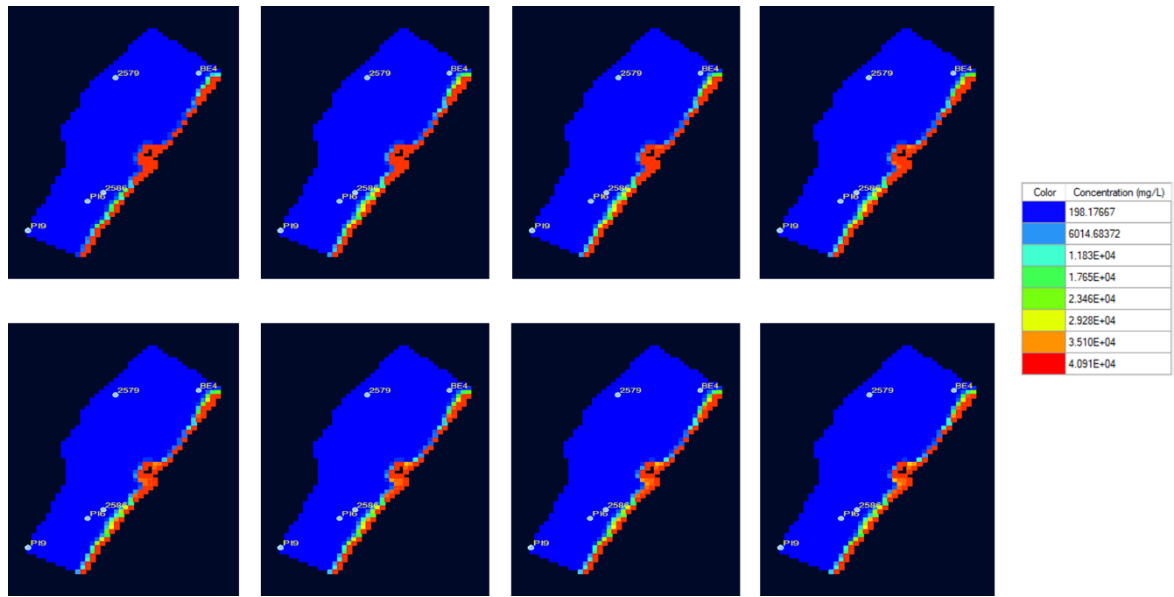
Fig. 70 TDS concentrations for the layer 1 considering a 100 l/s pumping rate (the legend is also the same for the following figures).
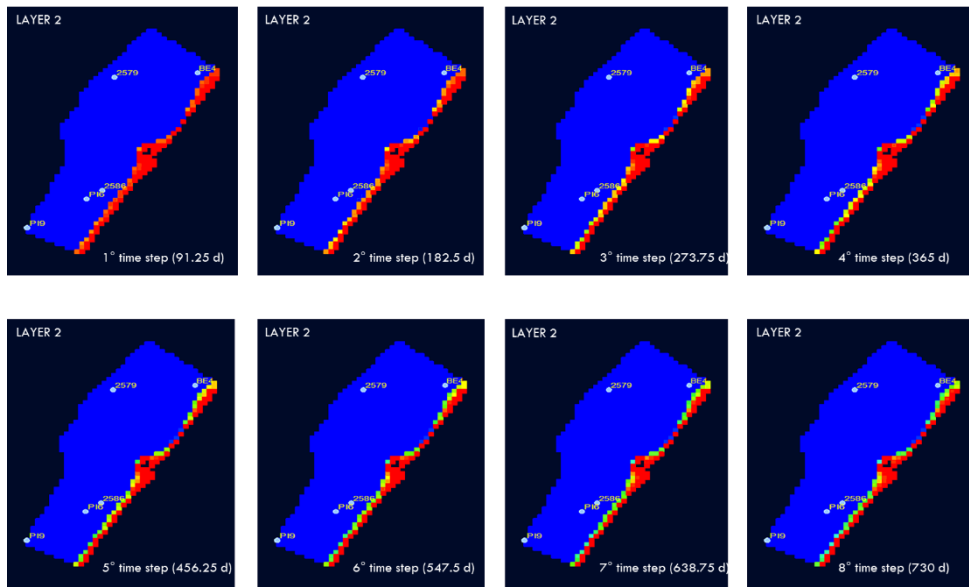

Fig. 71 TDS concentrations for the layer 2 considering a 100 l/s pumping rate.
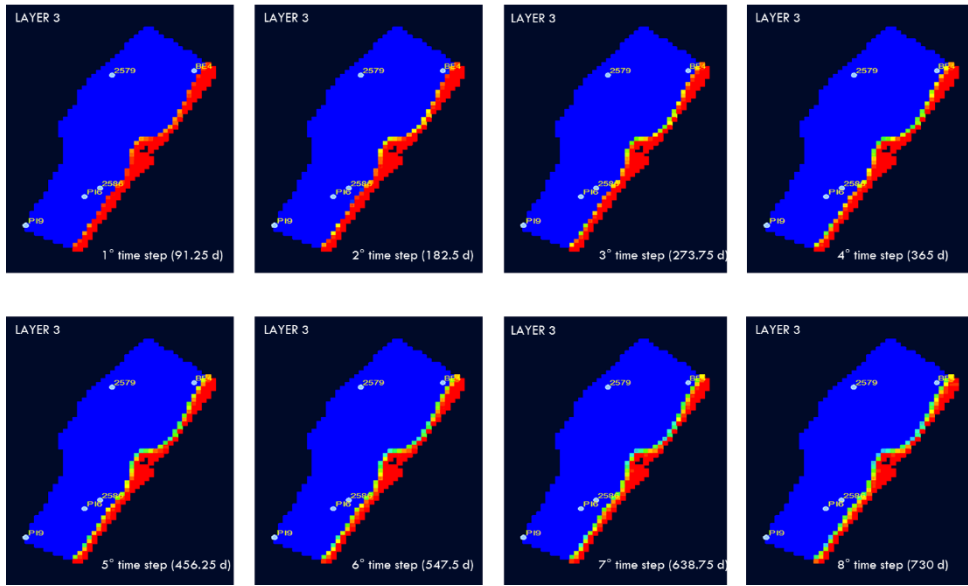
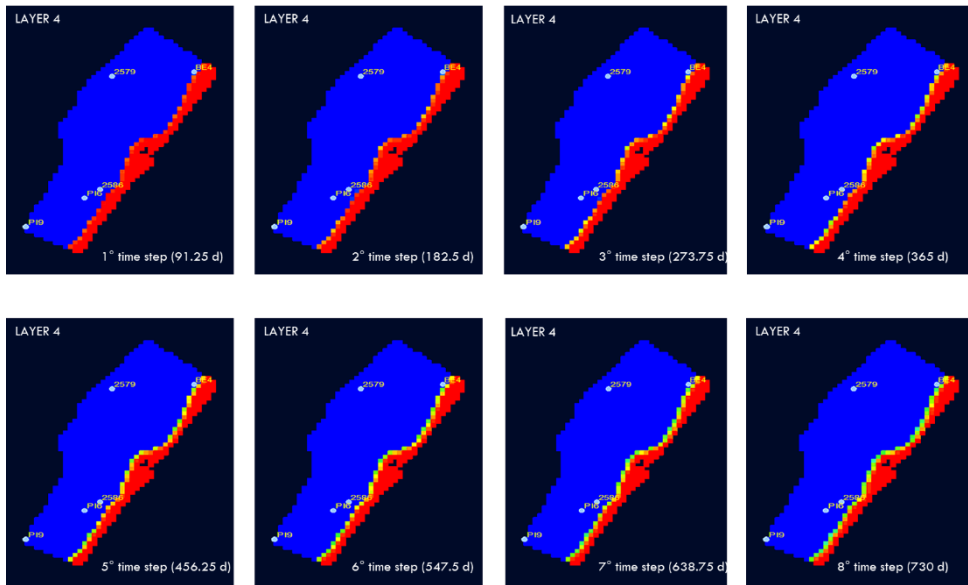***Fig. 72*** *TDS concentrations for the layer 3 considering a 100 l/s pumping rate.*

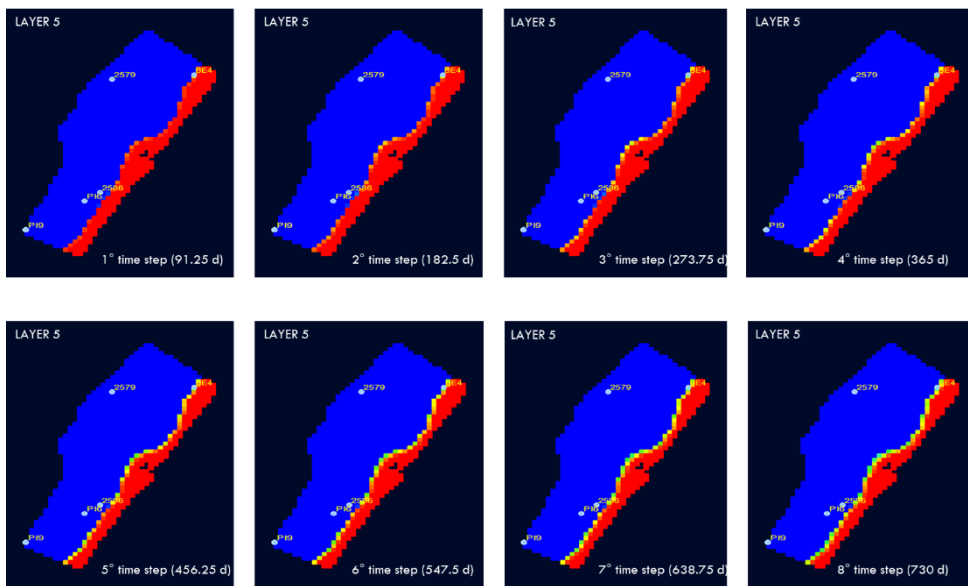***Fig. 73*** *TDS concentrations for the layer 4 considering a 100 l/s pumping rate.*

91

Fig. 74 *TDS concentrations for the layer 5 considering a 100 l/s pumping rate.*

Fig. 75 *TDS concentrations for the layer 6 considering a 100 l/s pumping rate.*

Fig. 76 *TDS concentrations for the layer 7 considering a 100 l/s pumping rate.*

92

Fig. 77 TDS concentrations for the layer 8 considering a 100 l/s pumping rate.

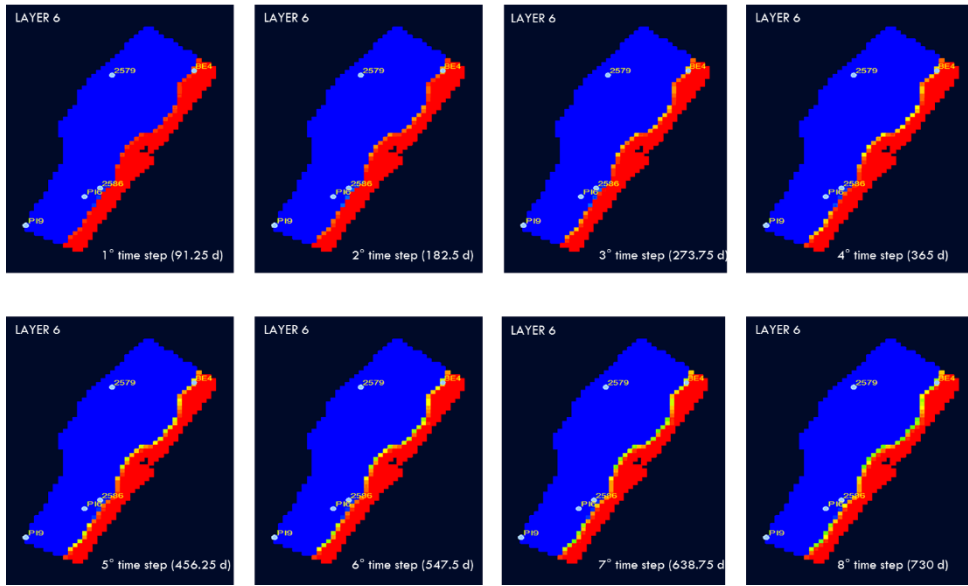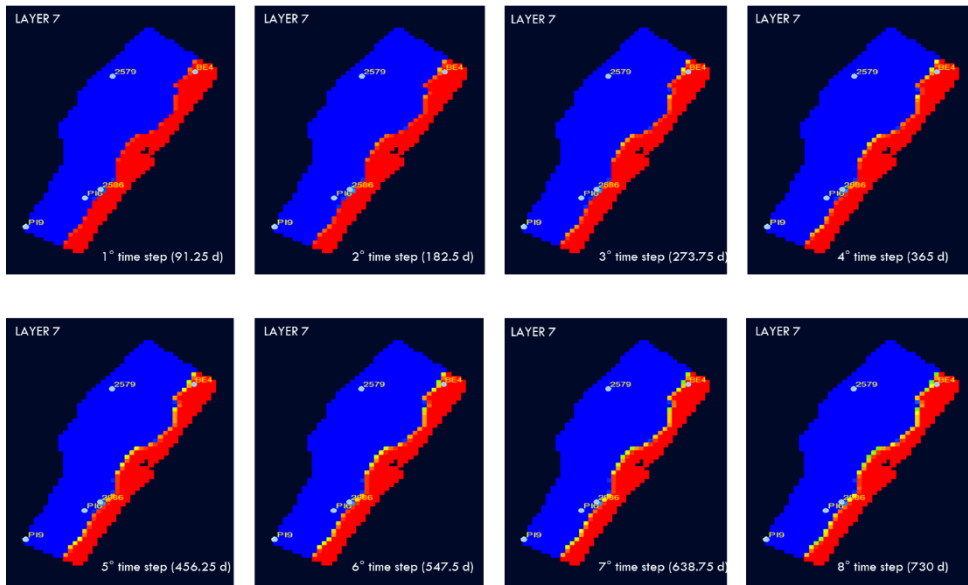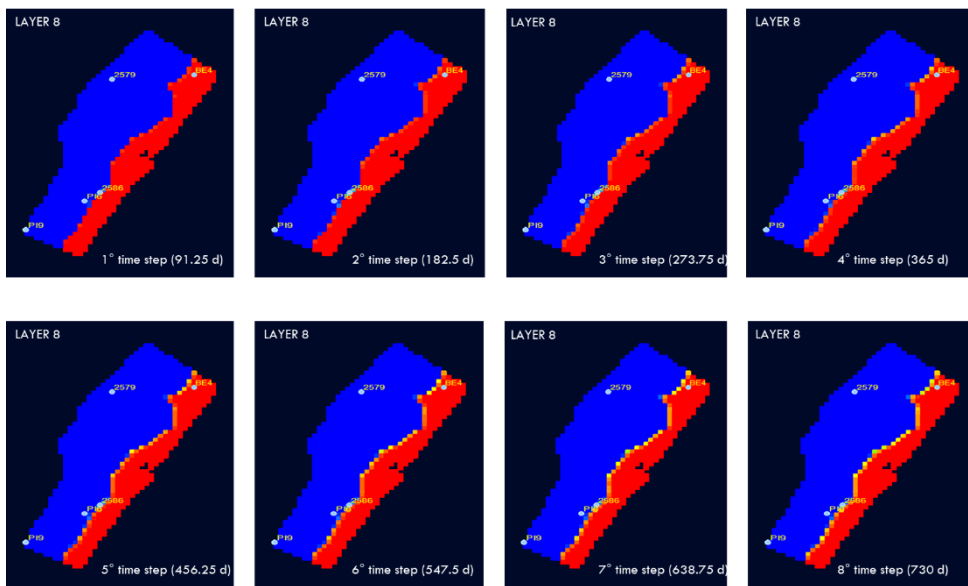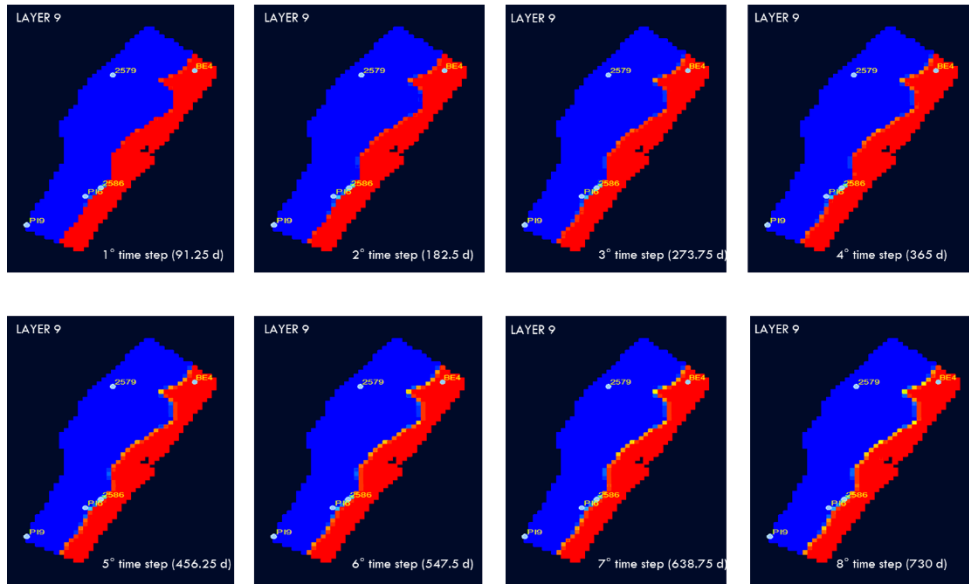*Fig. 78 TDS concentrations for the layer 9 considering a 100 l/s pumping rate.*
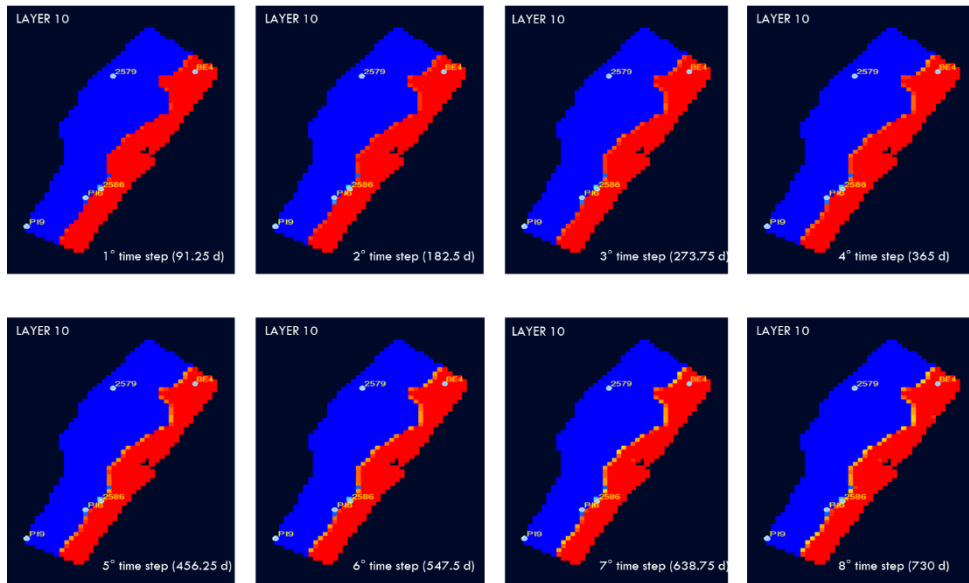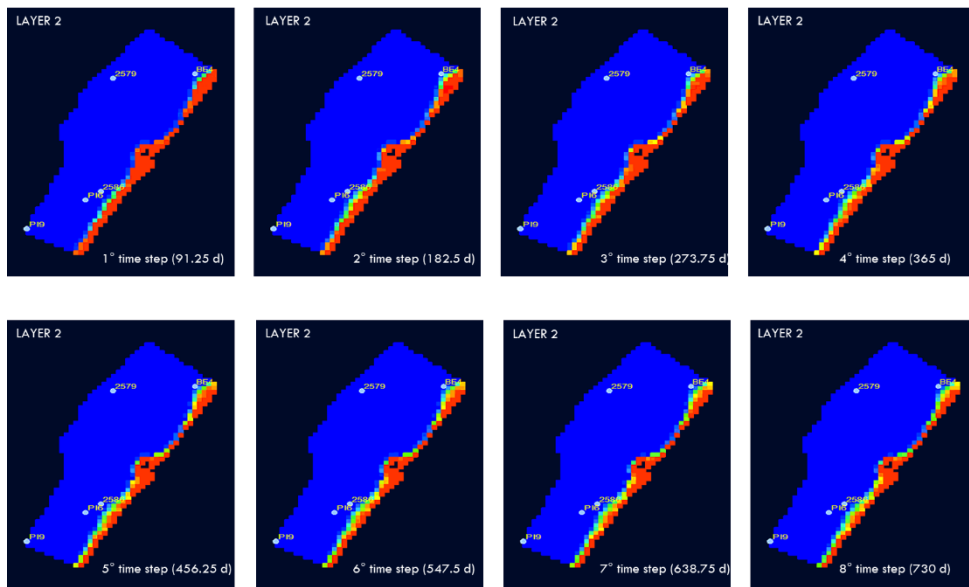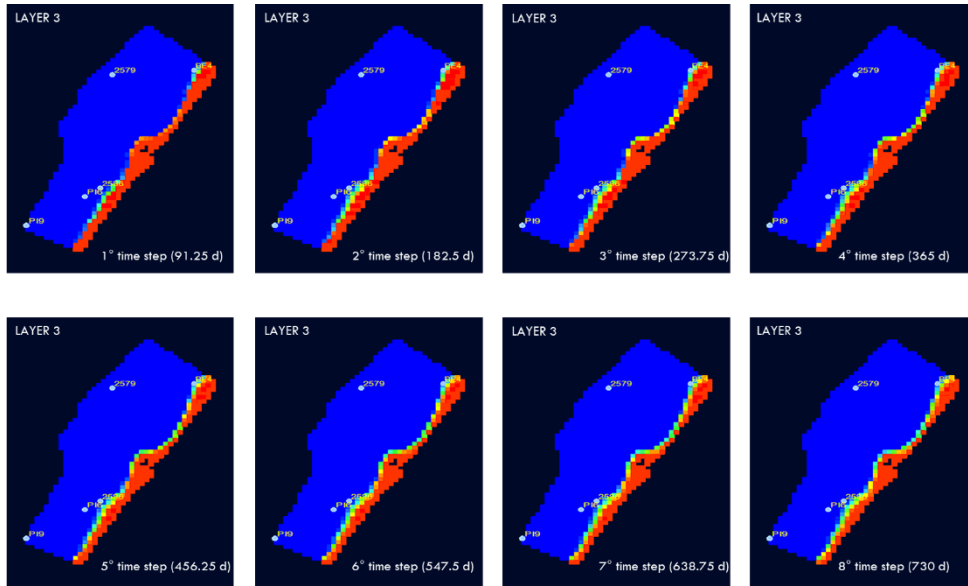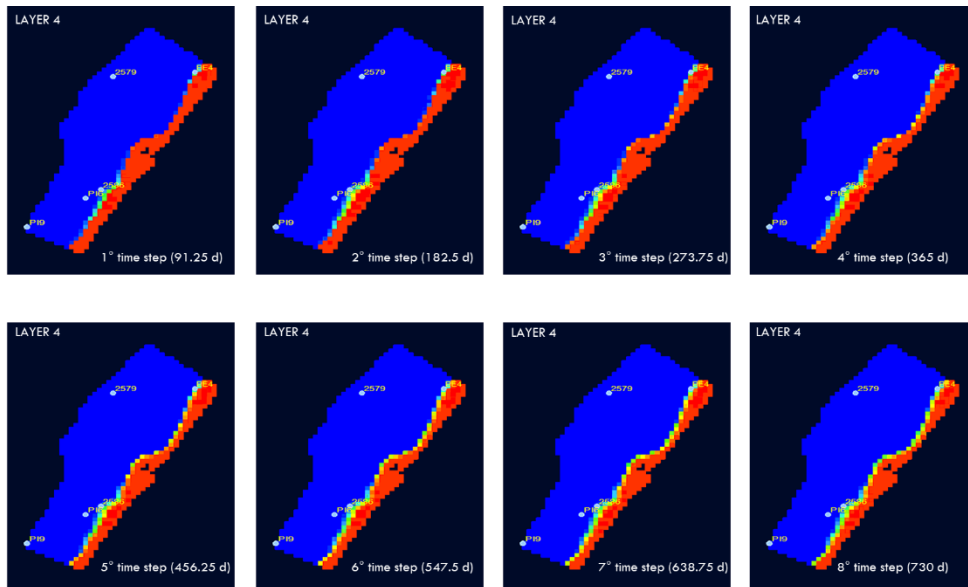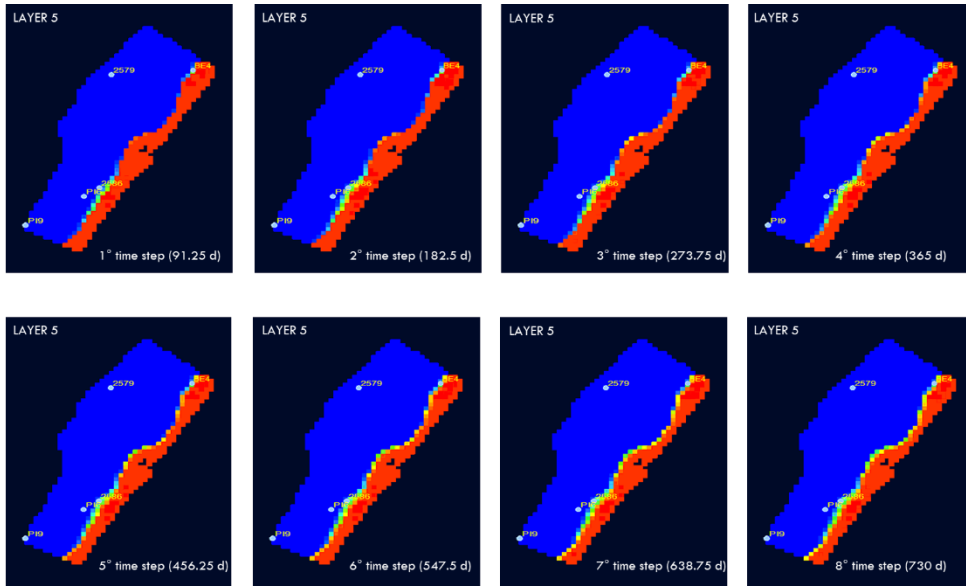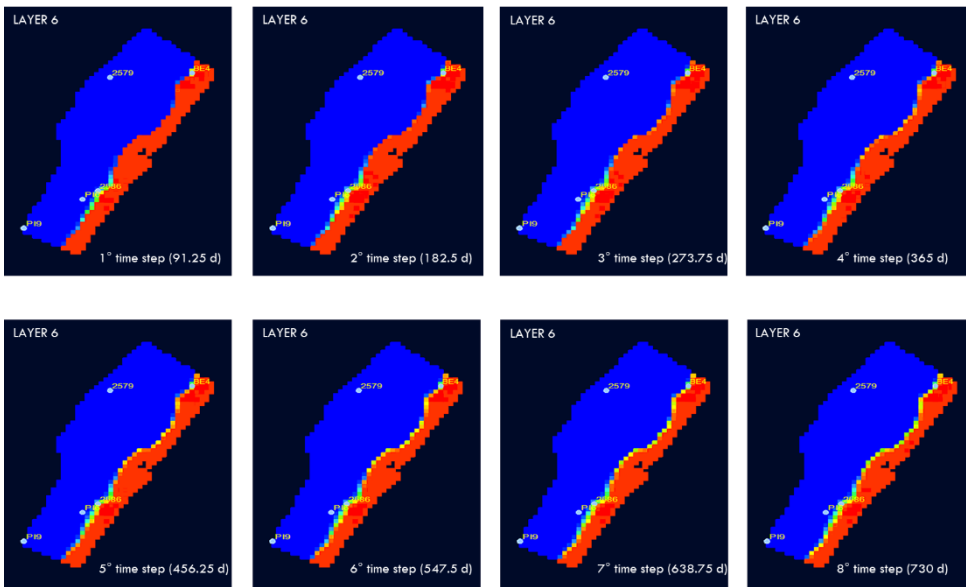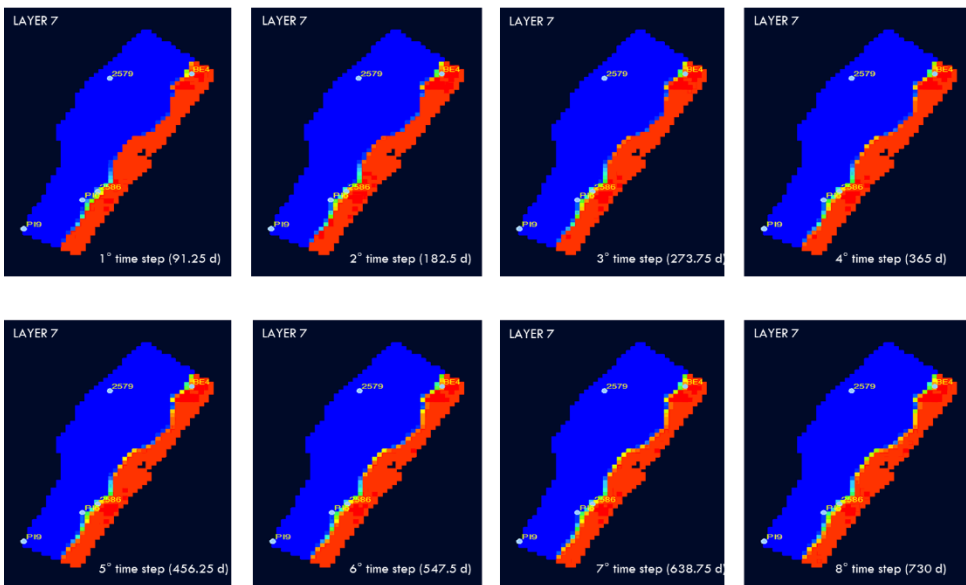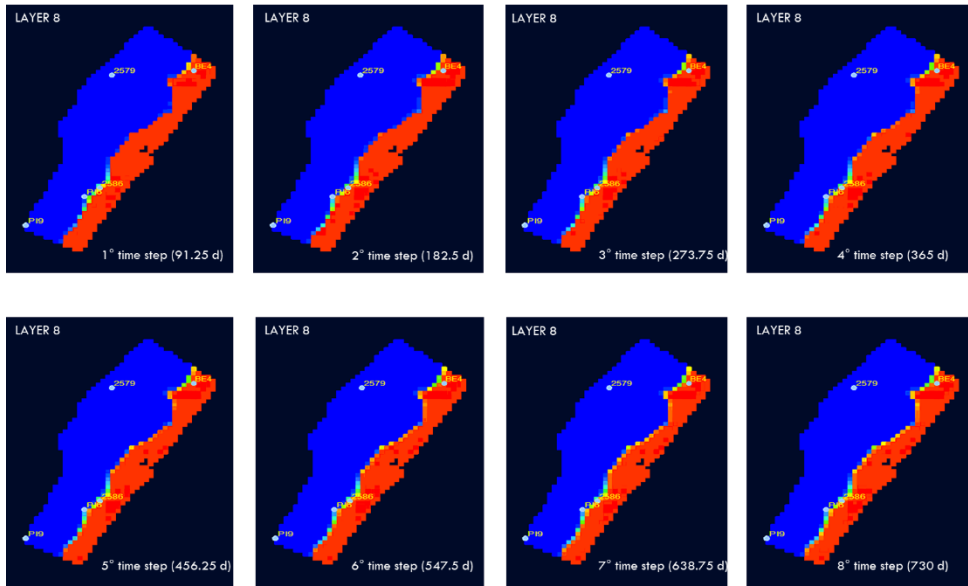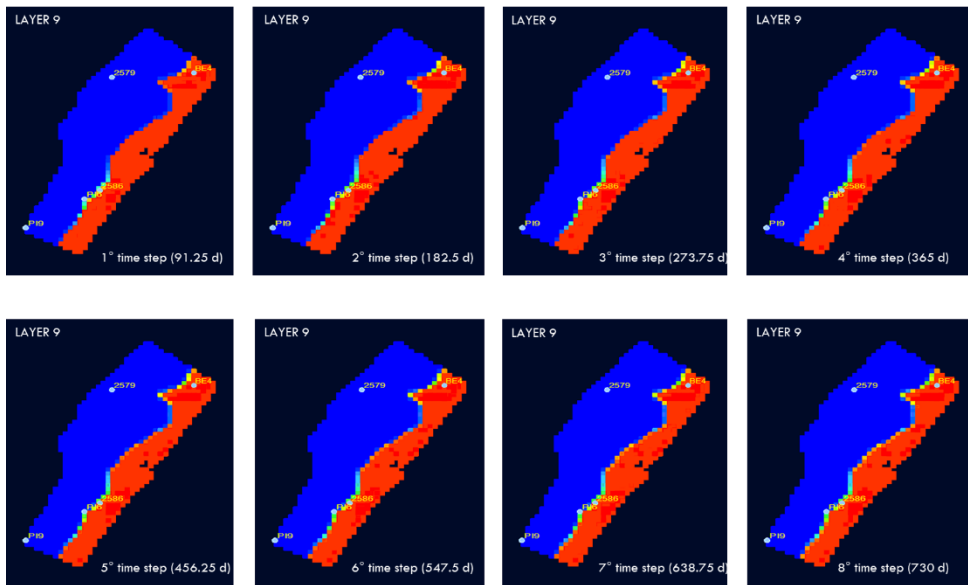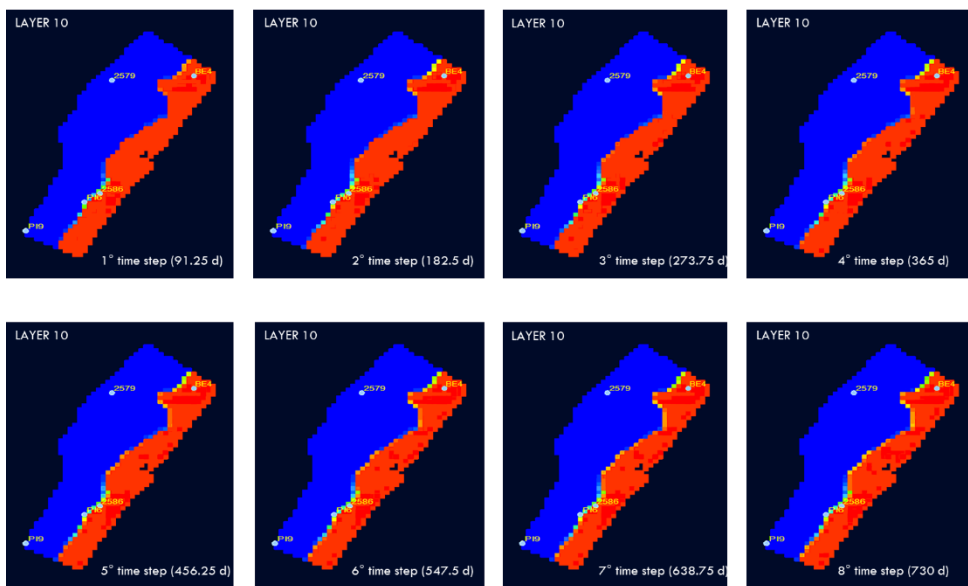

Fig. 79 TDS concentrations for the layer 10 considering a 100 l/s pumping rate.

93

12.   Conclusions

The excessive groundwater withdrawals can disrupt the equilibrium between fresh and saline groundwater due to seawater intrusion (SWI), thus enhancing the lateral and upconing movement of brackish groundwater and the subsequent salinization of fresh groundwater. These phenomena could be amplified in some areas where, due to peculiar geological and structural conditions, some preferential pathways are formed that facilitate the intrusion of seawater inland.

The results obtained from different investigation techniques, including geochemical tools and Electrical Resistivity Tomographies (ERT), highlighted the complexity of the hydrostratigraphic features of the Metaponto coastal plain. The articulated morphology may increase the vulnerability to SWI. For developing methodologies and knowledge for the safeguarding of the coastal aquifer groundwater, the multidisciplinary approach adopted can be useful for resource management purposes, e.g., to prevent upconing effects where they might be unexpected, i.e., far from the coast.

The ERT approach, with an optimal compromise between electrode distance and profile length, improved the characterization of the study area, highlighting the complexity of the erosion phenomena that characterize the subsurface. The previous geological knowledge of the subsurface stratigraphy/hydrostratigraphy was improved, indicating new erosion incisions, which could be considered of secondary importance from the global geological plain characterization perspective, but are essential to prevent salinization effects due to SWI. The previous works highlighted a good spatial analysis by Horizontal-to-Vertical Spectral Ratio (HVSR) methodology to define a synoptic map of the erosion substratum and the main paleovalley shapes. If the previous shallow ERT experiences were important to increase the knowledge in terms of SWI very close to the coastline, the results of this research activity highlighted how the use of deep ERT applications can detect in detail the complexity of the hydrostratigraphy in terms of incision shapes and paleovalley formation, where medium/high-permeability sediments are widespread located. These morphologic structures could be the major source of salinization risks for SWI, to be considered a key point for any management tools.

The obtained results demonstrate the opportunity to continue and strengthen the research on this aquifer. Further research efforts should pursue the integration of different methods to meet the need to manage SWI affordably: increase the knowledge of the geometric features of the aquifer, monitor and interpret water level, quality conditions, and trends. The widespread use of geophysical approaches continuously offers new possibilities to improve the knowledge of aquifer boundaries. The ERT approach in this work showed the need to define the relationship between the depth of investigation and lateral resolution to detect large erosion features (paleovalleys) in deep substrata, which are important vehicles for SWI. The site-specific approach in this field is fundamental.

The multidisciplinary approach underlying the research project can be useful for groundwater resources management purposes from both a quality and quantity point of view. An effective conceptualization of the Metaponto coastal plain was important for understanding the mechanisms involved in SWI and represents a useful tool to support groundwater management, simulating possible future scenarios with, for example, variations in rainfall and temperature. The proposed approach could be helpful for decision-makers to manage resource utilization while ensuring its availability and quality.

The evaluation of the effective recharge can be useful to identify the priority quantity protection measures for sustainable groundwater planning and management in the study area. The inverse hydrogeological water balance method allowed the estimation of effective infiltration for the entire hydrogeological basin.

According to the hydrochemical analysis of groundwater samples, the ion exchange processes are dominant in this coastal aquifer, showing the effects of SWI and the displacement of seawater by freshwater.

The overlay and index methods SINTACS and SINTACS-LU were applied to assess the groundwater vulnerability of the Metaponto coastal plain. The study area presents a growing population, tourist expansion and intensive agricultural practices. The land use parameter was added to the original SINTACS method because of its importance in the study area and its impact on groundwater vulnerability. The groundwater vulnerability to pollution was classified into low, moderate and high classes. The sector classified as highly vulnerable is closest to the sea and represents the area that most needs opportune management of groundwater resources. Map removal and single-parameter were the two types of sensitivity analysis performed in this research to understand the influence of the input parameters on the output. The intrinsic vulnerability assessment of the Metaponto coastal plain aquifer can assist in prioritizing groundwater protection measures and help in the selection of the most vulnerable areas for further investigation and monitoring. This is more important, considering that vulnerability assessment is gaining increasing attention because of the key role that groundwater quality plays in the study area.

The knowledge of potential intrinsic vulnerability and the issues related to groundwater quality represents a significant task to prevent and control the pollution of the resources. Indeed, identifying the aquifer zones characterized by high vulnerability represents a useful step for both groundwater management and communities' awareness concerning the resulting environmental problems. Furthermore, this research activity leads to new considerations concerning the link of the aquifer hydrogeological behaviour to the anthropogenic activities related to the release of pollutants in the subsurface and climate change.

Subsequently, the overlay-index GALDIT method was applied to assess the groundwater vulnerability to SWI. Groundwater resources are particularly exposed to quantitative and qualitative degradation due to unfavourable climate conditions worsened by climate change, the growing water demand, and the contamination caused by anthropogenic activities and the SWI process. The groundwater vulnerability assessment to SWI of the study area can support authorities and stakeholders in planning effective policies and strategies to protect coastal groundwater resources, including groundwater monitoring. The obtained intrinsic vulnerability map showed highly vulnerable areas in the proximity of the shoreline, occurring roughly parallel to the coast, within the first 500 m. The width of the coastal strip most vulnerable to SWI increases in the NE direction, reaching its maximum extension in the sector between the Basento and Bradano Rivers. Higher vulnerability to SWI was detected where the aquifer bottom deepens below sea level.

The sensitivity analysis was also performed to investigate the contribution of single parameters to the vulnerability index. According to its outcomes, the hydrogeological and topographical parameters, such as the aquifer hydraulic conductivity and the distance from the shore, have the greatest impact on groundwater vulnerability across the examined aquifer.

Qualitative degradation is a real risk that threatens the groundwater resources of the Metaponto aquifer. The SWI phenomenon can reduce the availability of good-quality groundwater in areas close to the coast.

The groundwater vulnerability map can be a useful tool for addressing coastal groundwater management to the protection from the SWI threat. The identification of the areas with potential high vulnerability can help to develop appropriate coastal groundwater strategies to face SWI in this area.

Numerical modeling applications were carried out to simulate the dynamic behaviour of the aquifer system under natural and anthropic driving forces to produce helpful predictive outcomes finalized

to understanding SWI phenomenon severity. Due to lack of data and prohibitive computational burden, it wasn't possible to perform numerical modeling of groundwater flow for the entire coastal plain. Instead, the research activity concentrated on the region that the GALDIT method's assessment of intrinsic vulnerability to SWI revealed to be potentially most vulnerable to this phenomenon. The MODFLOW and SEAWAT codes were used within the Visual MODFLOW Flex 7.0 software (© 2021 by Waterloo Hydrogeologic). Starting from the hydrogeological conceptualization of the coastal aquifer, a three-dimensional numerical model of groundwater flow was realized to simulate piezometric and salinity variations. Numerical simulation results confirm that most coastal aquifer supply comes from upstream aquifers. By comparing results between different scenarios of spatially distributed recharge values and pumping well rates, the effects of climate change in reducing direct recharge don't appear to be significant. On the contrary, particularly intense pumping rates above 100 l/s impact in terms of inland advancement of salinity expressed in terms of TDS concentration. Therefore, it is important to develop best practice proposals for pumping and optimal water resource management and, at the same time, to acquire further and more in-depth data to better define the SWI phenomenon in the study area. Only in this way it will be possible to define actions and interventions for mitigating the groundwater salinization risk, which will be strongly influenced by the aquifer's future management. Future scenarios will also depend on global climate change, local socioeconomic development and water requirements, environmental issues, and political choices.

Research on this aquifer system needs to be continued and expanded to improve the knowledge of the salinization process. In particular, in situ activities such as hydrogeological and geognostic surveys are essential for the consolidation and validation of the numerical model.

13. References

Adams, B., & Foster, S. (1992). Land-surface zoning for groundwater protection. *J. Inst. Water Environ. Manag.*, 6, 312-320.

Aladejana, J., Kalin, R., Sentenac, P., & Hassan, I. (2020). Hydrostratigraphic Characterisation of Shallow Coastal Aquifers of Eastern Dahomey Basin, S/W Nigeria, Using Integrated Hydrogeophysical Approach; Implication for Saltwater Intrusion. *Geosciences*, 10, 65.

Albinet, M., & Margat, J. (1970). Cartographie de la vulnérabilité de à la pollution des nappes d'eau souterraine. *Orléans France. Bull. BRGM*, 4, 13-22.

Aller, L., Bennett, T., Lehr, J., Petty, R., & Hackett, G. (1987). *DRASTIC: A Standardized System for Evaluating Ground Water Pollution Potential Using Hydrogeologic Settings.* Washington, DC, USA: U.S. Environmental Protection Agency.

Allocca, V., Manna, F., & De Vita, P. (2014). Estimating annual groundwater recharge coefficient for karst aquifers of the southern Apennines (Italy). *Hydrol. Earth Syst. Sci., 18 (2)*, 803-817.

Appelo, C., & Postma, D. (2004). *Geochemistry, Groundwater and Pollution.* London, England: CRC Press.

Babiker, I., Mohamed, M., Hiyama, T., & Kato, K. (2005). A GIS-based DRASTIC model for assessing aquifer vulnerability in Kakamigahara Heights, Gifu Prefecture, central Japan. *Sci. Total Environ. 345*, 127-140.

Bakker, M., Schaars, F., Hughes, J., Langevin, C., & Dausman, A. (2013). *Documentation of the seawater intrusion (SWI2) package for MODFLOW.* U.S. Geological Survey Techniques and Methods, book 6, chap. A46.

Barbulescu, A. (2020). Assessing Groundwater Vulnerability: DRASTIC and DRASTIC-Like Methods: A Review. *Water*, 12, 1356.

Bouzaglou, V., Crestani, E., Salandin, P., Gloaguen, E., & Camporese, M. (2018). Ensemble Kalman Filter Assimilation of ERT Data for Numerical Modeling of Seawater Intrusion in a Laboratory Experiment. *Water*, 10, 397.

Brindha, K., & Elango, L. (2015). Cross comparison of five popular groundwater pollution vulnerability index approaches. *J. Hydrol. 524*, 597-613.

Brückner, H. (1980). Marine Terrassen in Süditalien. Eine quartärmorphologische Studie über das Küstentiefland von Metapont. *Düsseldorfer Geographische Schriften, 14*, 1-235.

Canora, F., Musto, M., & Sdao, F. (2018). Groundwater recharge assessment in the carbonate aquifer system of the Lauria Mounts (southern Italy) by GIS-based distributed hydrogeological balance method. *Gervasi O. et al. (Eds.) Computational Science and Its Applications, Lecture Notes in Computer Science, 10961. Springer*, 166-181.

Canora, F., & Sdao, F. (2020). Hydrogeological characterization and groundwater vulnerability to pollution assessment of the High Basento River Valley carbonate hydrostructure (Southern Italy). *Italian Journal of Engineering Geology and Environment, 1*, 25-44.

Canora, F., D'Angella, A., & Aiello, A. (2015). Quantitative assessment of the sensitivity to desertification in the Bradano River basin (Basilicata, southern Italy). *J. Maps, 11*, 745-759.

Caputo, R., Bianca , M., & D'Onofrio, R. (2010). Ionian marine terraces of southern Italy: Insights into the Quaternary tectonic evolution of the area. *Tectonics, 29(4)*, TC4005.

Carsel, R., Mulkey, L., Lorber, M., & Baskin, L. (1985). The pesticide root zone model (PRZM): A procedure for evaluating pesticide leaching threats to ground water. *Ecol. Model. 30*, 49-69.

Celico, P. (1988). *Prospezioni idrogeologiche.* Napoli, Italy: Liguori.

Chachadi, A. G., & Lobo Ferreira, J. P. (2001). *Sea Water Intrusion Vulnerability Mapping of Aquifers Using GALDIT Method.* In: Elango L. and Jayakumar R. (2001, eds.) - Modelling in Hydrogeology. UNESCO-IHP, 143-155, Allied Publishers.

Chachadi, A. G., & Lobo Ferreira, J. P. (2005). Assessing aquifer vulnerability to sea-water intrusion using GALDIT method: Part 2 – GALDIT Indicators Description. *IAHS and LNEC, Proc. 4th Inter Celtic Colloquium on Hydrology and Management of Water Resources.* Guimarães, Portugal.

Chang, S., Chung, I., Kim, M., Tolera, M., & Koh, G. (2019). Application of GALDIT in Assessing the Seawater Intrusion Vulnerability of Jeju Island, South Korea. *Water, 11(9)*, 1824.

Ciaranfi, N., Ghisetti, F., Guida, M., Iaccarino, G., Lambiase, S., Pieri, P., Rapisardi, L., Ricchetti, G., Torre, M. Tortorici, L., & Vezzani, L. (1983). Carta Neotettonica dell'Italia meridionale. *Prog. Fin. Geodinamica Pubbl. 251*, 1-62.

Cilumbriello, A., Sabato, L., Tropeano, M., Gallicchio, S., Grippa, A., Maiorano, P., Mateu-Vicens, G., Rossi, C.A., Spilotro, G., Calcagnile, L., & Quarta, G. (2010). Sedimentology, stratigraphic architecture and preliminary hydrostratigraphy of the Metaponto coastal-plain subsurface (Southern Italy). *In Proceedings of the National Workshop Multidisciplinary Approach for Porous Aquifer Characterization.* (p. 67-84). Rome: Bersezio R., Amanti M., Eds. Memorie Descrittive della Carta Geologica d'Italia.

Civita, M. (1987). La previsione e la prevenzione del rischio di inquinamento delle acque sotterranee a livello regionale mediante le Carte di Vulnerabilità. *Proceedings of the Conference Inquinamento delle Acque Sotterranee: Previsione e Prevenzione*, (p. 9-18). Mantova, Italy.

Civita, M. (2005). *Idrogeologia Applicata e Ambientale.* Milano, Italy: CEA.

Civita, M. (2010). The combined approach when assessing and mapping groundwater vulnerability to contamination. *J. Water Resour. Prot. 2*, 14-28.

Civita, M., & De Maio, M. (1997). *SINTACS. Un Sistema Parametrico per la Valutazione e la Cartografia Della Vulnerabilità Degli Acquiferi All'inquinamento. Metodologia e Automazione, Quaderni di Tecniche di Protezione Ambientale.* Bologna, Italy: Pitagora Editrice.

Civita, M., & De Maio, M. (2000). *SINTACS R5 a New Parametric System for the Assessment and Automatic Mapping of Groundwater Vulnerability to Contamination.* Bologna, Italy: Pitagora Editrice.

Civita, M., & De Maio, M. (2001). Average ground water recharge in carbonate aquifers: a GIS processed numerical model. *Sciences et techniques de l'environnement. Mémoire hors-série*, 93-100.

Civita, M., & De Maio, M. (2004). Assessing and mapping groundwater vulnerability to contamination: The Italian "combined" approach. *Geofísica Int. 43*, 513-532.

Ckakraborty, S., Paul, P., & Sikdar, P. (2007). Assessing aquifer vulnerability to arsenic pollution using DRASTIC and GIS of North Bengal Plain: A case study of English Bazar Block, Malda District, West Bengal, India. *J. Spat. Hydrol. 7*, 101-121.

Cocco, E., Cravero, E., Di Geronimo, S., Mezzadri, G., Parea, G., Pescatore, T., Valloni, R., & Vinci, A. (1975). Lineamenti geomorfologici e sedimentologici del litorale alto ionico (Golfo di Taranto). *Boll. Soc. Geol. Ital. 94*, 993-1051.

Constable, S., Parker, R., & Constable, C. (1987). Occam′s inversion: a practical algorithm for generating smooth models from electromagnetic sounding data. *Geophysics, 52*, 289-300.

CORINE Land Cover (C.L.C.). (2018). *European Union, Copernicus Land Monitoring Service 2018.* Copenhagen, Denmark: European Environment Agency (EEA).

Corrado, G., Leo, P., Giannandrea, P., & Schiattarella, M. (2017). Constraints on the dispersal of Mt. Vulturepyroclastic products: Implications to mid-Pleistocene climate conditions in the foredeep domain of southern Italy. *Geomorphologie, 23*, 171-182.

Costall, A., Harris, B., & Pigois, J. (2018). Electrical resistivity imaging and the saline water interface in high-quality coastal aquifers. *Surv. Geophys.*, 39, 753-816.

Cotecchia, V. (2014). *Memorie descrittive della carta geologica d'Italia. Vol. 92: Le acque sotterranee e l'intrusione marina in Puglia: dalla ricerca all'emergenza nella salvaguardia della risorsa.* ISPRA Serv. Geologico d'Italia.

Cotecchia, V., D'ecclesiis, G., & Polemio, M. (1990). Studio geologico e idrogeologico dei monti di Maratea. *Geologia Applicata e Idrogeologia, XXV*, 139-179.

Custodio, E., & Llamas, M. (1996). *Hydrologia Subterranea.* Barcelona, Spain: Omega.

De Franco, R., Biella, G., Tosi, L., Teatini, P., Lozej, A., Chiozzotto, B., Giada, M., Rizzetto, F., Claude, C., Mayer, A., Bassan, V., & Gasparetto-Stori, G. (2009). Monitoring the saltwater intrusion by time lapse electrical resistivity tomography: the Chioggia test site (Venice Lagoon, Italy). *J. Appl. Geophys.*, 69, 117-130.

De Marsily, G. (1984). Spatial Variability of Properties in Porous Media: A Stochastic Approach. In J. Bear, & M. Corapcioglu, *Fundamentals of Transport in Porous Media* (p. 719-769). Leiden, The Netherlands: Martinus Nijhoff.

Doerfliger, N., Jeannin, P., & Zwahlen, F. (1997). Water vulnerability assessment in karst environments: A new method of defining protection areas using a multi-attribute approach and GIS tools (EPIK method). *Environ. Geol. 39*, 165-176.

Doglioni, C., Tropeano, M., Mongelli, F., & Pieri, P. (1996). Middle-late Pleistocene uplift of Puglia: an anomaly in the Apenninic foreland. *Memorie Società Geologica Italiana, 51*, 101-117.

Doherty, J. (2015). *Calibration and Uncertainty Analysis for Complex Environmental Models.* Brisbane, Australia: Watermark Numerical Computing.

Dörfligern, N., Dumon, A., Aunay, B., Picot, G., Moynot, C., & Bollard, M. (2011). *Influence de la montée du niveau de la mer sur le biseau salin des aquifères côtiers des DROM/COM, Rapport final.* Orléans, France: BRGM RP-60828-FR. BRGM.

Ducci, D., & Sellerino, M. (2013). Vulnerability mapping of groundwater contamination based on 3D lithostratigraphical models of porous aquifers. *Science of The Total Environment, 447*, 315-322.

Eftekhari, M., & Akbari, M. (2020). Evaluation of the SINTACS-LU model capability in the analysis of aquifer vulnerability potential in semiarid regions. *J. Appl. Res. Water Wastewater, 7*, 111-119.

Erostate, M., Huneau, F., Garel, E., Ghiotti, S., Vystavna, Y., Garrido, M., & Pasqualini, V. (2020). Groundwater dependent ecosystems in coastal Mediterranean regions: Characterization, challenges and management for their protection. . *Water Res., 172*, 115461.

European Environment Agency. (2012). *Water resources in Europe in the context of vulnerability. EEA 2012 state of water assessment.* Copenhagen.

Geological Survey of Italy. (2016). *Geological Map of Italy, 1:50,000 Scale.* Rome, Italy: ISPRA-Land Protection and Georesources Department.

Ghyben, B. (1888). Nota in verband met de voorgenomen putboring nabij Amsterdam. *Tijdschrift van Let Koninklijk Inst. Van Ing. 9*, 8-22.

Gioia, D., Bavusi, M., Di Leo , P., Giammatteo, T., & Schiattarella, M. (2020). Geoarchaeology and geomorphology of the Metaponto area, Ionian coastal belt, Italy. *J. Maps, 16*, 117-125.

Giorgi, F., & Lionello, P. (2008). Climate change projections for the Mediterranean region. *Global and Planetary Change, 63, 2-3*, 90-104.

Goldman, M., & Kafri, U. (2006). Hydrogeophysical applications in coastal aquifers. In H. B. Vereecken, *Applied Hydrogeophysics* (p. 233-254). Dordrecht, Netherlands: Springer:.

Grauel, A., & Bernasconi, S. (2010). Core-top calibration of δ18O and δ13C of G. ruber (white) and U. mediterranea along the southern Adriatic coast of Italy. *Marine Micropaleontology, 7, 3-4*, 175-186.

Guo, W., & Langevin, C. (2002). User's Guide to SEAWAT: A Computer Program for Simulation of Three-Dimensional Variable-Density Ground-Water Flow: Techniques of Water. In *Resources Investigations Book 6,Chapetr A7* (p. 77).

Gupta, P., Kumari, B., Gupta, S., & Kumar, D. (2020,). Nitrate-leaching and groundwater vulnerability mapping in North Bihar, India. *Sustain. Water Resour. Manag. 6* , 48.

Hamza, M., Added, A., Francés, A., & Rodríguez, R. (2007). Validité de l'application des méthodes de vulnérabilité drastic, sintacs et SI à l'étude de la pollution par les nitrates dans la nappe phréatique de Metline–Ras Jebel–Raf Raf (Nord-Est tunisien). *Comptes. Rendus Geosci. 339*, 493-505.

Hasan, M., Shang, Y., Jin, W., Shao, P., Yi, X., & Akhter, G. (2020). Geophysical Assessment of Seawater Intrusion into Coastal Aquifers of Bela Plain, Pakistan. *Water*, 12, 3408.

Herzberg, A. (1901). Die Wasserversorgung einiger nordseebader: J. Gasbeleucht. *Wasserversorg, 44*, 815-819.

Imbrenda, V., Coluzzi, R., Lanfredi, M., Loperte, A., Satriani, A., & Simoniello, T. (2018). Analysis of landscape evolution in a vulnerable coastal area under natural and human pressure. *Geomat. Nat. Hazards Risk, 9*, 1249–1279.

IPCC. (2022). *Climate Change 2022: Impacts, Adaptation, and Vulnerability. Contribution of Working Group II to the Sixth Assessment Report of the Intergovernmental Panel on Climate Change.* Cambridge, UK and New York, USA: Cambridge University Press.

IV Meeting CRYStallisation TECHnologies for prevention of SALt water INtrusion. Scanzano Jonico, Italy, 26-29 September 2002. (2003). *La ricerca europea per la riduzione dell'inquinamento salino delle acque sotterranee.* Polemio M. & Gallicchio G. CNR – IRPI, Bari.

Jahromi, M., Gomeh, Z., Busico, G., Barzegar, R., Samany, N., Aalami, M., Tedesco, D., Mastrocicco, M., & Kazakis, N. (2021). Developing a SINTACS-based method to map groundwater multi-pollutant vulnerability using evolutionary algorithms. *Environ. Sci. Pollut. Res. 28*, 7854-7869.

Javadinejad, S., Ostad-Ali-Askari, K., & Jafary, F. (2019). Using simulation model to determine the regulation and to optimize the quantity of chlorine injection in water distribution networks. , 5, . *Model. Earth Syst. Environ. 5*, 1015-1023.

Jesudhas, C., Chinnasamy, A., Muniraj, K., & Sundaram, A. (2021). Assessment of vulnerability in the aquifers of rapidly growing sub-urban: A case study with special reference to land use. *Arab. J. Geosci. 14*, 60.

Jha, M., Chowdhury, A., Chowdary, V., & Peiffer, S. (2007). Groundwater management and development by integrated remote sensing and geographic information systems: Prospects and constraints. *Water Resour. Manag. 21*, 427-467.

Kallioras, A., Pliakas, F., & Diamantis, I. (2010). Simulation of Groundwater Flow in a Sedimentary Aquifer System Subjected to Overexploitation. *Water Air Soil Pollut 211*, 177-201.

Kazakis, N., & Voudouris, K. (2015). Groundwater vulnerability and pollution risk assessment of porous aquifers to nitrate: Modifying the DRASTIC method using quantitative parameters. *J. Hydrol. 525*, 13-25.

Kazakis, N., Pavlou, A., Vargemezis, G., Voudouris, K., Soulios, G., Pliakas, F., & Tsokas., G. (2016). Seawater intrusion mapping using electrical resistivity tomography and hydrochemical data. An application in the coastal area of eastern Thermaikos Gulf, Greece. *Sci. Total Environ.*, 543, 373-387.

Kazakis, N., Spiliotis, M., Voudouris, K., Pliakas, F., & Papadopoulos, B. (2018). A fuzzy multicriteria categorization of the GALDIT method to assess seawater intrusion vulnerability of coastal aquifers. *Science of The Total Environment, 621*, 524-534.

Kim, I., Chung, I.-M., & Chang, S. (2021). Development of Seawater Intrusion Vulnerability Assessment for Averaged Seasonality of Using Modified GALDIT Method. *Water, 13(13)*, 1820.

Kirlas, M., Karpouzos, D., Georgiou, P., & Katsifarakis, K. (2022). A comparative study of groundwater vulnerability methods in a porous aquifer in Greece. *Appl. Water Sci.*, 12, 123.

Kirsch, R. (2009). *Groundwater Geophysics—A Tool for Hydrogeology.* Dordrecht, Netherlands: Springer.

Kumar, A., & Krishna, A. (2018). Groundwater vulnerability and contamination risk assessment using GIS-based modified DRASTIC-LU model in hard rock aquifer system in India. *Geocarto Int.*, 35, 1149-1178.

Kura, N., Ramli, M., Ibrahim, S., Sulaiman, W., Aris, A., Tanko, A., & Zaudi, M. (2015). Assessment of groundwater vulnerability to anthropogenic pollution and seawater intrusion in a small tropical island using index-based methods. *Environ Sci Pollut Res, 22*, 1512-1533.

Leonard, R., Knisel, W., & Still, D. (1987). GLEAMS: Groundwater loading effects of agricultural management systems. *Trans. Am. Soc. Agric. Eng. 30*, 1403-1418.

Lerner, D., Issar, A., & Simmers, I. (1990). *Groundwater recharge. A guide to understanding and estimating natural recharge.* Hannover, Germany: Heise.

Lobo Ferreira, J. P., Chachadi, A. G., Diamantino, C., & Henriques, M. J. (2005). Assessing aquifer vulnerability to sea-water intrusion using GALDIT method: Part 1 – Application to the Portuguese Aquifer of Monte Gordo. *IAHS and LNEC, Proc. 4th Inter Celtic Colloquium on Hydrology and Management of Water Resources.* Guimarães, Portugal.

Lobo Ferreira, J., & Cabral, M. (1991). Proposal for an operational definition of vulnerability for the European community's atlas of groundwater resources. *Meeting of the European Institute for Water.* Brussels: Groundwater Work Group.

Lodwick, W., Monson, W., & Svoboda, L. (1990). Attribute error and sensitivity analysis of map operations in geographical information systems: Suitability analysis. *Int. J. Geogr. Inf. Syst., 4*, 413-428.

Longhitano, S. (2015). Short-Term Assessment of Retreating vs. Advancing Microtidal Beaches Based on the Backshore/Foreshore Length Ratio: Examples from the Basilicata Coasts (Southern Italy). *Open J. Mar. Sci. 5*, 123-145.

Lotfata, A., & Ambinakudige, S. (2020). Degradation of groundwater quality in the coastal aquifers of the USA. *Sustain. Water Resour. Manag. 6*.

Luoma, S., Okkonen, J., & Korkka-Niemi, K. (2017). Comparison of the AVI, modified SINTACS and GALDIT vulnerability methods under future climate change scenarios for a shallow low-lying coastal aquifer in southern Finland. *Hydrogeol. J., 25*, 203-222.

Machiwal, D., Cloutier, V., Güler, C., & Kazakis, N. (2018a). A review of GIS-integrated statistical techniques for groundwater quality evaluation and protection. *Environ. Earth Sci. 77*, 681.

Machiwal, D., Jha, M., Singh, V., & Mohan, C. (2018b). Assessment and mapping of groundwater vulnerability to pollution: Current status and challenges. *Earth-Sci. Rev. 185*, 901-927.

Majandang, J., & Sarapirome, S. (Environ. Earth Sci. 68). Groundwater vulnerability assessment and sensitivity analysis in Nong Rua, Khon Kaen, Thailand, using a GIS-based SINTACS model. *2013*, 2025-2039.

Marquardt, D. (1963). An Algorithm For Least Squares Estimation Of Nonlinear Parameters. *J. Soc. Indust. Appl. Math. 11*, 431-441.

Martinelli, A., & Marchetti, G. (2000). *PROGETTO PRISMAS: Sintesi dei risultati.* Perugia, Italy: Convegno nazionale Progetto Interregionale PRISMAS, 9 novembre 2000.

Mavriou, Z., Kazakis, N., & Pliakas, F. (2019). Assessment of Groundwater Vulnerability in the North Aquifer Area of Rhodes Island Using the GALDIT Method and GIS. *Environments, 6(5)*, 56.

McDonald, M., & Harbaugh, A. (1984). *A modular three-dimensional finite-difference ground-water flow model.* U.S. Geological Survey Open-File Report 83-875.

Medici, G., Engdah, N., & Langman, J. (2021). A basin-scale groundwater flow model of the Columbia Plateau regional aquifer system in the Palouse (USA): Insights for aquifer vulnerability assessment. *International Journal of Environmental Research, 15(2)*, 299-312.

Mendoza, J., & Barmen, G. (2006). Assessment of groundwater vulnerability in the Río Artiguas basin, Nicaragua. *Environ. Geol.*, 50, 569-580.

Migliorini, C. (1937). Cenno sullo studio e sulla prospezione petrolifera di una zona dell'Italia meridionale. *2nd Petroleum world Congress, Paris* (p. 1-11). Roma: AGIP Report.

Moazamnia, M., Hassanzadeh, Y., Nadiri, A., & Sadeghfam, S. (2020). Vulnerability Indexing to Saltwater Intrusion from Models at Two Levels using Artificial Intelligence Multiple Model (AIMM). *Journal of Environmental Management, 255*, 109871.

Muzzillo, R., Canora, F., Polemio, M., & Sdao, F. (2022). Seawater intrusion vulnerability assessment by GALDIT method in the Metaponto coastal aquifer (Basilicata, Italy). *Italian Journal of Engineering Geology and Environment*, 32-41.

Muzzillo, R., Zuffianò, L. E., Canora, F., De Giorgio, G., Limoni, P. P., Polemio, M., & Sdao, F. (2021a). Hydrogeology and seawater intrusion proneness in the Metaponto plain aquifer (Basilicata, Italy). *Italian Journal of Engineering Geology and Environment, 1*, 139-149.

Muzzillo, R., Zuffianò, L., Rizzo, E., Canora, F., Capozzoli, L., Giampaolo, V., De Giorgio, G., Sdao, F., & Polemio, M. (2021b). Seawater Intrusion Proneness and Geophysical Investigations in the Metaponto Coastal Plain (Basilicata, Italy). *Water, 13(1)*, 53.

Napolitano, P., & Fabbri, A. (1996). Single-parameter sensitivity analysis for aquifer vulnerability assessment using DRASTIC and SINTACS. *HydroGIS 96: Application of Geographical Information Systems in Hydrology and Water Resources Management, Proceedings of the Vienna Conference, Vienna, Austria, 16-19 April 1996* (p. 559-566). Wallingford, UK: IAHS Pub.

National Research Council. (1993). *Ground Water Vulnerability Assessment: Predicting Relative Contamination Potential under Conditions of Uncertainty.* Washington, DC, USA: The National Academy Press.

Nguyen, F., Kemna, A., Antonsson, A., Engesgaard, P., Kuras, O., Ogilvy, R., Gisbert, J., Jorreto, S., & Pulido-Bosch, A. (2009). Characterization of seawater intrusion using 2D electrical imaging. *Near Surf. Geophys.*, 7, 377-390.

Nolan, B., Hitt, K., & Ruddy, B. (2002). Probability of nitrate contamination of recently recharged groundwaters in the conterminous United States. *Environ. Sci. Technol. 36*, 2138-2145.

Noori, R., Ghahremanzadeh, H., Kløve, B., Adamowski, F., & Baghvand, A. (2019). Modified-DRASTIC, modified-SINTACS and SI methods for groundwater vulnerability assessment in the southern Tehran aquifer. *J. Environ. Sci. Health, 54*, 89-91.

Ostad-Ali-Askari, K., & Shayannejad, M. (2021). Quantity and quality modelling of groundwater to manage water resources in Isfahan-Borkhar Aquifer. *Environ. Dev. Sustain. 23*, 15943-15959.

Ostad-Ali-Askari, K., Shayannejad, M., & Ghorbanizadeh-Kharazi, H. (2017). Artificial neural network for modeling nitrate pollution of groundwater in marginal area of Zayandeh-rood River, Isfahan, Iran. *KSCE J. Civ. Eng. 21*, 134-140.

Panagopoulos, G., Antonakos, A., & Lambrakis, N. (2006). Optimization of the DRASTIC method for groundwater vulnerability assessment via the use of simple statistical methods and GIS. *Hydrogeol. J. 14*, 894-911.

Parajka, J., & Szolgay, J. (1998). Grid-based mapping of long-term mean annual potential and actual evapotranspiration in Slovakia. *IAHS Publ., Series of Proc. and Rep., Intern. Assoc. Hydrol. Sc., 248*, 123-130.

Parea, G. C. (1986). I terrazzi marini tardo-pleistocenici del fronte della catena appenninica in relazione alla geologia dell'avanfossa adriatica (The Late Pleistocene marine terraces in front of the Apennines in relation to the geology of Adriatic Foredeep). *Memorie Società Geologica Italiana, 35*, 913-936.

Pastore, N., Cherubini, C., Doglioni, A., Giasi, C., & Simeone, V. (2020). Modelling of the Complex Groundwater Level Dynamics during Episodic Rainfall Events of a Surficial Aquifer in Southern Italy. *Water, 12*, 2916.

Pescatore, T., Pieri, P., Sabato, L., Senatore, M., Gallicchio, S., Boscaino, M., Cilumbriello, A., Quarantiello R., & Capretto, G. (2009). Stratigrafia dei depositi pleistocenico-olocenici dell'area costiera di Metaponto compresa fra Marina di Ginosa ed il Torrente Cavone (Italia meridionale): Carta geologica in scala 1:25,000. *Il Quat., 22*, 307-324.

Polemio, M., & Limoni, P. (2006). Groundwater pollution and risks for the coastal environment (southeastern Italy). *Predictions in Ungauged Basins: Promise and Progress* (p. 477-486). Sivapalan M., Wagener T., Uhlenbrook S., Zehe E., Lakshmi V., Liang X., Tachikawa Y., Kumar P., Eds.; IAHS Publications.

Polemio, M., & Ricchetti, E. (1991). Caratteri idrogeologici dell'acquifero della piana costiera di Metaponto (Basilicata). *Ricerca Scientifica e Istruzione Permanente, 93*, 417-426.

Polemio, M., & Zuffianò, L. E. (2020). Review of Utilization Management of Groundwater at Risk of Salinization. *Journal of Water Resources Planning and Management, 146(9)*, 20.

Polemio, M., Limoni, P. P., Mitolo, D., & Santaloia, F. (2002). Characterization Of Ionian-Lucanian Coastal Aquifer And Seawater Intrusion Hazard. *Proceedings Of 17th Saltwater Intrusion Meeting*, (p. 422-434). Delft, Netherlands.

Polemio, M., Limoni, P., Mitolo, D., & Santaloia, F. (2003). Characterisation Of The Ionian-Lucanian Coastal Plain Aquifer (Italy). *Boletin Geologico Y Minero, 114 (2)*, 225-236.

Polemio, M., Limoni, P., Mitolo, D., Santaloia, F., & Virga, R. (2005). Nitrate pollution and quality degradation of Ionian coastal groundwater (Southern Italy). In *Nitrates in groundwater* (p. 163-176). Rotterdam, Netherlands: Razowska-Jaworek L. & Sadurski A.

Polemio, M., Pambuku, A., Limoni, P., & Petrucci, O. (2011). Carbonate Coastal Aquifer of Vlora Bay and Groundwater Submarine Discharge (Southwestern Albania). *J. Coast. Res.*, 26-34.

Post, V. (2005). Fresh and saline groundwater interaction in coastal aquifers: Is our technology ready for the problems ahead? *Hydrogeology Journal, 13*, 120-123.

Praveena, S., & Aris, A. (2009). Groundwater Resources Assessment Using Numerical Model: A Case Study In Low-Lying Coastal Area. *Int. J. Environ. Sci. Technol., 7*, 135-146.

Radina, B. (1969). Idrogeologia del Bacino del fiume Basento. *Mem. Sc. Geol. 21*, 52.

Regione Basilicata. (2006). *I Suoli Della Basilicata.* Firenze, Italy: S.E.L.C.A.

Richard, C., & Nguyen Van Cu. (1961). Relation entre l a résistivité d'une eau et son taux de minéralisation. *L'eau, 1*, 22-24.

Rodier, J. (1975). *Analysis of Water.* New York: Wiley.

Romanazzi, A., & Polemio, M. (2013). Modelling of coastal karst aquifers for management support: a case study of Salento (Apulia, Italy). *Italian Journal of Engineering Geology and Environment, (1)*, 65-83.

Romanazzi, A., Gentile, F., & Polemio, M. (2015). Modelling and management of a Mediterranean karstic coastal aquifer under the effects of seawater intrusion and climate change. *Environ Earth Sci 74*, 115-128.

Rupert, M. (2001). Calibration of the DRASTIC ground water vulnerability mapping method. *Ground Water, 39*, 625-630.

Sabato, L., Cilumbriello, A., & Tropeano, M. (2018). *Note illustrative della Carta Geologica d'Italia alla scala 1:50.000, Foglio Geologico 508 Policoro.* ISPRA, Serv. Geol. d'It., Ed. System Cart.

Sahoo, S., Dhar, A., Kar, A., & Chakraborty, D. (2016). Index-based groundwater vulnerability mapping using quantitative parameters. *Environ. Earth Sci. 75*, 522.

Santoro, M. (1970). Sulla applicabilità della formula di Turc per il calcolo della evapotraspirazione effettiva in Sicilia. *Atti I Conv. I.A.H.*, (p. 105-114).

Satriani, A., Loperte, A., & Proto, M. (2011). Electrical resistivity tomography for coastal salt water intrusion characterization along the Ionian coast of Basilicata region (southern Italy). *IWTJ*, 83-90.

Satriani, A., Loperte, A., Imbrenda, V., & Lapenna, V. (2012). Geoelectrical surveys for characterization of the coastal saltwater intrusion in Metapontum forest reserve (southern Italy). *Int. J. Geophys.*, 1-8.

Sauer, D., Wagner, S., Bruckner, H., Scarciglia, F., Mastronuzzi, G., & Stahr, K. (2010). Soil development on marine terraces near Metaponto (Gulf of Taranto, southern Italy). *Quaternary International, 222(1-2)*, 48-63.

Scanlon, B., Healy, R., & Cook, P. (2002). Choosing appropriate techniques for quantifying groundwater recharge. *Hydrogeol. J., 10 (1)*, 18-39.

Scheidleger, A., Grath, J., & Lindinger, H. (2004). Saltwater intrusion due to groundwater overexploitation EEA inventory throughout Europe. *18th Saltwater Intrusion Meeting*, (p. 125). Cartagena, Spain.

Simmers, I. (1988). *Estimation of Natural Groundwater Recharge.* Boston, MA: D. Reidel Publishing Co.

Šimunek, J., Šejna, M., & van Genuchten, M. (2005). *The HYDRUS-1D Software Package for Simulating the One-Dimensional Movement of Water, Heat, and Multiple Solutes in Variably-Saturated Media.* Riverside, CA, USA: University of California.

Singh, A. (2015). Managing the environmental problem of seawater intrusion in coastal aquifers through simulation-optimization modeling. *Ecological Indicators, 48*, 498-504.

Stevenazzi, S., Bonfanti, M., Masetti, M., Nghiem, S., & Sorichetta, A. (2017). A versatile method for groundwater vulnerability projections in future scenarios. *J. Environ. Manag. 187*, 365-374.

Stewart, M. (1999). Geophysical investigations. In J. a. Bear, *Seawater intrusion in coastal aquifers. Concepts, methods and practices* (p. 9-50). Dordrecht, Netherlands: Kluwer Academic Publishers.

Summa, V., Margiotta, S., & Tateo, F. (2019). Correlation between geochemical, mineralogical and physical characters of sediments and salinization phenomena in a pilot area in the ionian plain (Southern Italy). *Geomatics, Natural Hazards and Risk, 10:1*, 1139-1154.

Taghavi, N., Niven, R., Paull, D., & Kramer, M. (2022). Groundwater vulnerability assessment: A review including new statistical and hybrid methods. *Sci. Total Environ.*, 822.

Tesoriero, A., & Voss, F. (1997). Predicting the probability of elevated nitrate concentrations in the Puget Sound Basin: Implications for aquifer susceptibility and vulnerability. *Groundwater, 35*, 1029-1039.

Trabelsi, N., Triki, I., Hentati, I., & Zairi, M. (2016). Aquifer vulnerability and seawater intrusion risk using GALDIT, GQISWI and GIS: case of a coastal aquifer in Tunisia. *Environ Earth Sci, 75*, 669.

Tropeano, M., Cilumbriello, A., Grippa, A., Sabato, L., Bianca, M., Gallicchio, S., Gallipoli, M.R., & Mucciarelli, M. (2011). Stratigraphy of the subsurface of the Metaponto Plain vs a geophysical 3D view of the late Pleistocene incised-valleys (Basilicata, Southern Italy). *Rendiconti online della Società Geologica Italiana, 17*, 187-193.

Tropeano, M., Cilumbriello, A., Sabato, L., Gallicchio, S., Grippa, A., Longhitano, S. G., Bianca, M., Gallipoli, M.R., Mucciarelli, M., & Spilotro, G. (2013). Surface and subsurface of the Metaponto coastal plain (Gulf of Taranto—Southern Italy): Present-day- vs. LGM landscape. *Geomorphology, 203*, 115-131.

Tropeano, M., Sabato, L., & Pieri, P. (2002). The Quaternary «Post-turbidite» sedimentation in the South-Apennines Foredeep (Bradanic Trough-Southern Italy). *Boll. Soc. Geol. Ital. 1*, 449-454.

Turc, L. (1954). Calcul du bilan de l'eau. Évaluation en fonction des précipitations et des températures. *IAHS Publ., 37*, 88-200.

Twarakavi, N., & Kaluarachchi, J. (2005). Aquifer vulnerability assessment to heavy metals using ordinal logistic regression. *Ground Water, 43*, 200-214.

United States Geological Survey. (2012). SEAWAT: A Computer Program for Simulation of Three-Dimensional Variable-Density Ground-Water Flow and Transport.

Vespasiano, G., Cianflone, G., Romanazzi, A., Apollaro, C., Dominici, R., Polemio, M., & De Rosa, R. (2019). A multidisciplinary approach for sustainable management of a complex coastal plain: The case of Sibari Plain (Southern Italy). *Marine and Petroleum Geology, 109*, 740-759.

Vezzani, L. (1967). I depositi plio-pleistocenici del litorale ionico della Lucania. *Atti Acc. Gioenia Sc. Nat. VI, 18*, (p. 159-180). Catania.

Vías, J., Andreo, B., Perles, M., Carrasco, F., Vadillo, I., & Jiménez, P. (2006). Proposed method for groundwater vulnerability mapping in carbonate (karstic) aquifers: The COP method. *Hydrogeol. J. 14*, 912-925.

Voss, C. (1984). *Finite Element Simulation Model for Saturated-Unsaturated Fluid Density-Dependent Groundwater Flow with Energy Transport or Chemically Reactive Single-Species Solute Transport.* Reston, VA, USA: U.S. Geological Survey.

Vrba, J., & Zaporec, A. (1994). Guidebook on Mapping Groundwater Vulnerability. *IAH International Contributions to Hydrogeology* (p. Volume 16, p. 131). Hannover, Germany: Heise Pub.

Wagenet, R., & Hutson, J. (1986). Predicting the fate of non-volatile pesticides in the unsaturated zone. *J. Environ. Qual. 15*, 315-322.

Webster, R., & Oliver, M. (2007). *Geostatistics for Environmental Scientists.* Chichester, UK: John Wiley & Sons.

Westaway, R., & Bridgland, D. (2007). Late Cenozoic uplift of southern Italy deduced from fluvial and marinesediments: Coupling between surface processes and lower-crustal flow. *Quat. Int., 175*, 86-124.

Younes, A., & Fahs, M. (2014). A semi-analytical solution for saltwater intrusion with very narrow transition zone. *Hydrogeol. J., 22*, 501-506.

Zheng, C., & Wang, P. (1999). *MT3DMS: A Modular Three-Dimensional Multispecies Transport Model for Simulation of Advection, Dispersion, and Chemical Reactions of Contaminants in Groundwater Systems; Documentation and User's Guide; Contract Report SERDP-99-1.* Vicksburg, MS, USA: U.S. Army Engineer Research and Development Center.

Zuffianò, L., Basso, A., Casarano, D., Dragone, V., Limoni, P., Romanazzi, A., Santaloia, F., & Polemio, M. (2015). Coastal Hydrogeological System of Mar Piccolo (Taranto, Italy). *Environ. Sci. Pollut. Res. 23*, 12502-12514.

Zwahlen, F. (2004). *Vulnerability and Risk Mapping for the Protection of Carbonate (Karst) Aquifers, Final Report (COST Action 620).* Brussels, Belgium: Report EUR 20912; European Commission.

14. Sitography

- https://www.un.org/en/conferences/ocean2022/facts-figures
- https://pesthomepage.org/frequently-asked-questions
- Piano di Monitoraggio Acque (regione.basilicata.it)
- https://www.regione.basilicata.it/giunta/files/docs/DOCUMENT_FILE_3032152.pdf

15.   Appendix

Scientific publications:

1. **Seawater Intrusion Proneness and Geophysical Investigations in the Metaponto Coastal Plain (Basilicata, Italy).** Muzzillo R., Zuffianò L.E., Rizzo E., Canora F., Capozzoli L., Giampaolo V., De Giorgio G., Sdao F. & Polemio M. Water, 2021, 13(1), 53 doi.org/10.3390/w13010053

2. **Hydrogeology and Seawater Intrusion Proneness in the Metaponto Plain Aquifer (Basilicata, Italy).** Muzzillo R., Zuffianò L.E., Canora F., De Giorgio G., Limoni P.P., Polemio M. & Sdao F. Italian Journal of Engineering Geology and Environment 2021, 1 doi:10.4408/IJEGE.2021-01.S-13 presented at the **7th National Congress of the Italian association of applied and environmental geology (AIGAA)**, Polo di Lecco – Politecnico di Milano, 23 - 24 September 2021

3. **Groundwater Vulnerability Assessment in the Metaponto Coastal Plain (Basilicata, Italy).** Canora F., Muzzillo R. & Sdao F. Water, 2022, 14(12) doi:10.3390/w14121851

4. **Seawater intrusion vulnerability assessment by GALDIT method in the Metaponto coastal aquifer (Basilicata, Italy).** Muzzillo R., Canora F., Polemio M. & Sdao F. Italian Journal of Engineering Geology and Environment 2022, 1 doi.org/10.4408/IJEGE.2022-01.O-03

5. **Numerical modeling of the groundwater flow and simulation of seawater intrusion in the Metaponto coastal plain (Basilicata, Italy)** *(in the process of submission)*